

**University of Alberta**

**Effective Parameters on Crack Initiation Stress in Low Porosity Rocks**

by

**Mohsen Nicksiar**

A thesis submitted to the Faculty of Graduate Studies and Research  
in partial fulfillment of the requirements for the degree of

**Doctor of Philosophy**

in

**Geotechnical Engineering**

Department of Civil and Environmental Engineering

©Mohsen Nicksiar

Spring 2013

Edmonton, Alberta

Permission is hereby granted to the University of Alberta Libraries to reproduce single copies of this thesis and to lend or sell such copies for private, scholarly or scientific research purposes only. Where the thesis is converted to, or otherwise made available in digital form, the University of Alberta will advise potential users of the thesis of these terms.

The author reserves all other publication and other rights in association with the copyright in the thesis and, except as herein before provided, neither the thesis nor any substantial portion thereof may be printed or otherwise reproduced in any material form whatsoever without the author's prior written permission.

*To my Mother for her precious love*

*To my Brother, Mehdi for his endless support*

*To my Father who will live in my heart forever*

*And to IRAN*

## **Abstract**

Laboratory testing of rocks is traditionally carried out to determine the peak strength using the ISRM Suggested Methods or other suitable standards. However, it is well known that in low-porosity crystalline rocks there are at least three distinct stages of compressive loading that can be readily identified if the stress–strain response is monitored during the loading process: (1) crack initiation, (2) unstable crack growth, i.e., crack coalescence and (3) peak strength. Crack initiation is noted as the first stage of stress-induced damage in low-porosity rocks. In addition, recent research suggests that crack initiation can be used as an estimate for the in situ spalling strength, commonly observed around underground excavations in massive to moderately jointed brittle rocks. Various methods have been proposed for identifying crack initiation in laboratory tests. These methods are evaluated using ten samples of Äspö Diorite and the results are compared with a simplified method, lateral strain response. Statistically, all methods give acceptable crack-initiation values. It is proposed that the ISRM Suggested Methods be revised to include procedures suitable for establishing the crack-initiation stress.

The stress-strain data from 376 laboratory tests carried out on samples of igneous, sedimentary and metamorphic rocks were analyzed to establish the onset of Crack Initiation (CI) stress. A statistical approach was used to find the geological parameters influencing crack initiation stress. Among various rock properties such

as grain size and mineralogy, the proportion of the hardest constituent mineral were found to correlate with CI stress. Foliation-induced anisotropy was found to affect the peak strength but its effect on CI stress was less pronounced. The CI stress to peak stress ratio ranged from 0.42 to 0.47 regardless of the material properties in uniaxial compression whereas this ratio ranged from 0.50 to 0.54 when confined. The crack initiation parameters for the Hoek-Brown spalling criterion for igneous rocks can be expressed in terms of the CI stress ratio and the tensile strength. A comparison of tensile strength from Brazilian and direct tension tests showed that the direct tensile strength was approximately 0.78 of the Brazilian tensile strength.

Crack initiation in the uniaxial compressive loading in rocks occurs well before the peak strength is reached. The factors that may influence the onset of cracking and possible initiating mechanisms were explored using a Discrete Element numerical approach. The numerical approach was based on grain-based model that utilized voronoi tessellation scheme to represent low porosity crystalline rocks such as granite. This approach enabled complete tracking of the failure process along the mineral grain boundaries. The effect of grain-size distribution (sorting coefficient ranging from 1.5 to 1.03), grain size (ranging from 0.75 mm to 2.25 mm), and the heterogeneities of different mineral grains (quartz, K-feldspar, plagioclase) were examined. The modelling revealed that crack initiation is a tensile mechanism in the low porosity rocks simulated, and that shear cracking along grain boundaries is only a prominent mechanism near the peak strength. It was also shown that the grain size distribution had the most significant effect on

peak strength and crack initiation stress. The peak strength ranges from 140 to 208 MPa as the grain size distribution varies from heterogeneous to uniform, respectively. However, the ratio of crack initiation to peak stress showed only minor variation, as the heterogeneity decreases. The other factors investigated had only minor effects on crack initiation and peak strength, and the crack initiation ratio.

## **Acknowledgements**

I would like to express my sincere gratitude to Prof. Derek C. Martin for his supervision, splendid guidance and encouragement during my PhD research program. His continuous support from the very beginning of the research when the topic was finalized up to my last day in Edmonton is warmly appreciated.

I would like to thank some other people at the University of Alberta who have been my support directly or indirectly during the last five years: Steve Gamble, Ann Jones and Prof. Clayton Deutsch. I specially thank Dr. Banafsheh Babakhani who generously spent her time on reviewing some of my papers and parts of my thesis.

I owe thanks to my family, my mother and brother, who encouraged me so much remotely from Iran and helped me out with their positive energy and financial aids. I could have never finished my graduate studies without their support. I am also thankful to our group members and all my friends especially Banafsheh who made my life full of happiness.

## Table of Content

<b>Chapter 1. Introduction.....</b>	<b>1</b>
1.1. Research focus .....	3
1.2. Research findings.....	4
1.3. Practical Implication .....	5
1.4. Reference .....	6
<b>Chapter 2. Literature Survey.....</b>	<b>9</b>
2.1. Mechanism of crack formation .....	9
2.2. Modes of crack tip displacement .....	9
2.3. Mechanism of cracking in rocks .....	10
2.4. Brittle failure process in rocks .....	16
2.5. Effect of material properties .....	29
2.5.1. Grain size .....	29
2.5.2. Texture .....	30
2.5.3. Grain size distribution.....	32
2.5.4. Elastic constants.....	33
2.5.5. Porosity .....	34
2.6. References.....	37
<b>Chapter 3. Evaluation of methods for determining crack initiation in compression tests on low porosity rocks .....</b>	<b>44</b>
3.1. Introduction.....	44
3.2. Stress-strain in laboratory compression tests.....	46
3.3. Methods for determining crack initiation in compression .....	48
3.3.1. Volumetric strain methods.....	49
3.3.2. Lateral strain methods.....	50

3.3.3. Acoustic emission method .....	54
3.3.4. Proposed Lateral Strain Response (LSR) method .....	55
3.4. Crack-initiation stress for Äspö Diorite .....	57
3.5. Discussion .....	59
3.6. Conclusion .....	63
<b>Chapter 4. Crack initiation stress in low porosity crystalline and sedimentary rocks .....</b>	<b>68</b>
4.1. Introduction .....	68
4.2. Sample description .....	69
4.2.1. Igneous rocks .....	69
4.2.2. Sedimentary Rocks .....	71
4.2.3. Metamorphic Rocks .....	74
4.3. Testing Methodology .....	75
4.3.1. Testing Procedure .....	75
4.3.2. Crack initiation stress measurement .....	76
4.3.3. Grouping of samples .....	77
4.4. Effect of material properties on crack initiation stress .....	79
4.4.1. Mineral composition .....	79
4.4.2. Effect of directional heterogeneity .....	80
4.5. Crack initiation for different loading paths .....	83
4.5.1. Uniaxial compression .....	83
4.5.2. Triaxial compression .....	84
4.5.3. Tensile loading .....	86
4.6. Estimation of crack initiation in triaxial compression .....	90
4.7. Conclusion .....	92
4.8. References .....	94

<b>Chapter 5. Factors affecting crack initiation in low porosity crystalline rocks .....</b>	<b>100</b>
5.1. Introduction.....	100
5.2. Crack initiation models in compression loading.....	102
5.3. UDEC modeling of brittle failure in intact rocks.....	107
5.3.1. Model setup.....	108
5.3.2. Block constitutive model .....	109
5.3.3. Contact constitutive model.....	110
5.4. Crack initiation stress.....	110
5.5. Modelling approach used to assess the effect of heterogeneity .....	113
5.6. Grain size distribution .....	113
5.7. Grain size .....	117
5.8. Mineralogy.....	117
5.9. Results and discussion .....	120
5.9.1. Crack initiation mechanism .....	120
5.9.2. Effect of heterogeneity induced by grain size distribution .....	123
5.9.3. Effect of grain size .....	124
5.9.4. Effect of mineralogy .....	125
5.10. Summary .....	127
5.11. Conclusion .....	129
5.12. References.....	131
<b>Chapter 6. Conclusion .....</b>	<b>137</b>
<b>Appendix 1.....</b>	<b>141</b>
<b>Appendix 2.....</b>	<b>143</b>
<b>Appendix 3.....</b>	<b>147</b>
<b>Appendix 4.....</b>	<b>159</b>

## Table of Tables

### ***Chapter 2:***

Table 2.1: The normalized value of crack initiation stress for different types of rocks .....	25
Table 2.2: Crack initiation stress calculation based on $\sigma_{cm}$ in different case studies .....	28
Table 2.3: Petrographic analysis of Forsmark granite and aplite, from Swedish Nuclear Fuel and Waste management Co. ....	33

### ***Chapter 3:***

Table 3.1: Comparison of results from different strain-based methods available for determining the crack-initiation stress of Äspö Diorite.....	59
---	----

### ***Chapter 4:***

Table 4.1: Grain size classification system of igneous rock samples .....	70
Table 4.2: Geological description of igneous specimens.....	72
Table 4.3: Geological description of sedimentary rock specimens .....	74
Table 4.4: Modal analysis of metamorphic specimen.....	75
Table 4.5: Spearman rank correlation coefficient between mineralogy and brittle failure parameters of fine and medium grained igneous rocks .....	80

### ***Chapter 5:***

Table 5.1: Material Properties used in the UDEC models. The bulk and shear modulus as well as normal and shear stiffness are changed in the mineral based models. ....	111
--	-----

Table 5.2: Elastic properties of igneous rock forming minerals .....	119
Table 5.3: Contact normal and shear stiffness based on Hooke's law for different minerals.....	119
Table 5.4: Modeling properties of Syenite and Gabbro.....	119
Table 5.5: Crack orientation in models with different attributes. Crack orientations are measured relative to the load direction .....	123
Table 5.6: Crack initiation stress peak stress in models with different grain size distribution. ....	125
Table 5.7: Crack initiation stress and peak stress in models with different average grain size when $S_o=1.03$ . ....	126
Table 5.8: Crack initiation stress and peak stress in models with different mineralogy and grain size distributions. ....	128

List of Figures

**Chapter 2:**

Figure 2.1: Typical stress strain response recorded in a uniaxial compressive test..... 10

Figure 2.2: Three models for axial crack initiation..... 12

Figure 2.3: Relationship between axial stress and volumetric strain for quartzite (left) and norite (right) in uniaxial compression test in conventional loading machine. Crack initiation and crack damage stress are marked by point A and B ..... 13

Figure 2.4: Idealized model for the initiation of the cracks (left) and most commonly observed features (right) ..... 14

Figure 2.5: Plots of volumetric stiffness and axial stress (red) and AE elastic impulse "energy" rate vs. axial stress for URL 240 level samples of granodiorite, grey granite and pegmatite..... 17

Figure 2.6: Rose diagram of the microcracks in samples parallel to the drill-core axis and untested sample. The horizontal microcracks correspond to the tectonically horizontal joints within the granite..... 18

Figure 2.7: Schematic illustration of different stages of fracture evolution ..... 20

Figure 2.8: Stress-strain diagram showing the elements of crack development. The volumetric strain has been calculated ..... 21

Figure 2.9: Variability of crack volume stiffness reversal with Poisson's ratio for 130 Level pink granite ..... 22

Figure 2.10: Strain guage data can be used in comination with AE event count.....	23
Figure 2.11: Effect of selected parameters on uniaxial compressive strength of the rock and failure duration.....	31
Figure 2.12: Influence of fabric on rock strength for the coarse grained granite, the angles are relative to sample axis.....	32
Figure 2.13: Photomicrograph of the granite (Top left, field view 5.6x4.2 mm) and Aplite (Top right, field view 2.9x2.2) from Forsmark site area; crossed polar. Voronoi model indicating different grain size distribution (Bottom).....	34
Figure 2.14: Effect of porosity on uniaxial compressive strength in limestone ...	36

***Chapter 3:***

Figure 3.1: Typical stress strain response recorded in a uniaxial compressive test. ....	47
Figure 3.2: Incremental distribution of acoustic emission activity measured by Thompson et al. (2006) during the confined testing of Westerly granite .....	48
Figure 3.3: Volumetric strain method proposed by Brace et al. (1966) to establish crack initiation .....	50
Figure 3.4: Crack Volumetric strain method proposed by Martin and Chandler (1994) to establish crack initiation.....	51
Figure 3.5: Lateral strain method proposed by Lajtai (1974) to establish crack initiation .....	52
Figure 3.6: Ratio of the lateral strain to axial stress using a data increment of 25 to establish crack initiation. Tangent line represented as dashed lines. ....	52

Figure 3.7: Extensional strain method proposed by Stacey (1981) to establish crack initiation .....	53
Figure 3.8: Poisson's ratio method proposed by Diederichs (2007) used to establish crack initiation. Tangent line represented as dashed lines. ....	54
Figure 3.9: Acoustic Emission count method proposed by Eberhardt et al. (1998) to establish crack initiation. Tangent line represented as dashed lines. ....	54
Figure 3.10: Example of the methodology used to establish the crack-initiation stress using the lateral strain response (LSR). Unstable crack growth is defined in Figure 3.1. (Top) Illustration of the LSR Methodology (Bottom) Example of the LSR result .....	56
Figure 3.11: Example of the measurement system; LVDTs and chain used to measure the axial and circumferential deformation, respectively. Photo provided by SKB.....	60
Figure 3.12: Sample of Äspö Diorite used to compare the crack-initiation stress using various methods. The specimen is mostly composed of Plagioclase, Oligoclase (in orange) and Anorthite (dark brown). Quartz grains are rarely observable as light coloured mineral while K-feldspars are not obvious in the specimen. ....	61
Figure 3.13: Relation between the uniaxial compressive strength (UCS) and the crack-initiation stress for Äspö diorite measured by LSR method. Also shown is the stress associated with onset of in-situ cracking (APSE) for Äspö diorite determined by Andersson et al. (2009) .....	62

**Chapter 4:**

Figure 4.1: Classification of igneous samples based on modal analysis .....	71
Figure 4.2: Example of the measurement system; LVDTs and chain used to measure the axial and circumferential deformation, respectively. Photo provided by SKB.....	76
Figure 4.3: Typical stress–strain response recorded in a uniaxial compressive test.....	77
Figure 4.4: Statistical distribution of unconfined compressive strength and crack initiation stress in (a) igneous, (b) sedimentary and (c) metamorphic rocks .....	78
Figure 4.5: Statistical distribution of unconfined compressive strength and crack initiation stress of (a) fine grained igneous; (b) medium grained igneous and (c) sedimentary samples .....	81
Figure 4.6: Crack initiation and peak stress in sedimentary rocks with different clay-carbonate content .....	82
Figure 4.7: Effect of directional anisotropy on (a) crack initiation and peak stress and (b) tensile strength. Peak (light colour) and crack initiation stress (dark colour) are measured from UCS stress-strain curve. Average stress values (in bold) and standard deviation.....	83
Figure 4.8: The relationship between crack initiation and peak stress in different rock types: (a) Igneous; (b) sedimentary and (c) metamorphic rocks.....	85
Figure 4.9: Relationship between crack initiation and peak stress in (a) igneous rocks, (b) metamorphic rocks, (c) Lac du Bonnet granite and (d) crack initiation stress ratios in triaxial compression .....	86

Figure 4.10: (a) Comparison of the mean Brazilian tensile strength of 20 samples and the mean tensile strength obtained from 10 Direct Tension tests; (b) Statistical distribution of direct to Brazilian tensile strength ratio for 10 available samples 88

Figure 4.11: Relationship between Brazilian and “dog-bone” Direct Tension tensile strength for various crystalline rocks: Olkiluoto Mica Gneiss, Forsmark granite, Lac du Bonnet granite (Ldb), Diabase and Marble. Error bars represent standard deviation ..... 88

Figure 4.12: Statistical distribution of crack initiation to tensile strength ratio of (a) Laxemar granite, (b) Laxemar quartz monzodiorite, (c) Forsmark metagranodiorite and (d) Olkiluoto mica gneiss. The Direct tensile strength values in the histograms are calculated using the relationship given in Figure 4.11. .... 89

Figure 4.13: Crack initiation stress from lab measurement, Griffith and Generalized Hoek-Brown failure criteria. (a) metagranodiorite; (b) granite; (c) quartz monzodiorite and (d) Lac du Bonnet granite ..... 92

**Chapter 5:**

Figure 5.1: Crack initiation (CI) stress versus uniaxial compressive strength (UCS) for low porosity igneous, sedimentary and metamorphic rocks. Regression line and its 95% confidence interval are shown as solid and dashed line, respectively ..... 102

Figure 5.2: Two models commonly used to explain crack initiation observed in laboratory tests. .... 104

Figure 5.3: Comparison of measured axial and lateral strain in a uniaxial compression tests subjected to 38 load-unload cycles. (a) Axial strain for 38 load-

unload cycles; (b) Lateral strain for 38 load-unload cycles; and (c) Permanent axial and lateral strain for 38 load-unload cycles .....	105
Figure 5.4: Comparison of volumetric strain reversal when applied stress is 183 MPa and 190 MPa, and slope of the axial and lateral strain for 190 MPa. (a) Volumetric strain reversal (b) Slope of axial and lateral strain for 190 MPa .....	107
Figure 5.5: Axial and lateral strains are recorded at the locations shown to monitor the sample response .....	110
Figure 5.6: Comparison of the crack initiation stress in a laboratory compression test and the methods used to establish crack initiation stress in the UDEC Model. (a) Stress strain response and crack initiation in a laboratory test; (b) Crack initiation in the UDEC model .....	113
Figure 5.7: Grain size distribution of the models with different sorting coefficient. The uniformity of the grain size increases from (a) to (d) .....	116
Figure 5.8: Location of 6 mineral-based models on Quartz–K-feldspar–Plagioclase diagram .....	118
Figure 5.9: Equivalent mineral stiffness based on Hooke's law .....	120
Figure 5.10: Relationship between the quantity of tensile and shear cracks, expressed as a percentage of the total contacts, for each approximate 0.07 load increment. The applied stress is normalized to the peak strength. CI refers to crack initiation and CD refers to crack damage (unstable crack growth) obtained by strain-based methods .....	121
Figure 5.11: The direction of cracks measured in the four models ( $S_o=1.5, 1.14, 1.05$ and $1.03$ ) .....	122

Figure 5.12: Crack initiation stress as a function of peak stress in models with different grain size distribution.....	124
Figure 5.13: Crack initiation stress as a function of average grain size when $S_o=1.03$ .....	126
Figure 5.14: Crack initiation stress and peak stress in models with different mineralogy and grain size distributions. ....	127
Figure 5.15: Relation between crack initiation stress (CI) and peak uniaxial compressive strength (UCS) found in the grain-based numerical models.....	129

***Appendix 1:***

Figure A1.1: Äspö diorite stress-strain curves in unconfined compressive strength test.....	141
Figure A2.1: Lateral Strain, normalized tensile cracks and change in Poisson's ratio in models with different grain size distribution, (a) $S_o= 1.50$ ; (b) $S_o= 1.14$ ; (c) $S_o= 1.05$ and (d) $S_o=1.03$ .....	143
Figure A2.2: Lateral Strain, normalized tensile cracks and change in Poisson's ratio in models with different average grain size, (a) fine; (b) fine to medium and (c) medium grain size.....	144
Figure A2.3: Lateral strain, normalized tensile cracks and change in Poisson's ratio in models with various mineral contents. All models have uniform grain size distribution. Graphs a-f correspond to model 1-6, respectively.....	145
Figure A2.4: Lateral Strain, normalized tensile cracks and change in Poisson's ratio in models with various mineral contents. All models have the same grain	

size distribution as Figure 5.7-a. Graphs a-f correspond to model 1-6  
respectively. .... 146

# Chapter 1. Introduction

The stability of the underground excavations depends on the mechanical behaviour and the interaction of in-situ stresses to the rock mass. In order to predict the response of the rock mass to the stress change, the failure mechanism has been thoroughly investigated. Brittle failure is always thought of as a tensile mechanism and the formation of the first fracture is also the start of failure of the material. In this respect, the initiation and propagation of the newly formed cracks are the precursor to any brittle failure.

Glass rods subjected to a constant tensile stress were used by Griffith (1921) to support his energy theory for rupture of brittle solids. Griffith used a constant tensile stress loading system to demonstrate that the tensile strength of a material depended on the size of the internal cracks embedded within the material. The traction on these crack surfaces is lost when subjected to tensile loading. The crack tips are regarded as zones of stress concentration such that the application of a modest tensile boundary stress is adequate to rupture the internal crack tip. In these experiments, as in any direct tension test for brittle solids, the tensile stress required to initiate a crack is essentially the same as the ultimate tensile strength. Hence in tension, crack initiation is synonymous with rupture. Griffith (1924) applied his energy concepts to the rupture of rock in compression, and suggested that the strength of rock in unconfined compression was 8 times its tensile strength. Laboratory tests have shown that the uniaxial compressive strength is approximately 15 to 20 times the tensile strength and therefore the Griffith criterion is seldom used to predict the rupture strength of rock in compression. However, the initiation of cracking in compressive loading occurs well before peak strength and at values that are approximately equal to 8 times the tensile strength, which is similar to Griffith's original criterion. Whether this is fortuitous

or not is unknown, however, the onset of cracking in compression has been identified as a material property that is observed in the laboratory compression testing of common crystalline rocks (Stacey, 1981, Martin, 1993).

In 1963, Cook studied the initiation of cracks in underground excavation using seismic events. He found that most of the events will be caused by new fractures which are analogous to Griffith cracks and aligned parallel to the boundaries of excavation at the Witwatersrand gold mine. This type of cracking has been studied by Hallbauer et al. (1973) for rock bursts in deep mines and Fairhurst and Cook (1966) in rock samples and the results showed that these cracks will not produce unstable collapse in uniform compressive stress field. Fairhurst and Cook (1966) evaluated slabbing observed around South African tunnels. They concluded that the cracks are initiated parallel to the maximum stress in compression. Hoek and Brown (1980) evaluated the performance of square tunnels in South Africa and found that when the far-field maximum stress magnitude exceeded 0.15 the uniaxial compressive strength, slabbing was observed around the underground opening. Martin et al. (1999) converted the Hoek and Brown Criterion to a maximum tangential stress and found that when the maximum tangential stress exceeded approximately 0.4 of the UCS, slabbing was observed. Stacey (1981) noted that slabbing was observed at stress values well below peak UCS strength using extensional strain. This criterion has been evaluated in Löttschberg base tunnel, Switzerland by Rojat et al. (2009) to analyze the stress-induced problem associated with TBM excavated tunnel at the depth of over 1000m and particularly at 4 locations with different lithologies from gneiss to granite. In all cases, it was reported that the in-situ slabbing (spalling) strength is far less than the uniaxial compressive strength and hence using the peak strength is problematic for evaluating the spalling strength. Most recently Martin and Christiansson (2009) and Andersson (2007) have suggested that crack initiation from laboratory uniaxial compressive tests could be used as a lower bound estimate for the in-situ spalling strength. Hence having a reliable method

for determining crack initiation in laboratory tests would be beneficial for studies of rock mass in underground excavation.

The ISRM (Bieniawski and Bernede, 1979) makes no mention of crack initiation in its “Suggested Methods for Determining the Uniaxial Compressive Strength and Deformability of Rock Materials”. Nonetheless various authors have proposed different methods for identifying crack initiation (e.g. Brace, 1964; Bieniawski, 1967; Lajtai, 1974; Stacey, 1981; Martin, 1993; Eberhardt et al., 1998 and Diederichs et al., 2004). Therefore, proposing a robust method for determining crack initiation stress would be necessary.

### **1.1. Research focus**

In this thesis, the initiation of the new cracks in brittle rocks is studied from the following aspects:

- Methods to measure crack initiation stress
- Mechanism controlling the initiation of the cracks
- Rock characteristics governing the initiation of the cracks
- Effect of confinement on crack initiation stress
- Numerical simulation of crack initiation stress and the modes of cracking

In Chapter 3, the pros and cons of different methods of crack initiation stress measurement will be reviewed. The purpose of this chapter is to find a methodology that is robust enough to propose as a guideline in crack initiation stress measurement.

In Chapter 4, the role of mineralogy, average grain size and directional anisotropy on crack initiation under low confinement is explored in samples of different rock types. The effect of confinement on crack initiation stress is also studied. Moreover, the ratio of crack initiation stress to peak strength is also investigated

from the unconfined and triaxial compression test results. The available spalling criteria, Griffith and Hoek-Brown, are also studied in this chapter.

In Chapter 5, the uniaxial compressive strength test will be modelled using Discrete Element Methods (DEM) with special interest on capturing the initiation of the cracks. This model will then be used to find the cracking behaviour of the samples as geometrical and mineralogical heterogeneities have been applied to the models. Moreover, the model which best describes the process of brittle failure will be described using the numerical and lab data.

## **1.2. Research findings**

Numerical and empirical methods are presented to find the procedure of fulfilling the abovementioned approaches. These methodologies will be started from the simplest models to the sophisticated examples that demonstrate the characteristics of real data.

In the third chapter, five strain based methods to measure crack initiation stress will be categorized according to the input parameters. The steps for each method will be presented and the ambiguities on their measurement will be discussed. Knowing all the weaknesses, the robust method of crack initiation stress measurement is introduced. Crack initiation stress is then measured for samples of Äspö diorite using all the reviewed methods as well as newly introduced Lateral Strain Response (LSR) method. The results clearly showed that the LSR method is statistically accurate.

In the fourth chapter, the effect of geology and loading condition on crack initiation stress for different rock types will be analyzed using newly introduced Lateral Strain Method (LSR). The results will be statistically compared with other rock properties confirming the crack initiation stress is positively correlated to the hardest rock forming mineral. In metamorphic rocks, the directional anisotropy affects peak strength. However, Crack initiation stress remained unchanged for the samples of different foliation angle relative to the loading direction. Crack

initiation stress is also studied in triaxial compression. The results showed that crack initiation to peak strength ratio increases as the confinement pressure is increased. Finally spalling criteria have been studied using the results from uniaxial and compressional test. Accordingly, Hoek-Brown spalling criterion for igneous rocks can be expressed in terms of crack initiation stress ratio and tensile strength to have a better estimation of spalling strength.

Considering the limitations in studying the effect of material properties on brittle failure parameters using lab data, numerical modelling is used. In chapter five, crack initiation stress and peak strength have been measured from 20 models. These models represent models with different grain size distribution, average grain size and mineralogy. The results show that the effect of grain size distribution is more pronounced on crack initiation and peak stress compared to other parameters. Finally two generally accepted cracking models, force-chain and sliding crack model, are evaluated during brittle failure of the samples concluding that the force-chain model better describes the cracking, especially at the early stage of loading. Shearing mechanism becomes more dominant as stress levels approach to the peak strength.

### **1.3. Practical Implication**

Stress induced failure within a rock mass is closer to the crack initiation stress levels. The methodology for damage initiation threshold detection is not fully provided according to the available standards of ISRM or ASTM. It is therefore essential to understand the crack initiation stress mechanism and also the controlling parameters.

Ambiguities associated with the use of these thresholds for modelling criteria of spall prediction will be clarified if the effective parameters on crack initiation are discovered. Moreover, having the relationship between crack initiation stress in intact rock and the rock mass spalling criteria, spalling stress can be estimated from the lab crack initiation stress.

## 1.4. Reference

- Andersson, C.J., 2007, Äspö Hard Rock Laboratory. Äspö Pillar Stability Experiment, Final report. Rock mass response to coupled mechanical thermal loading: SKB TR-07-01.
- Bieniawski, Z.T., 1967, Mechanism of brittle fracture of rock: Part I—theory of the fracture process: *International Journal of Rock Mechanics and Mining Sciences & Geomechanics Abstracts*, v. 4, no. 4, p. 395-404, IN11-IN12, 405-406.
- Bieniawski, Z.T., and Bernede, M.J., 1979, Suggested methods for determining the uniaxial compressive strength and deformability of rock materials: Part 1. Suggested method for determining deformability of rock materials in uniaxial compression: *International Journal of Rock Mechanics and Mining Sciences & Geomechanics Abstracts*, v. 16, no. 2, p. 138-140
- Brace, W.F., 1964, Brittle Fracture of Rock. in Judd, W.R., ed., *State of Stress in the Earth's Crust*: New York, Elsevier, p.111-181.
- Diederichs, M.S., Kaiser, P.K., and Eberhardt, E., 2004, Damage initiation and propagation in hard rock during tunnelling and the influence of near-face stress rotation: *International Journal of Rock Mechanics and Mining Sciences*, v. 41, no. 5, p. 785-812.
- Eberhardt, E., Stead, D., Stimpson, B., and Read, R.S., 1998, Identifying crack initiation and propagation thresholds in brittle rock: *Canadian Geotechnical Journal*, v. 35, no. 2, p. 222-233.
- Fairhurst, C., and Cook, N.G.W., 1966, The phenomenon of rock splitting parallel to direction of maximum compression in the neighborhood of a surface, in 1st congress of the international society of rock mechanics: Lisbon, p. 687-692.

- Griffith, A.A., 1921, The Phenomena of Rupture and Flow in Solids: Philosophical Transactions of the Royal Society of London. Series A, Containing Papers of a Mathematical or Physical Character, v. 221, p. 163-198.
- Griffith, A.A., 1924, Theory of rupture, in Proceedings of the First International Congress of Applied Mechanics: Delft, p. 55-63.
- Hallbauer, D.K., Wagner, H., and Cook, N.G.W., 1973, Some observations concerning the microscopic and mechanical behaviour of quartzite specimens in stiff, triaxial compression tests: International Journal of Rock Mechanics and Mining Sciences & Geomechanics Abstracts, v. 10, no. 6, p. 713-726.
- Hoek, E., and Brown, E.T., 1980, Underground excavations in rocks: London, Institution of Mining and Metallurgy.
- Lajtai, E.Z., 1974, Brittle fracture in compression: International Journal of Fracture, v. 10, no. 4, p. 525-536.
- Martin, C.D., 1993, The strength of massive Lac du Bonnet granite around underground openings. [PhD Thesis]: Department of Civil and Geological Engineering, University of Manitoba, Wininpeg, Man.
- Martin, C.D., and Christiansson, R., 2009, Estimating the potential for spalling around a deep nuclear waste repository in crystalline rock: International Journal of Rock Mechanics and Mining Sciences, v. 46, no. 2, p. 219-228.
- Martin, C.D., Kaiser, P.K., and McCreath, D.R., 1999, Hoek-Brown parameters for predicting the depth of brittle failure around tunnels: Canadian Geotechnical Journal, v. 36, no. 1, p. 136-151.
- Rojat, F., Labiouse, V., Kaiser, P.K., and Descoedres, F., 2009, Brittle Rock Failure in the Steg Lateral Adit of the Lötshberg Base Tunnel, Springer Wien 42, 341 p.

Stacey, T.R., 1981, A simple extension strain criterion for fracture of brittle rock:  
International Journal of Rock Mechanics and Mining Sciences &  
Geomechanics Abstracts, v. 18, no. 6, p. 469-474.

## **Chapter 2. Literature Survey**

Brittle failure in rocks is always under attention in different fields of rock mechanics such as stability in underground excavations. The formation of a failure plane in a rock mass or intact rock, results from the initiation of small cracks. The process of crack initiation depends on the mechanical behaviour and stress interaction of the mineral crystals. At the microscopic scale, these small cracks are first formed along the grain boundaries of crystals which rupture under applied load.

### **2.1. Mechanism of crack formation**

The initiation of cracks was first studied by Griffith (1921) who examined the crack propagation from small defects, so-called "Griffith Cracks", in glass rods. These flaws will lose the traction on their surface under tensile loading. Cracks propagate when an excess in energy due to loading develops, which in turn is balanced by an increase in crack length. Griffith (1924) expanded his failure criterion to describe compressive loading under uniaxial and biaxial compressive stress fields. He proposed that the cracks propagate along the flaws due to local induced tensile stress on the crack tips. Although Griffith failure criterion estimates the uniaxial compressive strength of a material as eight times its tensile strength, the lab works indicate the peak stress is 15-20 times the tensile strength in crystalline rocks.

### **2.2. Modes of crack tip displacement**

In Griffith's study, cracks are initiated when the tensile stress concentrates at the crack tips and exceeds the tensile strength. Accordingly cracking can be defined

by the concept of Linear Elastic Fracture Mechanics (LEFM). Assuming a flat sharp crack with zero width, three possible displacements are considered on the crack tips when it is subjected to loading: (1) mode I, tensile; (2) mode II, in-plane shear and (3) mode III, anti-plane shear (Broek, 1986; Figure 2.1).

According to LEFM, cracks occur when the stress intensity factor exceeds a critical value, known as fracture toughness,  $K_{IC}$  (Ingraffea, 1987). Stress intensity factor ( $k$ ) is the magnitude of the stress at the crack tip, which is a function of the applied stress. This stress is a function of the distance from the crack tip and the direction of the flaws relative to the applied stress.

### 2.3. Mechanism of cracking in rocks

In rocks, the Griffith flaws are regarded as the grain boundaries. During loading, stress can be concentrated at these flaws resulting in microcrack initiation. For rocks, microcracks are divided into four types according to Kranz (1979):

- 1- Grain boundary cracks which are formed along the grain boundaries;
- 2- Intragranular cracks which are formed within one grain;
- 3- Intergranular cracks which are propagated from the grain boundaries to the inside of a grain;
- 4- Multi-granular cracks (or transgranular cracks) which are propagated from the grain boundaries and cross several grains.

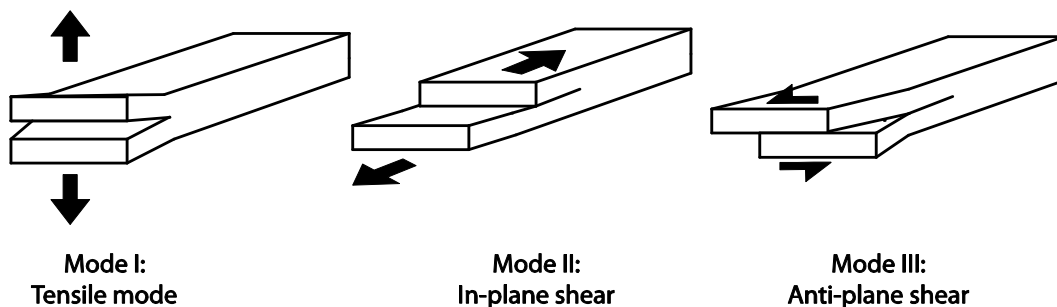
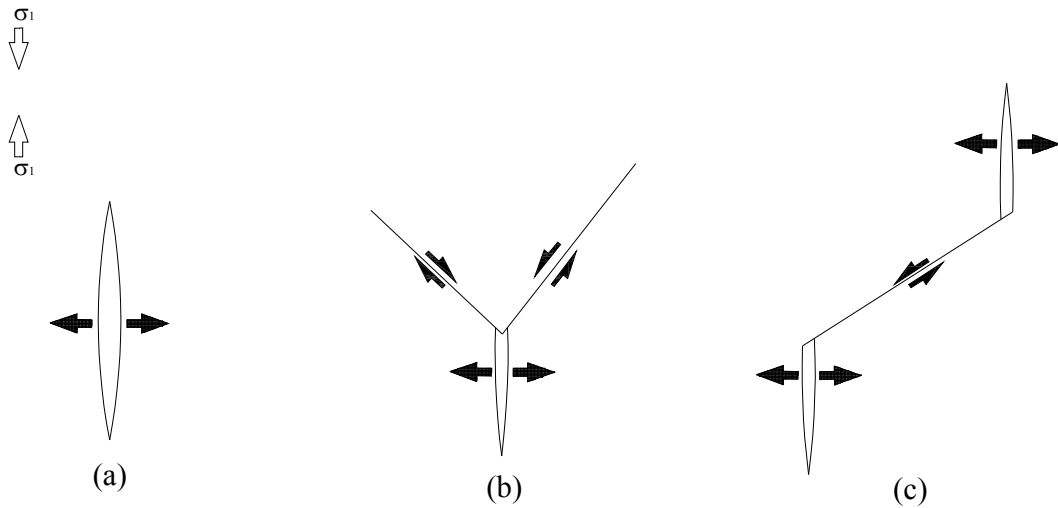


Figure 2.1: Typical stress strain response recorded in a uniaxial compressive test

Brace et al. (1966) have investigated the brittle failure in rocks under uniaxial compressive loading. In their experiments, the stress-strain response of coarse-grained granite, medium-grained marble and fine-grained aplite was studied to determine the rock behaviour through to failure. They found, when the volumetric strain curve deviates from linearity, cracks initiate. At this stress level, the grain boundaries would be more visible due to grain separation. Brace et al. (1966) introduced three models by which the formation of the cracks was probable:

- 1- Axial cracks, which are formed along the grain boundaries or the cleavage within the cracks (Figure 2.2a).
- 2- Open cracks, which are formed at the junction of grain boundaries of three pre-existing cracks. Sliding on two inclined crack surfaces is accommodated by opening at the axial cracks (Figure 2.2b).
- 3- Axial cracks, which are formed at both ends of a pre-existing crack or grain boundaries which is inclined to the sample axis (Figure 2.2c).

The first probable model was rejected by Brace et al. (1966) because the isolated axial cracks should be opened and closed completely with a hysteresis. Bieniawski (1967a) investigated the brittle failure mechanism using uniaxial, biaxial and triaxial tests on norite and quartzite. The volumetric strain vs. axial stress curve has been used to determine the stress level required to initiate fracture (Figure 2.3).



**Figure 2.2: Three models for axial crack initiation (based on Brace et al., 1966)<sup>1</sup>**

The term fracture initiation was introduced by Bieniawski (1967b) as the failure process by which pre-existing cracks in a material start to extend. Crack initiation stress was also defined separately as the formation of one or more cracks independently. He considered the mechanism of fracture initiation as the shear movement of grains over their boundaries, i.e., pre-existing cracks. Wawersik and Brace (1971) found that the initiated cracks are the stable extension of pre-existing flaws that are propagated along grain boundaries in granite and diabase under uniaxial compressive loading. The cracking can be extended within grains at higher stress levels relative to the crack initiation stress.

The generation of the tensile stress along the defects results in initiation and propagation of the microcracks due to stress concentration or differential elastic deformation. These microcracks along the grain boundaries or inside a grain (intergranular cracks) and initiate and propagate parallel or sub-parallel to the direction of the maximum stress. The deformation of the grains under uniaxial loading has been studied by Tapponnier and Brace (1976) using Scanning Electron Microscope (SEM).

<sup>1</sup> In the original document the direction of  $\sigma_1$  was incorrectly shown to be perpendicular to the axis of axial cracks that has been corrected here.

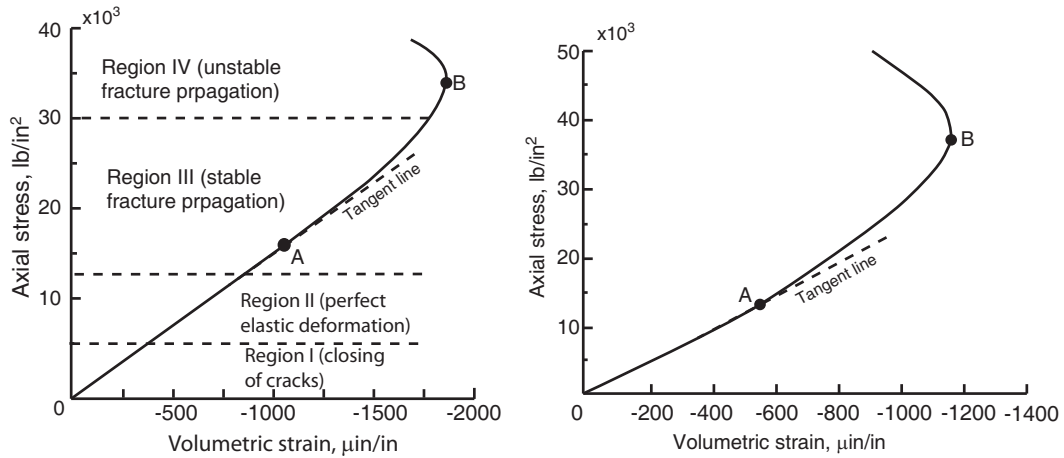


**Figure 2.3: Relationship between axial stress and volumetric strain for quartzite (left) and norite (right) in uniaxial compression test in conventional loading machine. Crack initiation and crack damage stress are marked by point A and B (after Bieniawski, 1967b)**

In this experiment, different samples of Westerly Granite were tested under different axial loading. Examination of the samples which were loaded to the crack initiation stress showed that most of the newly formed cracks are formed along grain boundaries or healed cracks which are oriented up to  $30^\circ$  to maximum compression.

SEM observation showed that most of the cracks are isolated and interface cracks which intersect at high angle interfaces of different minerals (Figure 2.4a and Figure 2.4c). Interface cracks are caused by local tensile stress at the interface of two solids with different elastic properties. However, the cracks formed in a shearing mode were insignificant (Figure 2.4b). The same conclusion was also published earlier by Lisowski (1959). Brace (1964) suggests that the cracks are initiated by rupture along the grain boundaries on Solenhofen Limestone, Marble, Blair dolomite, Webatuck dolomite, Dunham dolomite, Westerly granite, Cheshire quartzite and Fredrick diabase under multiaxial compressional loading.

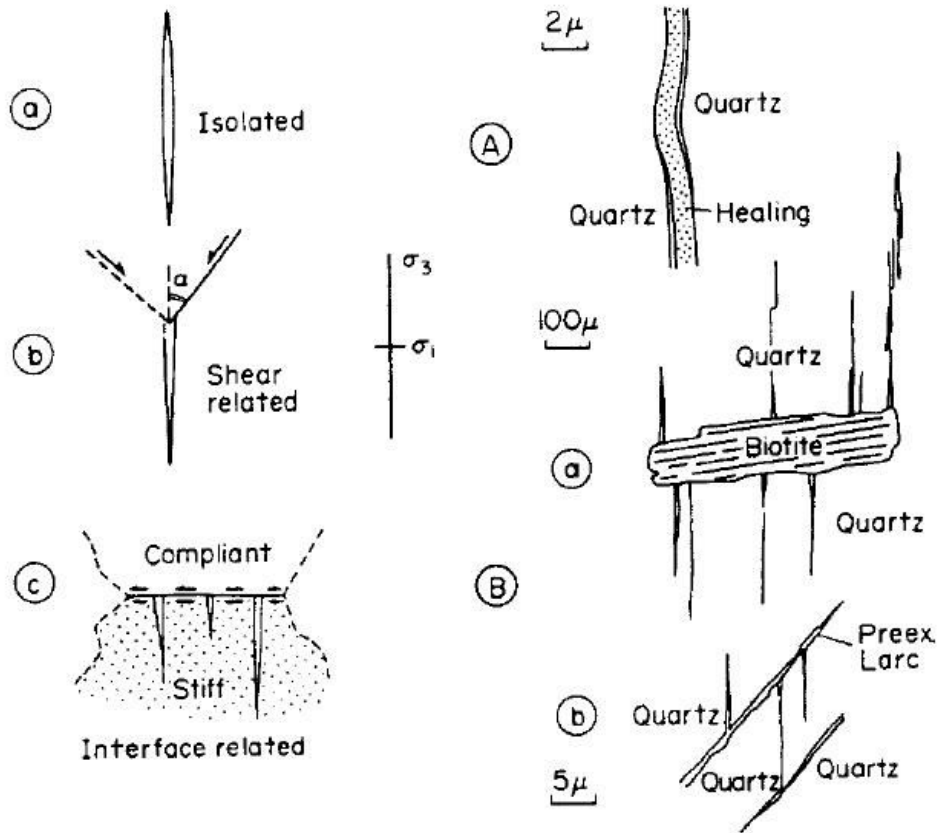


Figure 2.4: Idealized model for the initiation of the cracks (left) and most commonly observed features (right) (after Brace et al., 1966)

Grain boundary cracking was described later by Walsh (1965) as the lateral elastic distortion of the mineral grains and slight movement or sliding of grains or parts of grains under the applied load. Bieniawski (1967a) studied the initiation of the fracture in norite and quartzite in uniaxial compressive regime. It was found that cracks propagate due to the shear movement of the crack faces close to the pre-existing crack tip. Lajtai and Lajtai (1974) examined two confined specimens of plaster of Paris to build up a model for the brittle failure mechanism. Plaster was used because it behaves elastically during the early stage of fracture development. In their models, the fractures grow from the flaws in two modes:

- 1- Tensile fracture, extending parallel to the load
- 2- Normal shear fracture perpendicular to the maximum compression

The formation of the tensile fracture is due to the tensile stress concentration but it was found from the model that the normal shear fracture is actually a crushed zone forming from numerous tiny tensile cracks.

Hallbauer et al. (1973) found out that intergranular cracks are the most common type of cracking caused by the point loading of quartz grains in fine grained argillaceous quartzite under triaxial compression. Observation of the thin sections showed that the majority of the fractures, during triaxial compression, are oriented  $\pm 10^\circ$  relative to the long axis of the specimens which is parallel to the axis of the maximum stress. The initiation of crack has been defined as the total extension strain of the rock when it exceeds a critical value (Stacey, 1981). This critical value is dependent on the rock type characteristics. Martin and Chandler (1994) proposed that the dilation at the point of crack initiation is only registered by the lateral strain gauge and must reflect the axial cracks parallel to the direction of the maximum applied load. Kaiser et al. (2001) has carried out a research on heterogeneous sphalerite to show that under low confinement conditions, local tensile stresses will be generated due to material heterogeneity. This stress concentration results in crack initiation parallel to the maximum compressive stress. Further research on microscopic behaviour of rocks under compressive loading confirmed the formation and growth of the microscopic cracks. These cracks are formed at around half of the unconfined compressive strength of the sample and roughly parallel to the direction of maximum stress (Kranz, 1979; Brace et al., 1966; Tapponnier and Brace, 1976; Peng and Johnson, 1972).

Acoustic Emission (AE) is a low-energy seismic event which will be generated by any inelastic deformation such as grain dislocation or crack initiation (Hardy, 1981).

The sequential initiation of the cracks has been discussed further by Eberhardt et al. (1999a) using both strain gauge data and acoustic emission sensors (Figure 2.5). The samples were Lac du Bonnet granodiorite (average grain size: 1mm), granite (average grain size: 3mm) and pegmatite (average grain size: 20mm).

Both the volumetric stiffness vs. axial strain curve and AE impulse "energy" rate has been used to obtain more accurate data. By virtue of these methods, two modes of crack initiation have been found as  $\sigma_{ci}$  and  $\sigma_{ci2}$  which are caused by grain boundary and intergranular cracks in feldspar's, respectively.

Tromans and Meech (2002) have also shown that in the case of intragranular cracking, the cracks tend to propagate parallel to the axial load even if the crystallographic axes of the minerals changes from grain to grain relative to the maximum axial stress.

Akesson et al. (2004) used a combination of fluorescent and polarized microscopy to investigate the microcrack development in medium grained granite (average grain size: 2 mm) under dynamic cyclic loading. The maximum loading was 122 MPa which is 60% of the uniaxial compression strength (200 MPa). The fluorescent images of the samples from the loaded drill core show a higher abundance of intragranular cracks compared to unloaded samples. The results indicate that intragranular cracks initiate in uniaxial loading, while the transgranular cracks do not show clear differences between the tested and untested samples (Figure 2.6).

## **2.4. Brittle failure process in rocks**

The study of brittle failure, as a progressive process in rocks, was started by Brace (1964) and Bieniawski (1967b) for different rock types. Accordingly, the brittle failure can be divided into several stages using the strain response of the sample under compressive loading.

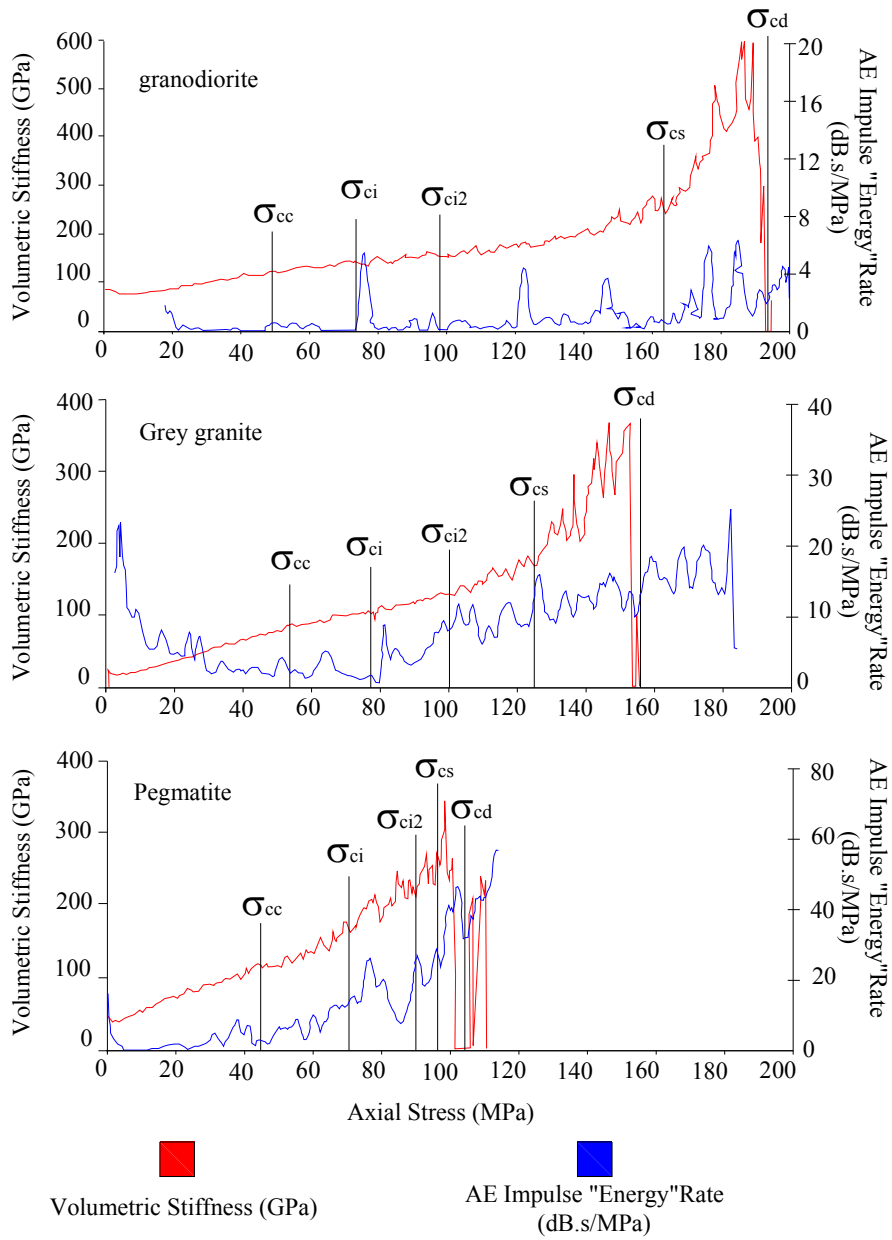


**Figure 2.5: Plots of volumetric stiffness and axial stress (red) and AE elastic impulse "energy" rate vs. axial stress for URL 240 level samples of granodiorite, grey granite and pegmatite (based on Eberhardt et al., 1999a)**

Crack closure stress is defined as the stress at which pre-existing cracks are closed and is marked on the axial strain curve as the onset of linear stress-strain behaviour. Crack initiation stress is marked on the lateral strain curve as where it

deviates from linearity and is defined as the stress in which the new tensile cracks are formed. These are seen as propagating in stable manner. Unstable crack growth region is started at the stress of crack damage where the sample is failed shortly after, even if the stress is not increased. Crack damage stress is marked on the volumetric strain curve when it reaches the maximum contraction and then reversed and dilates.

Several methodologies have been introduced in literature to measure crack initiation stress with the early works of Brace (1964) and Bieniawski (1967b) using volumetric strain curve. In this approach crack initiation stress is defined where volumetric strain versus axial stress curve deviates from linearity. In 1974, Lajtai proposed different stages of brittle failure according to the initiation and propagation of cracks (Figure 2.7). According to his definition, brittle failure process can be divided in 4 categories:

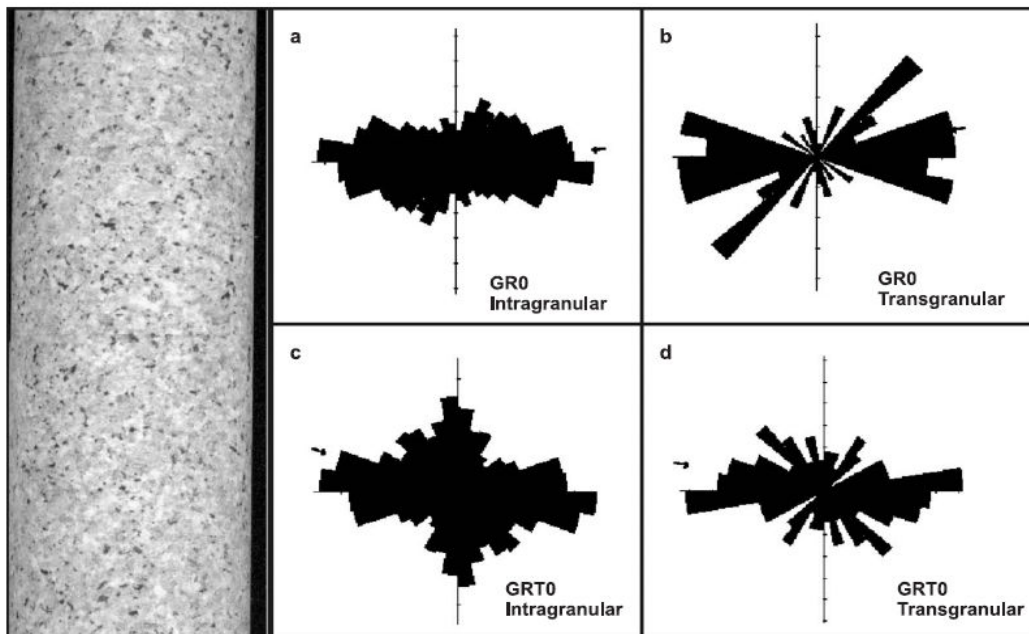


**Figure 2.6: Rose diagram of the microcracks in samples parallel to the drill-core axis and untested sample. The horizontal microcracks correspond to the tectonically horizontal joints within the granite (after Akesson et al., 2004)**

- 1- Macroscopic tensile fractures (CT).
- 2- Macroscopic normal shear fracture start forming which is propagated at the yield point of axial stress-strain curve (Cs).
- 3- Macroscopic inclined shear fracture developed by expanding normal shear fracture (CI).
- 4- The macroscopic fault (which separates material into two pieces) forms after material failure (CR).

In this method, the crack initiation stress can be measured from the lateral strain-axial stress, where the curve deviates from linearity. A similar method has been used by Stacey (1981) using axial strain instead of axial stress.

However, noting the difficulty in using lateral strain gauge data, Martin and Chandler (1994) suggested using crack volumetric strain to identify crack initiation calculated by subtracting the elastic volumetric strains from the total measured volumetric strains (Figure 2.8).

Several difficulties have been encountered by Eberhardt et al. (1998) using this method, mostly dealt with uncertainty in Poisson's ratio determination due to non-linearity of lateral strain curve. This uncertainty can affect crack initiation values of up to  $\pm 40\%$  change in crack initiation stress for a little change of  $\pm 0.05$  in Poisson's ratio. The same assessment has been made by the author on Lac du Bonnet granite of Cold Spring quarry and the change of 30% relative to the actual Poisson's ratio has been found (Figure 2.9).

Eberhardt et al. (1998) used several techniques to detect crack initiation for Lac du Bonnet granite such as stress-strain data, moving point regression technique and acoustic emission (AE).

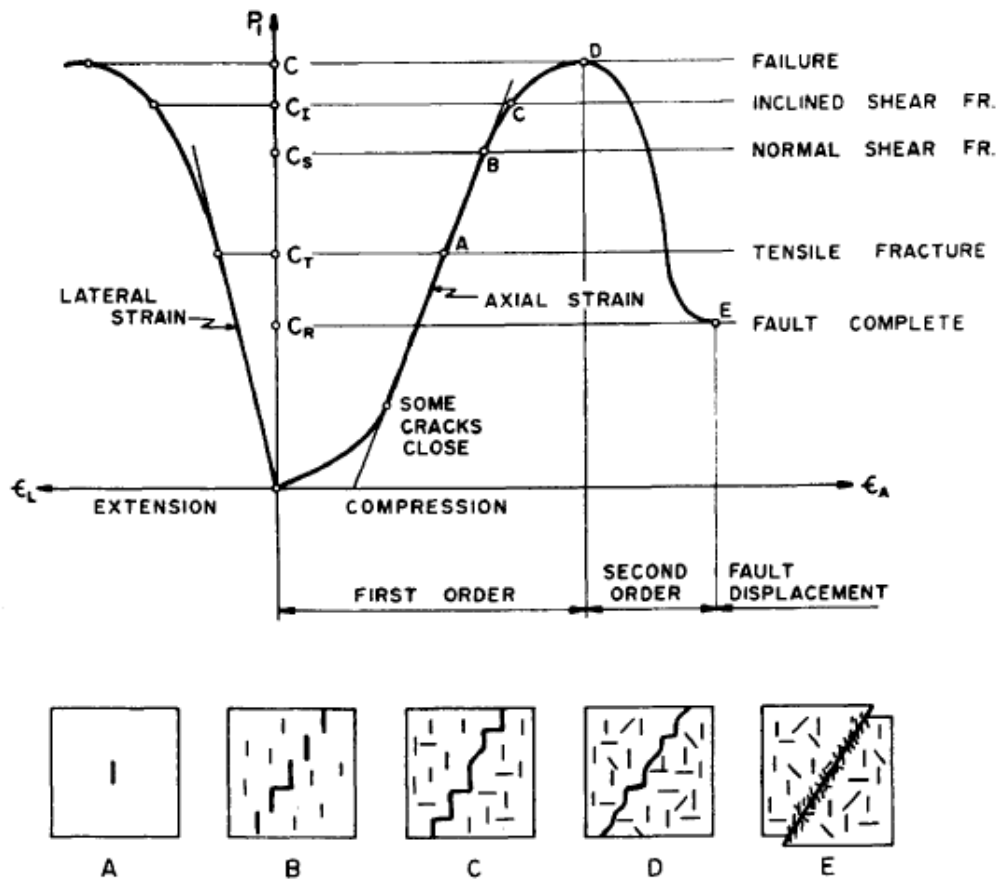
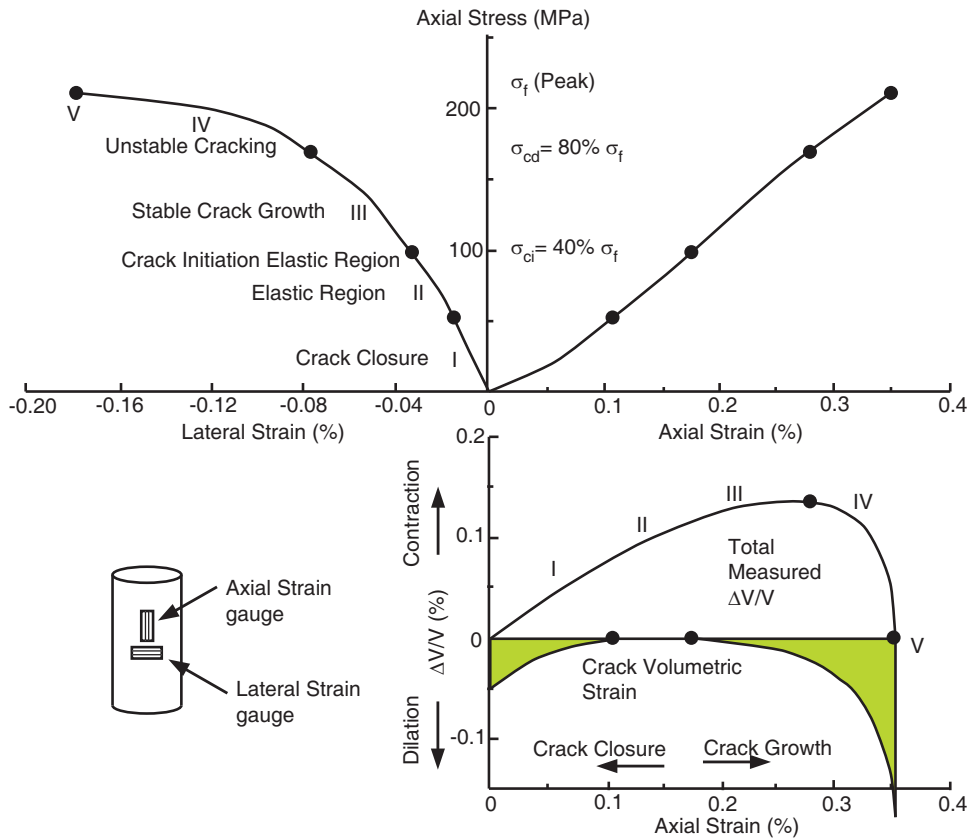


Figure 2.7: Schematic illustration of different stages of fracture evolution (after Lajtai, 1974)

These methods can be used together in order to find a more reliable result (Figure 2.10). However, the insignificant AE activity at the stage of crack initiation has made it difficult to differentiate between the background noise and the cracking-source acoustic events. Lockner (1993) found a good correlation between AE activity and inelastic strain in Westerly Granite to quantify damage accumulation in brittle rocks. Although the crack initiation stress is independent of damage accumulation, crack damage stress reduces significantly in the early stages of the test and reaches a threshold as the damage accumulates in the sample. AE techniques have been used by many authors for rock burst assessment or roof fall prediction (Alcott et al., 1998; Butt et al., 2000).



**Figure 2.8: Stress-strain diagram showing the elements of crack development. The volumetric strain has been calculated (after Martin and Chandler, 1994).**

Although several methods have been applied to understand crack initiation mechanism such as using Scanning Electron Microscope (SEM) images of the deformed sample, the mechanism involved in fracture development needs to be more investigated.

It was first noted by Brace (1964) that the stress required for internal fracturing depends solely on the properties of the rock. The loading condition or sample geometry has no effect on the stress at which cracks are initiated (Bieniawski, 1967b; Bieniawski, 1966).

This conclusion was supported by the results found by Martin and Chandler (1994). They found that although the peak strength reduces as sample volume is increased, the crack initiation stress appears to be unaffected. The different

sample geometry will result in different stress distributions which does not affect the initiation of the crack. Brace et al. (1966) found out the normalized value of crack initiation to peak stress level is 0.45 for granite, 0.5 for marble and 0.55 for aplite. Also, Bieniawski (1967b) showed that crack initiation stress ratio in compression and tension is different. The crack initiation stress in compression was 35% of maximum load while in tension was 94.5%.

For crack damage in compression the stress was 73% while in tensional regime; it was 96.5% of the maximum load in norite. It was also confirmed by Martin and Chandler (1994) that cracks initiate when the load first exceeds about 0.4 of the peak strength. If the value is calculated from simple petrographic investigation, the information can be used to back-calculate the rock mass strength parameters.

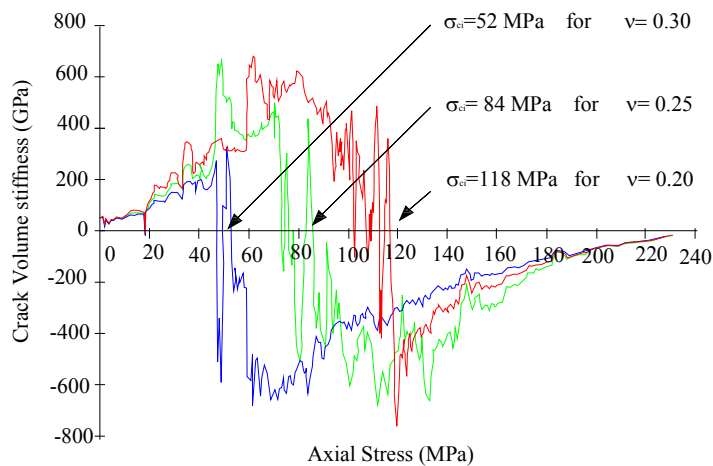


**Figure 2.9: Variability of crack volume stiffness reversal with Poisson's ratio for 130 Level pink granite (after Eberhardt et al., 1998)**

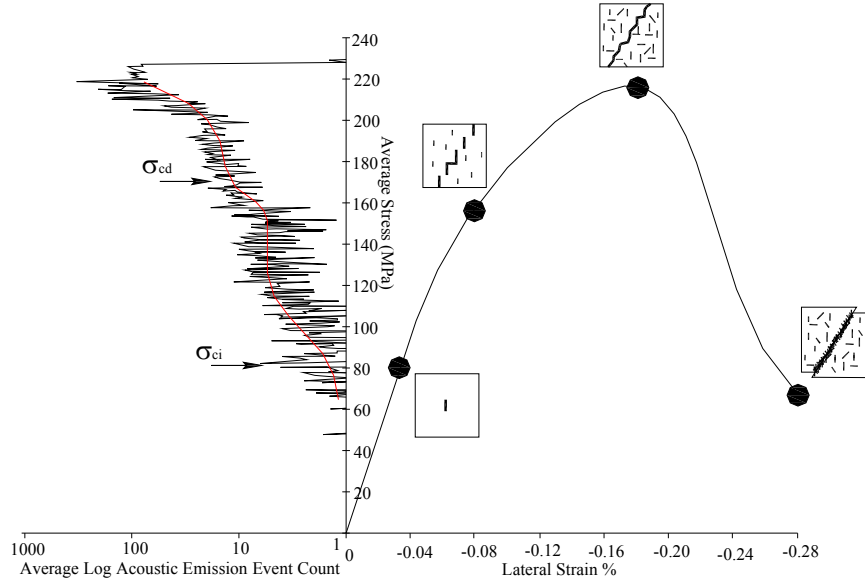


**Figure 2.10: Strain gauge data can be used in combination with AE event count (based on Lajtai 1974; Martin and Chandler, 1994; Eberhardt et al., 1998)**

Cai et al. (2007) developed a method to back calculate the rock mass strength parameters such as UCS, cohesion and friction angle from Acoustic Emission (AE) monitoring data associated with Finite Element Method (FEM) stress analysis. In his research, the stress level at the AE initiation is calculated by FEM (elastic) analysis. Thereafter, the results are back-calculated using generalized crack initiation stress thresholds of brittle rock to find rock mass strength parameters (Cai et al. 2004):

$$f_{\rightarrow \min} = \sum_{i=1}^n (\sigma_1 - \sigma_3 - A \sigma_{cm}) \quad (2-1)$$

or

$$f_{\rightarrow \min} = \sum_{i=1}^n (\sigma_1 - \sigma_3 - A \frac{2c_m \cos \phi_m}{1 - \sin \phi_m})$$

where:

A is the ratio of crack initiation to crack damage stress which in most cases is in the range of 0.4-0.6 and  $c_m$  and  $\phi_m$  are the equivalent cohesive strength and angle of friction of the rock mass, respectively.

On the other hand, careful study of crack initiation stress and uniaxial compressive stress prove that the crack initiation stress ratio is constant for different types of rock and is between 0.37-0.52 (Table 2.1). Cai et al. (2004) have also noted that crack initiation stress can be calculated from rock mass strength ( $\sigma_{cm}$ ) in various rock types. In the general form  $\sigma_1 - \sigma_3 = A \sigma_{cm}$  for crack initiation in which “A” is between 0.4-0.5 for massive to moderately jointed rock mass and 0.5-0.6 for highly jointed rock mass (Table 2.2).

**Table 2.1: The normalized value of crack initiation stress for different types of rocks**

Rock type	CI Stress (MPa)	Method	UCS (MPa)	CI/UCS	Ref.
Granite (coarse grain)	113 ( $\pm 17$ )	$\Delta V/V$ vs. $\sigma_{axial}$	225 ( $\pm 4.9$ )	0.5 $\pm$ 0.07	(Brace et al., 1966)
	90 (Min) – 130 (Max)	4 samples	218 (Min) - 238 (Max)	0.41-0.57	
Marble (medium grain)	20	$\Delta V/V$ vs. $\sigma_{axial}$	46	0.45	(Brace et al., 1966)
	-	1 sample	-	-	
Aplite (fine grain)	270	$\Delta V/V$ vs. $\sigma_{axial}$	600	0.45	(Brace et al., 1966)
	260 (Min) – 280 (Max)	2 samples	595 (Min) - 605 (Max)	0.43-0.47	
Norite	83.73	$\Delta V/V$ vs. $\sigma_{axial}$	307 $\pm$ 6	0.27	(Bieniawski, 1967a)
	-	6 samples	-	-	
Quartzite	113.76	$\Delta V/V$ vs. $\sigma_{axial}$	297 ( $\pm 3$ )	0.38	(Bieniawski, 1967a)
	-	12 samples	-	-	
Westerly Granite	250	$\Delta V/V$ vs. $\sigma_{axial}$	540	0.46	(Tapponnier and Brace, 1976)
	-	-	-	-	
Lac du Bonnet	Granodiorite	AE Impulse "energy" Rate vs. $\sigma_{axial}$	200	0.4	(Eberhardt et al., 1999b)
		-	5 samples	-	
	Granite	AE Impulse "energy" Rate vs. $\sigma_{axial}$	182	0.44	
		-	5 samples	-	
	Pegmatite	AE Impulse "energy" Rate vs. $\sigma_{axial}$	118	0.61	(Eberhardt et al., 1999b)
		-	-	-	

**Table 2.1: continued**

Rock type		CI Stress (MPa)	Method	UCS (MPa)	CI/UCS	Ref.		
Forsmark	Grano-diorite	115 (±21)	Crack Volumetric Strain	226 (±28)	0.51	(Glamheden et al., 2007)		
		60 (Min)- 187 (Max)	47 samples	157 (Min)- 289 (Max)	-			
	Pegma-tite	121 (±28)	Crack Volumetric Strain	228 (±21)	0.53			
		100 (Min)- 140 (Max)	10 samples	192 (Min)- 266 (Max)	-			
	Granite (Aplite)	169 (±29)	Crack Volumetric Strain	310 (±58)	0.55			
		125 (Min)- 200 (Max)	5 samples	229 (Min)- 371 (Max)	-			
	Bunt Sandstone		27	Onset of dilatancy	60		0.45	(Gowd and Rummel, 1980) <sup>1</sup>
			-	-	-		-	
Solenhofen Limestone		200	Onset of dilatancy	350	0.57	(Heard, 1960) <sup>2</sup>		
		-	-	-	-			

<sup>2</sup> - The data extracted from Ashby and Sammis (1989)

**Table 2.1: continued**

Rock type		CI Stress (MPa)	Method	UCS (MPa)	CI/UCS	Ref.
Aminadav Dolomite	Xenotopic	77.2 ( $\pm 35$ )	Crack Volumetric Strain	89.6 ( $\pm 41$ )	0.87	(Hatzor and Palchik, 1997)
		43 (Min)- 130 (Max)	5 samples	43 (Min)- 138 (Max)	0.73-1.00	
	Hypidiotopic	134 ( $\pm 57$ )	Crack Volumetric Strain	193 ( $\pm 56$ )	0.69	
		90 (Min)- 238 (Max)	6 samples	120 (Max) - 274 (Min)	0.48-0.98	
	Idiotopic	115.83 ( $\pm 55$ )	Crack Volumetric Strain	169 ( $\pm 83$ )	0.69	
		57 (Min)- 290 (Max)	6 samples	57 (Max)- 290 (Min)	0.57-0.82	
Åspo	Diorite	170 ( $\pm 29$ )	Lateral Strain Response	311 ( $\pm 58$ )	0.55	Author's note
		126 (Min)- 200 (Max)	8 samples	230 (Min)- 371 (Max)	0.35-0.56	
	Diorite	141 ( $\pm 18$ )	Lateral Strain Response	302 ( $\pm 26$ )	0.47	
		120 (Min)- 162 (Max)	5 samples	231 (Min)- 371 (Max)	0.42-0.61	

**Table 2.2: Crack initiation stress calculation based on  $\sigma_{cm}$  in different case studies (after Cai et al., 2004)**

Case Study	Lithology	Geological Description	CI
URL Mine-by	Granite	-	(0.44-0.47) $\sigma_{cm}$
SKB ZEDEX	Diorite	-	(0.55) $\sigma_{cm}$
SNO	Norite	Fine grained- Jointed	(0.4-0.5) $\sigma_{cm}$
Creighton	-	Jointed	(0.53) $\sigma_{cm}$
Löesberg Tunnel	Granite	Massive	(0.6) $\sigma_{cm}$

Interests in stress-induced cracking during an underground excavation, leads to the investigation of the stress concentration which is required to initiate and propagate cracks. Initiation of newly formed cracks can be used to assess the mechanical response of rocks such as rock burst risk assessment (Alcott et al., 1998), roof fall prediction (Butt et al., 2000), rock slope stability, rock damage evaluation and large-scale underground cavern stability monitoring (Young, 1993; Maejima et al., 2003).

In 1966, Fairhurst and Cook found out slabbing is most probable in the zone of maximum compression, caused by a tensile mechanism at the compressive stress regime. They showed that the slabbing stress is slightly above the strength of the rock defined by Griffith Theory. Hoek and Brown (1980) studied the magnitude of far-field stress which caused slabbing in square tunnels in South Africa. They reported the slabbing strength is 0.15 times the maximum far-field stress. Converting far-field to tangential stress, the stress magnitude required for slabbing will be 40% of uniaxial compressive strength (Martin et al., 1999).

Diederichs (2007) used micromechanical investigations of samples in association with field data to correlate the crack initiation and crack damage stress limit with potential spalling. He proposed the crack initiation stress and crack damage stress as the limitations for spalling in deep excavations. Martin and Christiansson

(2009) have also found that the ratio of rock mass spalling strength to uniaxial compressive strength was slightly above the onset of crack initiation measured in the lab. It has been also found from lab results that the crack initiation stress is a constant proportion of the peak stress in uniaxial loading regime. The same results have been reported by Andersson and Martin (2009) in which yield strength of the rock mass can be estimated from laboratory crack initiation stress in the absence of in situ stress.

## **2.5. Effect of material properties**

Considering crack initiation as a material property, geological properties of rocks have been studied to find the parameters which control the variation in crack initiation stress. Moreover, the geological characteristics of materials that affect uniaxial compressive strength can also be considered as effective parameters on crack initiation stress due to the constant crack initiation stress ratio.

### ***2.5.1. Grain size***

It was noted by Griffith (1921) that an increase in the size of flaws in a glass rod results in a decrease in the strength of the material. The same consequence on rock strength will be expected due to variation in grain size. The first investigation of the effect of grain size on the strength of rocks has been done by Skinner (1959) who has shown that the UCS in anhydrite decreases as the grain size is increased. Hugman and Friedman (1979) have also shown that the ultimate strength is inversely related to mean grain size in carbonate rocks even if the sample is tested in triaxial conditions with confining stresses up to 200 MPa. Similar results have also been reported by Olsson (1974) for dolomite and Prikryl (2001) for granites. Hatzor and Palchik (1997) have found higher crack initiation stress is expected in finer grained dolomite with low porosity. The initiation and propagation of fracture in crystalline rocks are related to the grain size, however in the case of different mineralogical composition the effect of heterogeneity is prominent which decreases the crack initiation stress.

### 2.5.2. *Texture*

In addition to grain size, grain shape, grain boundary geometry and grain orientation relative to the principal stress can change the material properties. Brace (1961) suggested that the strength of a rock with serrated grain boundaries is different from relatively straight borders, even if grain size, shape and composition remain constant. Dunn et al. (1973) and Digby (1981) have shown that rock stiffness in granular material depends on the number of contacts between the grains. In similar research with Meng and Pan (2007), higher strength and shorter failure duration have been monitored for sandstone with siliceous cement relative to that for argillaceous cement (Figure 2.11). They also mentioned that line-contact between grains increases the strength and decreases the failure duration compared to those with point-contact. Hugman and Friedman (1979) have shown that anhedral<sup>3</sup> crystalline dolomite is weaker and less brittle than euhedral<sup>4</sup> or microcrystalline limestone. This variation in brittleness of rocks is described by the stress concentration on the grain boundary edges. Tapponnier and Brace (1976) found that the crack initiation stress is started from the grain boundaries in Westerly granite. Similar results have been found by Eberhardt et al. (1999b) and Everitt and Lajtai (2004) that the cracks are initiated along the grain boundaries, first between neighbouring feldspar and quartz grains and then, within feldspar grains.

---

<sup>3</sup> Crystal with a rounded or indeterminate form

<sup>4</sup> Crystal completely bounded by its own rational face

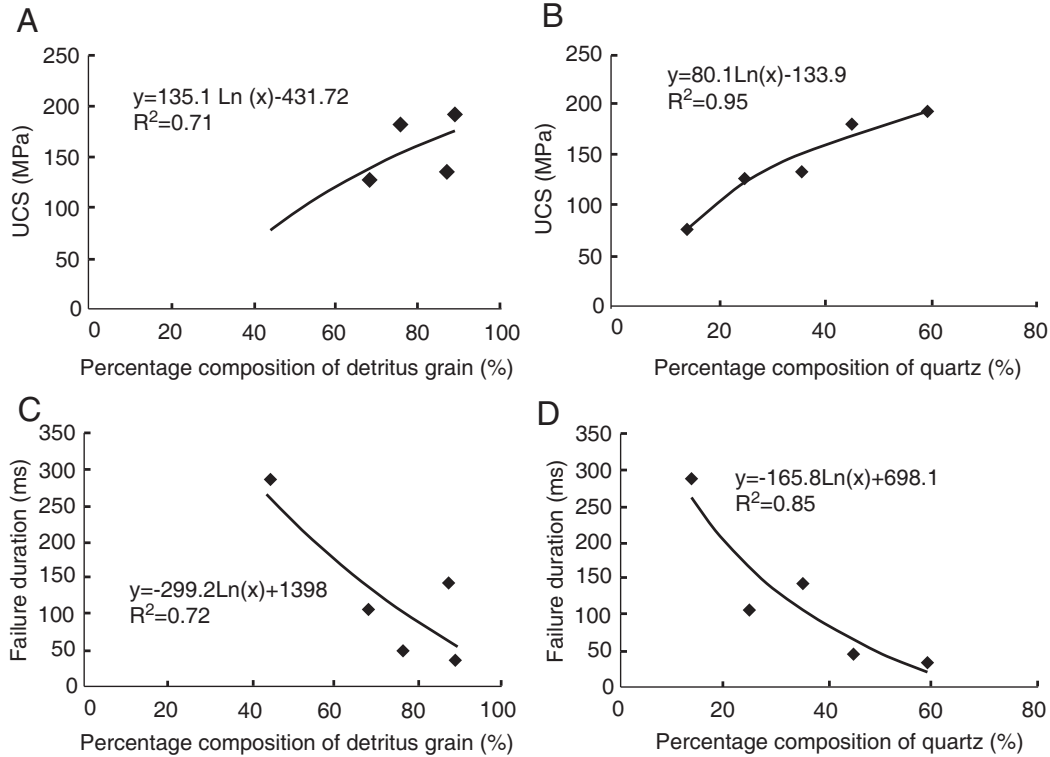


**Figure 2.11: Effect of selected parameters on uniaxial compressive strength of the rock and failure duration (after Meng and Pan, 2007)**

Mlakar et al. (1993) have recorded the presence of low amplitude AE events associated with intergranular cracking in early stages of loading, while high amplitude events associated with intragranular cracking and transgranular cracking in the later stages of the loading cycle.

Everitt and Lajtai (2004) have investigated the effect of fabric orientation on coarse-grained Lac du Bonnet granite (Figure 2.12). The weakest sample has been reported when the layering intersects the core axis in the angle of  $20^\circ$  to  $40^\circ$ . The rock is stronger when this orientation is  $0^\circ$  to  $15^\circ$ .

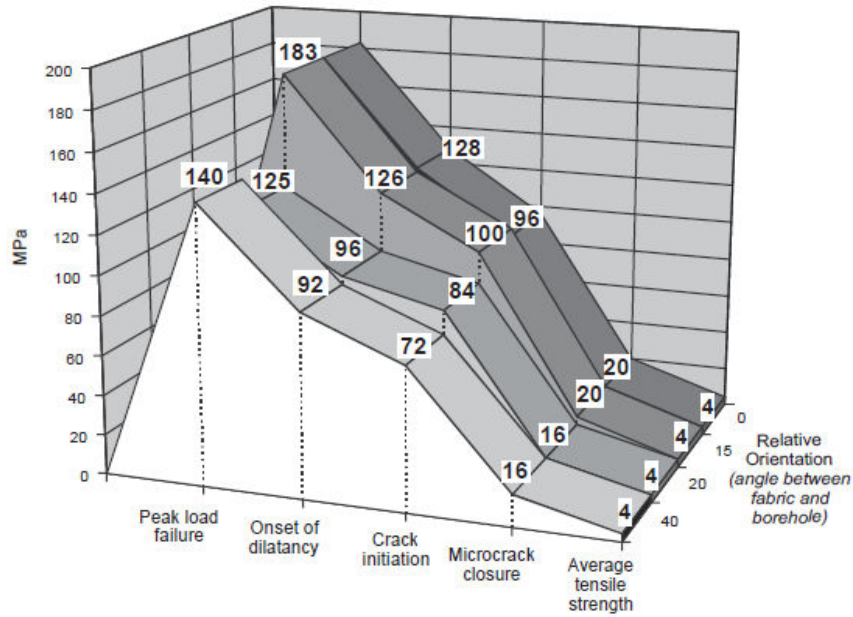


**Figure 2.12: Influence of fabric on rock strength for the coarse grained granite, the angles are relative to sample axis (after Everitt and Lajtai, 2004)**

Although it is concluded that the stress concentration along the grain boundary tips resulted in grain separation along the flaws, when the heterogeneity increased, the crack initiation process is facilitated. This process mostly resulted from differential elastic deformation of the grains.

### **2.5.3. Grain size distribution**

It was shown in the Section 2.3 that a tensile mechanism causes the crack initiation. In order to generate tensile stress, there must be a mismatch between the grain shapes (to generate point load) or elastic contrasts. Grain size, on the other hand, can also be regarded as another factor. The effect of grain size on the UCS is well understood, however in case of uniform grain size distribution, no porosity and same grain type the stress distribution is uniform. The uniform stress distribution results in a higher crack initiation stress compared to non-uniform specimens.

In order to show this effect the results from two series of tests on granite and aplite with almost the same mineralogy are presented in Table 2.3.

Although both rocks have the same mineralogy, the difference in the grain size distribution range (0.1-2 mm for granite and 0.1-0.6 mm for aplite) resulted in different brittle failure stress levels. This factor will be modeled numerically by defining different grain size distribution using the Discrete Element Method in Chapter 5 (see Figure 2.13 as an example).

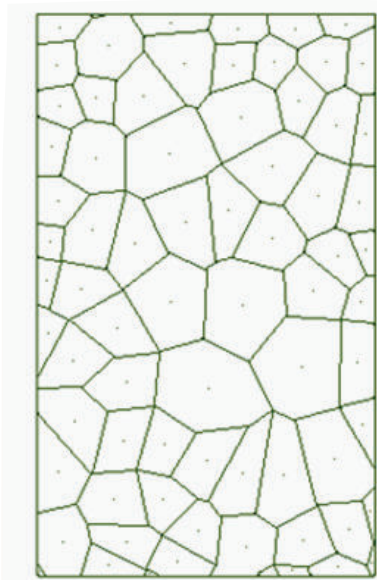
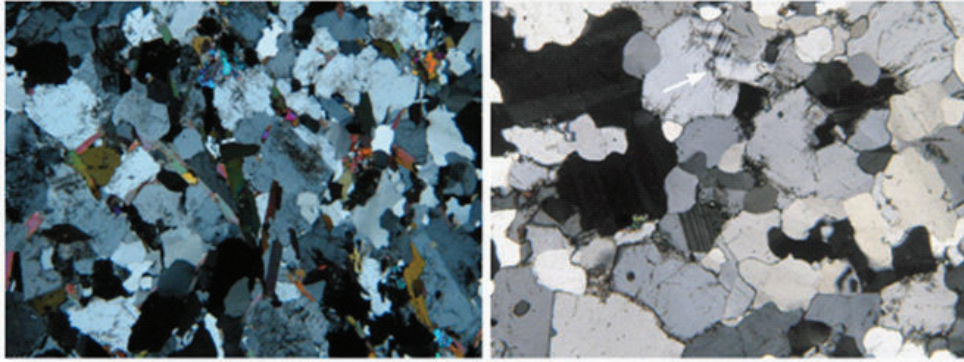
#### **2.5.4. Elastic constants**

The effect of grain type or mineral content on the initiation and propagation of the cracks can be expressed in terms of heterogeneity in the minerals' elastic constants. Stearns (1968) showed that dolomites are more intensely fractured than limestone when both are deformed under similar condition. Hugman and Friedman (1979) found that the dolomite content correlates well with strength of rocks only when the texture is kept constant.

Alteration in stress distribution by different elastic deformation of the grains has been explained by Dey and Wang (1981) who have proposed that mismatch in elastic moduli of two minerals causes additional boundary traction. Palchik and Hatzor (2002) have reported UCS as a function of porosity and elastic modulus in fairly homogeneous limestone whereas the role of individual grain size is not significant in the case of heterogeneity.

**Table 2.3: Petrographic analysis of Forsmark granite and aplite, from Swedish Nuclear Fuel and Waste management Co. (Glamheden et al., 2007)**

	Mineralogy (%)				grain size (mm)	CI (MPa)	No. Samples
	Quartz	K-feldspar	Plagioclase	Biotite			
Granite	34.6	22.8	37.6	4.4	0.1-2	116	47
Aplite	34.5	30.7	27.2	6.9	0.1-0.6	169	5



Voronoi Tessellation representing uniform grain size



Voronoi Tessellation representing heterogeneous grain size

**Figure 2.13: Photomicrograph of the granite (Top left, field view 5.6x4.2 mm) and Aplite (Top right, field view 2.9x2.2) from Forsmark site area; crossed polar (based on Glamheden et al., 2007). Voronoi model indicating different grain size distribution (Bottom)**

Dissimilarity in elastic constants of the minerals causes differential deformation of the neighbouring grains which results in the formation of tensile stresses across the grain boundaries.

### **2.5.5. Porosity**

It was previously mentioned that according to the Griffith theory, macroscopic fractures start at pre-existing flaws, so-called "Griffith Cracks". These flaws will

enlarge and spread under the influence of applied stress. The principal difficulty in applying the Griffith theory of rocks is identification of Griffith Cracks. Stress concentration along these defects will cause crack initiation and propagation in the material. These flaws can be presented in the form of small mineralogical defects such as cleavage, grain boundaries or porosity. Farquhar et al. (1994) have found an exponential relationship between uniaxial compressive strength and porosity. The same results had also been reported by Dunn et al. (1973), Hushino (1974) and Dearman et al. (1978). They have also shown that the crack damage stress approaches its maximum value when porosity decreases and elastic modulus increases simultaneously (Figure 2.14).

There are other factors which indirectly influence crack initiation such as moisture and temperature. For instance, Lajtai and Dzik (1996) have shown that at 100% humidity, the crack initiation points in feldspar and quartz are no longer distinguishable. In spite of the abovementioned research, the exact mechanism of crack initiation is not entirely understood. In the next section, several researches on the crack initiation and propagation mechanism had been outlined.

In this research, the different methods of crack initiation stress measurement have been reviewed and the new method, which is based only on stress-strain data, is established.

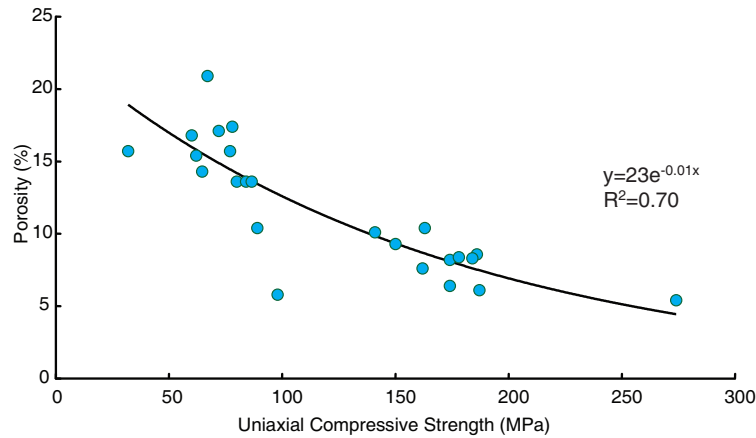


**Figure 2.14: Effect of porosity on uniaxial compressive strength in limestone (based on Palchik and Hatzor, 2002)**

The stress-strain response of different types of rocks will be collected and investigated for determination crack initiation stress. The effect of confinement on the crack initiation stress is also studied and defined using Hoek-Brown failure criteria.

Thereafter, numerical modelling will be used to model brittle failure under uniaxial loading. The results will be analyzed for different material properties such as grain size, grain size distribution and mineralogy. Finally, the initiation and propagation of the cracks are investigated under different material properties.

## 2.6. References

- Akesson, U., Hansson, J., and Stigh, J., 2004, Characterisation of microcracks in the Bohus granite, western Sweden, caused by uniaxial cyclic loading: *Engineering Geology*, v. 72, no. 1-2, p. 131-142.
- Alcott, J.M., Kaiser, P.K., and Simser, B.P., 1998, Use of microseismic source parameters for rockburst hazard assessment: *Pure and applied geophysics*, v. 153, no. 1, p. 41-65.
- Andersson, J.C., and Martin, C.D., 2009, The Äspö pillar stability experiment: Part I—Experiment design: *International Journal of Rock Mechanics and Mining Sciences*, v. 46, no. 5, p. 865-878.
- Bieniawski, Z.T., 1967a, Mechanism of brittle fracture of rock: Part II—experimental studies: *International Journal of Rock Mechanics and Mining Sciences & Geomechanics Abstracts*, v. 4, no. 4, p. 407-408, IN13-IN14, 409-418, IN15-IN18, 419-423.
- Bieniawski, Z.T., 1967b, Mechanism of brittle fracture of rock: Part I—theory of the fracture process: *International Journal of Rock Mechanics and Mining Sciences & Geomechanics Abstracts*, v. 4, no. 4, p. 395-404, IN11-IN12, 405-406.
- Bieniawski, Z.T., 1966, Mechanism of rock fracture in compression: *Meg.* 459.
- Brace, W.F., 1964, Brittle Fracture of Rock. in Judd, W.R., ed., *State of Stress in the Earth's Crust*: New York, Elsevier, p.111-181.
- Brace, W.F., 1961, Dependence of fracture strength of rocks on grain size: *Bull. Miner. Inds. Exp. Stn. Penn. St. Univ.*, v. 76, p. 99-103.
- Brace, W.F., Paulding, B., and Scholz, C., 1966, Dilatancy in the fracture of crystalline rocks: *Journal of Geophysical Research*, v. 71, p. 3939-3953.

- Broek, D., 1986, Elementary Engineering Fracture Mechanics, Martinus Nijhoff publishers, Boston, 496pp.
- Butt, S.D., Mukherjee, C., and Lebars, G., 2000, Evaluation of acoustic attenuation as an indicator of roof stability in advancing headings: International Journal of Rock Mechanics and Mining Sciences, v. 37, no. 7, p. 1123-1131.
- Cai, M., Kaiser, P.K., Tasaka, Y., Maejima, T., Morioka, H., and Minami, M., 2004, Generalized crack initiation and crack damage stress thresholds of brittle rock masses near underground excavations: International Journal of Rock Mechanics and Mining Sciences, v. 41, no. 5, p. 833-847.
- Cai, M., Morioka, H., Kaiser, P.K., Tasaka, Y., Kurose, H., Minami, M., and Maejima, T., 2007, Back-analysis of rock mass strength parameters using AE monitoring data: International Journal of Rock Mechanics and Mining Sciences, v. 44, no. 4, p. 538-549.
- Dearman, W.R., Baynes, E.J., and Irfan, T.Y., 1978, Engineering grading of weathered granite: Engineering Geology, v. 12, p. 345-374.
- Dey, T.N., and Wang, C., 1981, Some mechanisms of microcrack growth and interaction in compressive rock failure: International Journal of Rock Mechanics and Mining Sciences & Geomechanics Abstracts, v. 18, no. 3, p. 199-209.
- Diederichs, M.S., 2007, The 2003 Canadian Geotechnical Colloquium: Mechanistic interpretation and practical application of damage and spalling prediction criteria for deep tunneling: Canadian Geotechnical Journal, v. 44, p. 1082-1116.
- Digby, P.J., 1981, The effect of elastic moduli of porous granular rocks: Journal of applied mechanics, v. 48, no. 4, p. 803-809.

- Dunn, D.E., Lafountain, L.J., and Jackson, R.E., 1973, Porosity Dependence and Mechanism of Brittle Fracture in Sandstones, v. 78, no. 14, p. 2403-2417.
- Eberhardt, E., Stead, D., and Stimpson, B., 1999a, Quantifying progressive pre-peak brittle fracture damage in rock during uniaxial compression, v. 36, p. 361-380.
- Eberhardt, E., Stimpson, B., and Stead, D., 1999b, Effect of grain size on the initiation and propagation threshold of stress-induced brittle fracture: Rock Mechanics and Rock Engineering, v. 32, no. 2, p. 81-99.
- Eberhardt, E., Stead, D., Stimpson, B., and Read, R.S., 1998, Identifying crack initiation and propagation thresholds in brittle rock: Canadian Geotechnical Journal, v. 35, no. 2, p. 222-233.
- Everitt, R.A., and Lajtai, E.Z., 2004, The influence of rock fabric on excavation damage in the Lac du Bonnet granite: International Journal of Rock Mechanics and Mining Sciences, v. 41, no. 8, p. 1277-1303.
- Fairhurst, C., and Cook, N.G.W., 1966, The phenomenon of rock splitting parallel to direction of maximum compression in the neighborhood of a surface, in 1st congress of the international society of rock mechanics: Lisbon, p. 687-692.
- Farquhar, R.A., Somerville, J.M., Smart, B.G.D., and Heriot-Watt, U., 1994, Porosity as a Geomechanical Indicator: An Application of Core and Log Data and Rock Mechanics, in European Petroleum Conference, SPE, p. 481.
- Glamheden, R., Fredriksson, A., Roshoff, K., Karlsson, J., Hakami, H., and Christiansson, R., 2007, Rock Mechanics Forsmark, Site descriptive modelling, Forsmark stage 2.2: R-07-31, 277 p.
- Gowd, T.N., and Rummel, F., 1980, Effect of confining pressure on the fracture behaviour of a porous rock: International Journal of Rock Mechanics and Mining Sciences & Geomechanics Abstracts, v. 17, no. 4, p. 225-229.

- Griffith, A.A., 1921, The Phenomena of Rupture and Flow in Solids: Philosophical Transactions of the Royal Society of London. Series A, Containing Papers of a Mathematical or Physical Character, v. 221, p. 163-198.
- Griffith, A.A., 1924, Theory of rupture, in Proceedings of the First International Congress of Applied Mechanics: Delft, p. 55-63.
- Hallbauer, D.K., Wagner, H., and Cook, N.G.W., 1973, Some observations concerning the microscopic and mechanical behaviour of quartzite specimens in stiff, triaxial compression tests: International Journal of Rock Mechanics and Mining Sciences & Geomechanics Abstracts, v. 10, no. 6, p. 713-726.
- Hardy, H.R., 1981, Applications of acoustic emission techniques to rock and rock structures: a state of the art review. in Drnevich and Gray, ed., Acoustic Emission in Geotechnical Engineering Practice, ASTM STP750, ASTM, p.4-92.
- Hatzor, Y.H., and Palchik, V., 1997, The influence of grain size and porosity on crack initiation stress and critical flaw length in dolomites: International Journal of Rock Mechanics and Mining Sciences, v. 34, no. 5, p. 805-816.
- Heard, H.C., 1960, Transition from brittle fracture to ductile flow in Solenhofen limestone as a function of temperature, confining pressure, and interstitial fluid pressure. in Griggs, D. and Handin, J., eds., Rock Deformation, Geol. Soc. Am. Memoir 79, p.193-226.
- Hoek, E., and Brown, E.T., 1980, Empirical strength criterion for rock masses: Journal of the Geotechnical Engineering Division, v. 106, no. 9, p. 1013-1035.
- Hugman, R. H. H. III., and Friedman, M., 1979, Effects of Texture and Composition on Mechanical Behavior of Experimentally Deformed Carbonate Rocks, v. 63, no. 9, p. 1478-1489.

- Hushino, K., 1974, Effect of porosity on strength of clastic sedimentary rock, in the 3rd Congress of International Society of Rock Mechanics, vol.1, Balkema, Rotterdam, p. 511.
- Ingraffea, A.R., 1987, Theory of crack initiation and propagation in rocks. in Atkinson, B.K., ed., Fracture mechanics of rocks, Elsevier, p.71-110.
- Kaiser, P.K., Yazici, S., and Maloney, S., 2001, Mining-induced stress change and consequences of stress path on excavation stability — a case study: International Journal of Rock Mechanics and Mining Sciences, v. 38, no. 2, p. 167-180.
- Kranz, R.L., 1979, Crack growth and development during creep of Barre granite: International Journal of Rock Mechanics and Mining Sciences & Geomechanics Abstracts, v. 16, no. 1, p. 23-35.
- Lajtai, E.Z., 1974, Brittle fracture in compression: International Journal of Fracture, v. 10, no. 4, p. 525-536.
- Lajtai, E.Z., and Dzik, E.J., 1996, Searching for the damage threshold in intact rock, in the 2nd North American Rock Mechanics Symposium. NARMS 96, a regional conference of ISRM, ISRM.
- Lajtai, E.Z., and Lajtai, V.N., 1974, The evolution of brittle fracture in rocks: Geological Society of London, v. 130, p. 1-18.
- Lisowski, A., 1959, Failure types of rock cubic specimens in the light of the theory of elasticity: Bulletin of De l'Accademic Polonaise des Science, v. 7, p. 341-351.
- Lockner, D., 1993, The role of acoustic emission in the study of rock fracture: International Journal of Rock Mechanics and Mining Sciences & Geomechanics Abstracts, v. 30, no. 7, p. 883-899.

- Maejima, T., Morioka, H., Mori, T., and Aoki, K., 2003, Evaluation of loosened zones on excavation of a large underground rock cavern and application of observational construction techniques: *Tunnelling and Underground Space Technology*, v. 18, no. 2-3, p. 223-232.
- Martin, C.D., and Chandler, N.A., 1994, The progressive fracture of Lac du Bonnet granite: *International Journal of Rock Mechanics and Mining Sciences & Geomechanics Abstracts*, v. 31, no. 6, p. 643-659.
- Martin, C.D., and Christiansson, R., 2009, Estimating the potential for spalling around a deep nuclear waste repository in crystalline rock: *International Journal of Rock Mechanics and Mining Sciences*, v. 46, no. 2, p. 219-228.
- Martin, C.D., Kaiser, P.K., and McCreath, D.R., 1999, Hoek-Brown parameters for predicting the depth of brittle failure around tunnels: *Canadian Geotechnical Journal*, v. 36, no. 1, p. 136-151.
- Meng, Z., and Pan, J., 2007, Correlation between petrographic characteristics and failure duration in clastic rocks: *Engineering Geology*, v. 89, no. 3-4, p. 258-265.
- Mlakar, V., Hassani, F.P., and Momayez, M., 1993, Crack development and acoustic emission in potash rock: *International Journal of Rock Mechanics and Mining Sciences & Geomechanics Abstracts*, v. 30, no. 3, p. 305-319.
- Olsson, W.A., 1974, Grain Size Dependence of Yield Stress in Marble: *J. Geophys. Res.*, v. 79, no. 32, p. 4859-4862.
- Palchik, V., and Hatzor, Y.H., 2002, Crack damage stress as a composite function of porosity and elastic matrix stiffness in dolomites and limestones: *Engineering Geology*, v. 63, no. 3-4, p. 233-245.
- Peng, S., and Johnson, A.M., 1972, Crack growth and faulting in cylindrical specimens of chelmsford granite: *International Journal of Rock Mechanics*

- and Mining Sciences & Geomechanics Abstracts, v. 9, no. 1, p. 37-42, IN5-IN6, 43-60, IN7-IN14, 61-74, IN15-IN18, 75-86.
- Prikryl, R., 2001, Some microstructural aspects of strength variation in rocks: International Journal of Rock Mechanics and Mining Sciences, v. 38, no. 5, p. 671-682.
- Skinner, W.J., 1959, Experiments on the compressive strength of anhydrite: Engineer, v. 207, p. 255-259.
- Stacey, T.R., 1981, A simple extension strain criterion for fracture of brittle rock: International Journal of Rock Mechanics and Mining Sciences & Geomechanics Abstracts, v. 18, no. 6, p. 469-474.
- Stearns, D.W., 1968, Certain aspects of fracture in naturally deformed rocks, in N.S.F. Advanced Science Seminar in Rock Mechanics, Air Force Cambridge Research Lab. Spec. Rept., p. 97.
- Tapponnier, P., and Brace, W.F., 1976, Development of stress-induced microcracks in Westerly Granite: International Journal of Rock Mechanics and Mining Sciences & Geomechanics Abstracts, v. 13, no. 4, p. 103-112.
- Tromans, D., and Meech, J.A., 2002, Fracture toughness and surface energies of minerals: theoretical estimates for oxides, sulphides, silicates and halides: Minerals Engineering, v. 15, no. 12, p. 1027-1041.
- Walsh, J.B., 1965, The effect of cracks on the compressibility of rocks: Journal of Geophysical Research, v. 70, no. 2, p. 381-389.
- Wawersik, W.R., and Brace, W.F., 1971, Post failure behaviour of granite and diabase: Rock Mechanics and Rock Engineering, v. 3, no. 2, p. 61-85.
- Young, R.P., 1993, Seismic methods applied to rock mechanics: ISRM news journal, v. 1, no. 3, p. 4-18.

# **Chapter 3. Evaluation of methods for determining crack initiation in compression tests on low porosity rocks<sup>5</sup>**

## **3.1. Introduction**

Griffith (1921) used a constant tensile stress loading system to support his energy theory for rupture of brittle solids. In these experiments, as in any direct tension test for brittle solids the tensile stress required to initiate a crack is essentially the same as the ultimate tensile strength. Hence in tension, crack initiation is synonymous with rupture (Bieniawski, 1967b). Griffith (1924) using a two-dimensional approach, applied his energy concepts to the rupture of rock in compression, and suggested that the rupture of rock in unconfined compression was 8 times its tensile strength. In 1963, Murrell extended Griffith's theory to triaxial stress conditions, which gave a ratio of uniaxial compressive strength to tensile strength of 12. Laboratory tests have shown that the uniaxial compressive strength is approximately 15 to 20 times the tensile strength for most rocks and therefore the Griffith based criteria is seldom used to predict the rupture strength of rocks in compression. Nonetheless researchers have clearly identified that crack initiation is a characteristic of common low porosity crystalline rocks that is routinely observed in laboratory testing (Brace et al., 1966; Stacey, 1981; Martin and Chandler, 1994).

---

<sup>5</sup> A version of this chapter has been published as a paper by journal of Rock Mechanics and Rock Engineering:

Nicksiar, M., and Martin, C. D. (2012). "Evaluation of Methods for Determining Crack Initiation in Compression Tests on Low-Porosity Rocks." *Rock Mechanics and Rock Engineering*, 45(4), 607-617.

In 1963, Cook studied the initiation of cracks around Witwatersrand gold mines using seismic events. He found that the events were associated with the formation of cracks associated with the mining front where the compressive stress concentrations were the greatest. Fairhurst and Cook (1966) evaluated the formation of thin slabbing, observed around deep South African tunnels commonly referred to as spalling. They concluded that the formation of the slabs could be explained using the extension of Griffith cracks in a compressive stress field growing parallel to the maximum compressive stress. This slabbing process was also examined by Stacey (1981) using an extensional strain criterion developed from laboratory compression tests.

The performance of square tunnels in South Africa was evaluated by Hoek and Brown (1980) who found that when the far-field maximum stress magnitude exceeded 0.15 of the uniaxial compressive strength, spalling was observed around the underground opening. Martin et al. (1999) converted the Hoek and Brown criterion to a maximum tangential stress criterion and found that when the maximum tangential stress exceeded approximately 0.4 of the uniaxial compressive strength, slabbing was observed. This criterion was applied by Rojat et al. (2009) to the Löttschberg tunnel, Switzerland to analyze the stress-induced problems associated with tunnel boring machine excavated tunnel at the depth of over 1000 m. They concluded that in all cases the in-situ spalling strength was significantly lower than the laboratory uniaxial compressive strength and hence using the peak laboratory strength is problematic for evaluating the spalling strength for tunnel design. More recently Martin and Christiansson (2009) and Andersson and Martin (2009) have suggested that crack initiation from laboratory uniaxial compressive tests could be used as an estimate for the in-situ spalling strength. Hence having a reliable method for determining crack initiation in laboratory tests might benefit the engineering community when estimating the spalling strength.

The ISRM makes no mention of crack initiation in its “Suggested Methods for Determining the Uniaxial Compressive Strength and Deformability of Rock

Materials” (Bieniawski and Bernede, 1979). Nonetheless various authors have proposed different methods for identifying crack initiation, (e.g. Martin and Chandler, 1994; Brace et al., 1966; Bieniawski, 1967b; Lajtai, 1974; Stacey, 1981; Eberhardt et al., 1998; Diederichs et al., 2004). The purpose of this paper is to review and evaluate the various methods that have been proposed to identify crack initiation, using 10 laboratory tests of Äspö granodiorite. The results are compared to those obtained from a simplified methodology.

### 3.2. Stress-strain in laboratory compression tests

The ISRM Suggested Methods (Brown, 1981) for “Determining Uniaxial Compressive Strength and Deformability of Rock Materials” suggests measuring and plotting the axial stress versus axial ( $\varepsilon_{ax}$ ) and lateral ( $\varepsilon_{lat}$ ) strains response as illustrated in Figure 3.1. Also plotted in Figure 3.1 is the calculated volumetric strain ( $\Delta V/V$ ) given by:

$$\frac{\Delta V}{V} \approx \varepsilon_{ax} + 2\varepsilon_{lat} \quad (3.1)$$

Since the early work of Brace et al. (1966) and Bieniawski (1967b) it is now recognized that the stress-strain response in both unconfined and confined tests for low porosity rocks displays four important inflections: (1) crack closure, observed in the axial strain as the starting point of linearity; (2) crack initiation, observed in the lateral strain as the inflection point in lateral strain; (3) start of unstable crack growth, observed in the volumetric strain as the maximum volumetric strain; and (4) peak, observed in the axial strain as the point of maximum stress (see Figure 3.1).

Crack closure may or may not be present in the stress-strain response as it simply depends on the volume of cracks that exist in the samples being tested. At stress magnitudes above crack initiation it has been shown by many researchers that stress-strain response is dominated by the initiation and growth of cracks (Brace et al., 1966; Bieniawski, 1967b; Lajtai, 1974; Hallbauer et al., 1973).

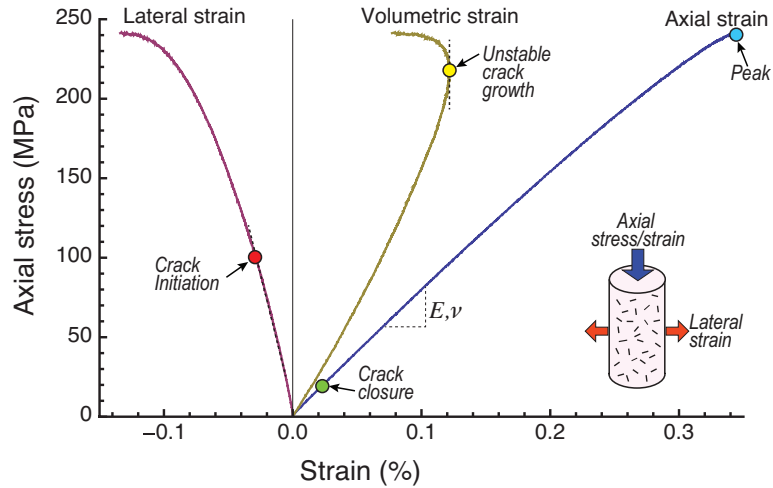


**Figure 3.1: Typical stress strain response recorded in a uniaxial compressive test.**

Acoustic emission (AE) monitoring techniques used by Lockner (1993) to locate the sources of the cracking within confined cylinders of granite showed that initially the cracks were distributed uniformly throughout the specimen. However, as the peak stress was approached the cracks coalesced on the boundary of the sample, eventually propagating across the sample as a discrete zone of AE activity as the load was maintained. Moore and Lockner (1995) investigated the crack density in the vicinity of this AE zone and concluded that the crack density in this zone was an order of magnitude greater than that found in undeformed samples. Thompson et al. (2006) performed three triaxial compression experiments of Westerly granite where the load was applied in such a way as to maintain a constant AE-rate. The results indicate that these findings were valid for both slow and fast loading rate. They also clearly showed that the change from stable crack initiation and growth to unstable crack coalescence occurs abruptly near peak strength that in its final stage may lead to formation of a fault (Figure 3.2).

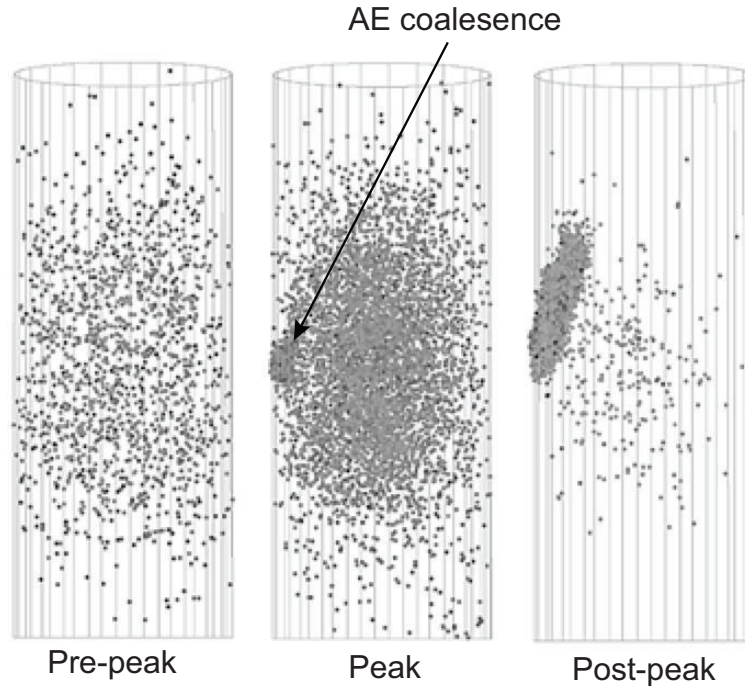


**Figure 3.2: Incremental distribution of acoustic emission activity measured by Thompson et al. (2006) during the confined testing of Westerly granite**

These findings help explain the change in the volumetric strain response from contraction to dilation observed in the stress-strain response, at the onset of unstable crack growth (see Figure 3.1). The researches over the past 40 years have clearly shown that behaviour of low porosity rocks in compression is linked to the initiation and growth of cracks. In the next section we review the methods that are used to establish the stress magnitude associated with crack initiation.

### **3.3. Methods for determining crack initiation in compression**

The methods that researchers have used to establish the load associated with the onset of crack initiation during laboratory compression loading have relied primarily on the measured strains. The methods utilized either the volumetric strain or the lateral strain, and have been modified by various researchers and at times augmented by acoustic emission techniques. These methods are reviewed below, and a new method that utilizes the lateral strain is introduced. It is assumed that the methods used to measure the lateral strain are accurate and reliable.

### 3.3.1. Volumetric strain methods

One of the earliest studies that utilized volumetric strain to establish the onset of dilatancy in compression was carried out by Brace et al. (1966). They examined the stress-strain response of granite, marble and aplite measured with strain gauges. They noted that the onset of dilatancy could be established using volumetric strain by examining when the volumetric strain deviated from the early linear portion. Figure 3.3 illustrated the approach used by Brace et al. (1966). Brace et al. (1966) found that the onset of dilatancy when normalized to its peak values varied from an average of 0.45 for granite, 0.5 for marble and 0.55 for aplite. Bieniawski (1967a) conducted similar experiments on norite and quartzite. Using microscopic images and the volumetric strain method he concluded that fracture/crack initiation in uniaxial compression is not affected by specimen shape, loading platens or loading machine and that the mechanism of fracture in compression is essentially the same in uniaxial and triaxial compression.

Martin and Chandler (1994) noted that crack initiation is difficult to identify from the axial-stress volumetric-strain curve, particularly if the specimen already contains a high density of cracks. They proposed that crack initiation could be determined using a plot of crack volumetric strain versus axial strain. Crack volumetric strain  $(\Delta V/V)_{cr}$  is calculated by subtracting the elastic volumetric strain  $(\Delta V/V)_{el}$  from the calculated volumetric strains  $(\Delta V/V)$ .

$$\left(\frac{\Delta V}{V}\right)_{cr} = \frac{\Delta V}{V} - \left(\frac{\Delta V}{V}\right)_{el} \quad (3.2)$$

where:

$$\left(\frac{\Delta V}{V}\right)_{el} = \frac{2\nu - 1}{E}(\sigma_1 + 2\sigma_3) \quad (3.3)$$

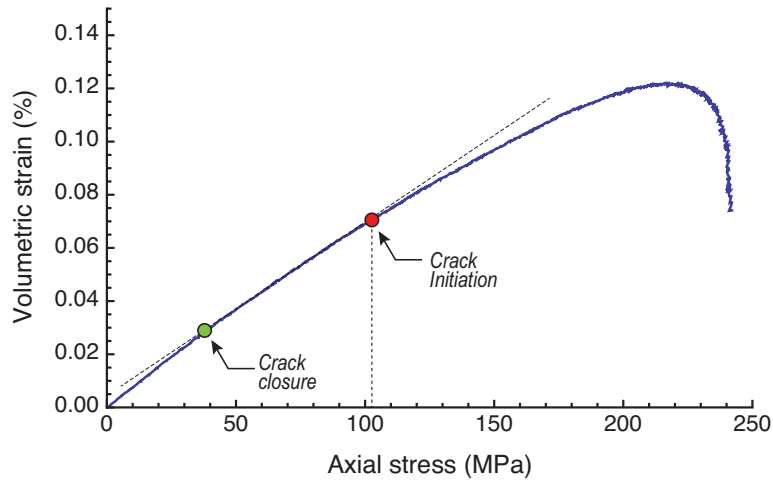


**Figure 3.3: Volumetric strain method proposed by Brace et al. (1966) to establish crack initiation**

The elastic volumetric strains are calculated using the elastic constants ( $E, \nu$ ) from the linear portion of the stress-strain curves in Figure 3.1. As shown in Figure 3.4 the method is less subjective than the previous method and can be readily programmed. One of the critiques of the method is that the Crack Initiation stress is influenced by the elastic constants, and therefore extra care must be exercised when determining those constants (Eberhardt et al., 1998). The method is also more difficult to use when there are a significant volume of cracks prior to testing. These cracks influence the determination of Poisson's ratio and according to Eberhardt et al. (1998) this uncertainty can significantly affect the crack initiation values.

### **3.3.2. Lateral strain methods**

It is well known that the lateral strain is more sensitive than the axial strain to the growth of cracks in the region of the stress-strain response before the onset of unstable crack growth. Consequently several researchers examined methods to establish the crack-initiation stress based on the lateral strains. Lajtai (1974) suggested that the axial strains remained linear from crack closure through to the onset of unstable crack growth in Figure 3.1. Hence Lajtai (1974) applied the

methodology used by Brace et al. (1966) for the Volumetric Strain method to the lateral strain.

Lajtai (1974) proposed that the crack-initiation stress could be established by defining the onset where the lateral strains deviated from linearity (Figure 3.5). This approach is also subjective if the stress strain response deviates from the typical stress-strain response due to intense pre-existing cracks.

Because the lateral strain more clearly defines the onset of cracking, changes in the ratio of the lateral strain to axial stress can also indicate the onset of cracking. This approach that is also introduced by Eberhardt et al. (1998) as lateral stiffness method, can be easily programmed and can take advantage of the large number of data points that are collected during a compression test. Given that a test may contain 1000 data points the ratio of the lateral strain to axial stress can be determined over various increments to assess the sensitivity of the crack initiation to the chosen increment. Figure 3.6 shows the ratio for a data increment of 25. The data in Figure 3.6 have also been smoothed using a moving median technique.

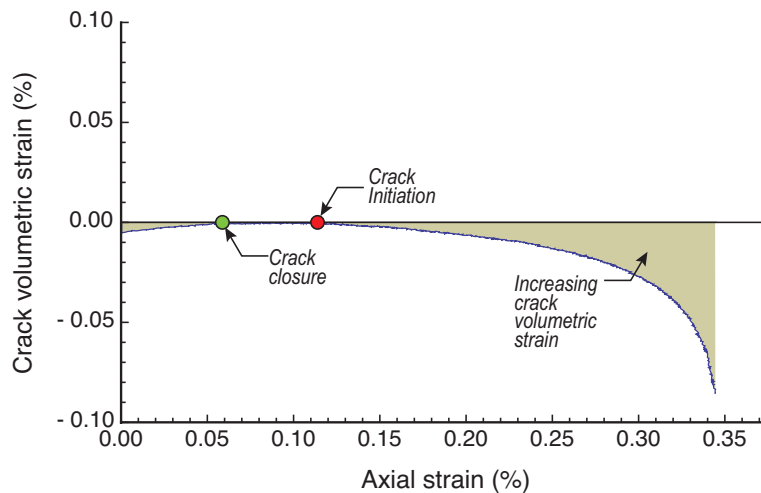


**Figure 3.4: Crack Volumetric strain method proposed by Martin and Chandler (1994) to establish crack initiation**

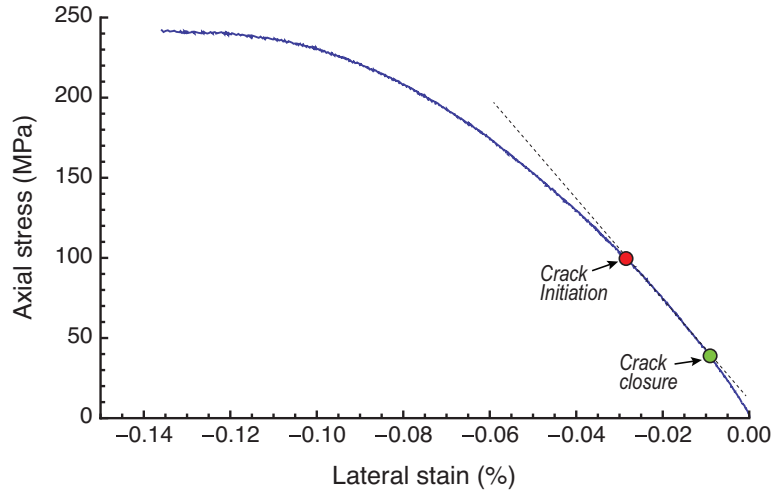


**Figure 3.5: Lateral strain method proposed by Lajtai (1974) to establish crack initiation**

Stacey (1981) observed that stress-induced failure observed around South African gold mines could be estimated using an extensional strain criterion. Stacey (1981) suggested that the extensional strain criterion in laboratory tests could be determined using plots of lateral strain versus axial strain (Figure 3.7).

In essence Stacey was also indirectly defining the crack-initiation stress, although the crack-initiation stress was not used by Stacey to assess tunnel stability.

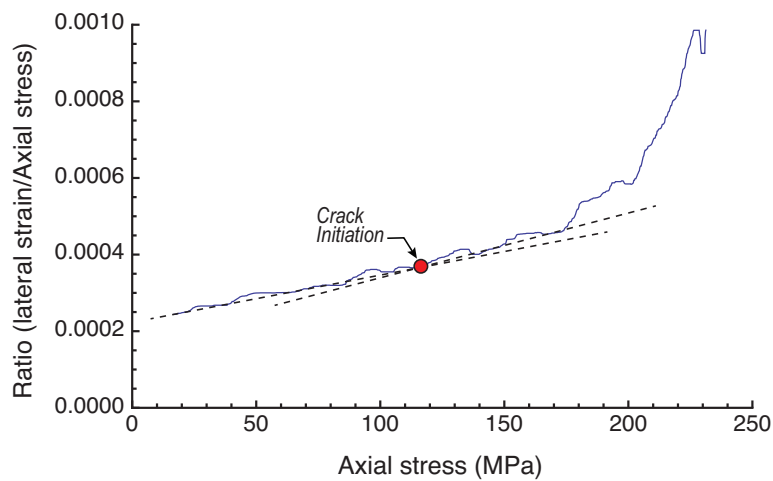


**Figure 3.6: Ratio of the lateral strain to axial stress using a data increment of 25 to establish crack initiation. Tangent line represented as dashed lines.**

Inspection of Figure 3.7 shows that the lateral strain versus axial strain is nonlinear for essentially its entire length. Andersson et al. (2009) also noted that applying Stacey's extensional strain approach was problematic because of the nonlinearity. This issue may simply be related to the impact of modern day data acquisition. It is now common to acquire many 100s data points during the loading of a test sample while inspection of Stacey's original figure shows that the interpretation was made with only 10s of data points. Moreover, marking the linear behaviour on lateral strain curve may not be easily possible especially in presence of pre-existing cracks. Hence, as illustrated in Figure 3.7 this increase in data frequency makes inflection points more difficult to detect.

Diederichs (2007) examined crack initiation using a discrete element program and proposed that the change in Poisson's ratio should be a suitable indicator for establishing the stress magnitudes associated with crack initiation. Diederichs suggested that plotting the Poisson's ratio versus the log of the axial stress should be suitable for establishing the stress magnitude associated Crack Initiation (Figure 3.8).

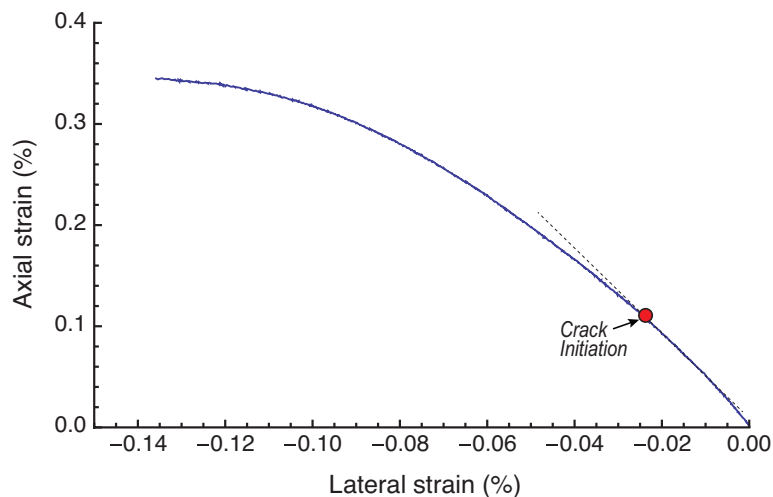


**Figure 3.7: Extensional strain method proposed by Stacey (1981) to establish crack initiation**

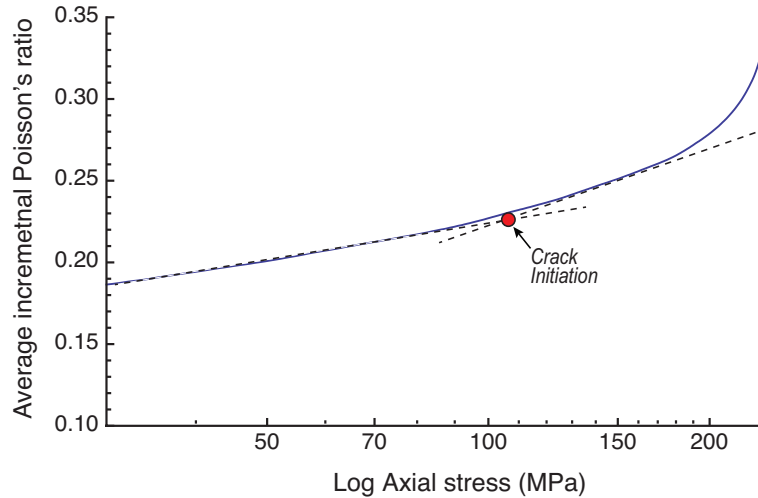


**Figure 3.8: Poisson's ratio method proposed by Diederichs (2007) used to establish crack initiation. Tangent line represented as dashed lines.**

### 3.3.3. Acoustic emission method

Eberhardt et al. (1998) have used several techniques to detect crack initiation for Lac du Bonnet granite such as stress-strain data, moving point regression technique and acoustic emission (AE). Acoustic Emission (AE) is a low-energy seismic event which is generated by inelastic deformation such as grain dislocation or crack initiation (Hardy, 1981).

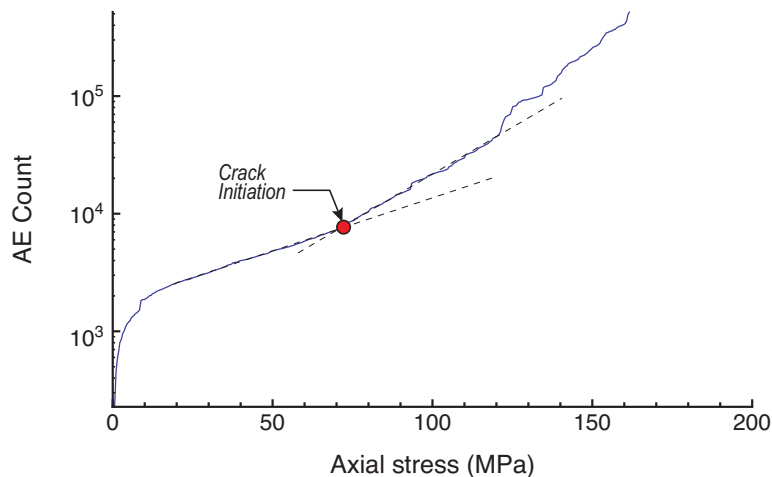


**Figure 3.9: Acoustic Emission count method proposed by Eberhardt et al. (1998) to establish crack initiation. Tangent line represented as dashed lines.**

These techniques can be used together in order to find a more reliable result (Figure 3.9). But the insignificant AE activity in crack initiation stages has made it difficult to differentiate between the background noise and the cracking-source acoustic events.

#### ***3.3.4. Proposed Lateral Strain Response (LSR) method***

Since the crack initiation is detectable on the lateral strain curve, the new methodology utilizing the lateral strain response should be used to establish the stress magnitude associated with crack initiation. As discussed previously, beyond the onset of unstable crack growth the lateral strain increases significantly, (see Figure 3.1).

Therefore, the lateral strain response from zero stress to the onset of unstable crack growth is examined for changes as the axial stress is applied. To detect changes in the lateral strain response (LSR), the loading response is compared to a linear reference line response taken from the onset of unstable crack growth to zero stress (Figure 3.10a). The LSR method simply evaluates the difference between the measured loading response and the linear reference line. This difference is plotted as a function of axial stress and the maximum difference is taken as the onset of crack initiation (Figure 3.10b). The methodology can be summarized as follows:

- 1- Determine onset of unstable crack growth where total volumetric strain reversal occurs (see Figure 3.1)
- 2- Determine the linear lateral strain-reference line
- 3- Find the change in lateral strain ( $\Delta LSR$ ) between the loading and linear reference line
- 4- Plot the axial stress versus change in lateral strain ( $\Delta LSR$ )
- 5- Determine the maximum change in lateral strain difference and the associated axial stress.

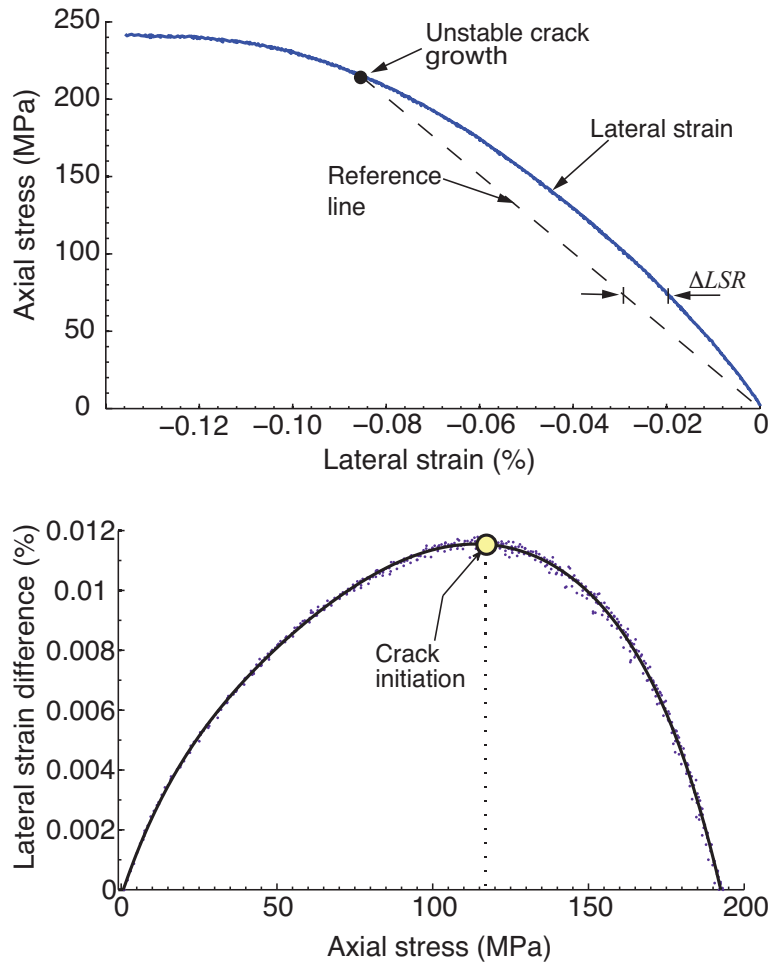


**Figure 3.10: Example of the methodology used to establish the crack-initiation stress using the lateral strain response (LSR). Unstable crack growth is defined in Figure 3.1. (Top) Illustration of the LSR Methodology (Bottom) Example of the LSR result**

This methodology is amenable to programming in Mathematica or Matlab and has been used by the authors to examine the stress-strain response in a variety of rock types. A polynomial equation can be used to establish a best fit to the data which facilitates finding the maximum LSR value and the associated crack-initiation stress. An attractive feature of the proposed method is that it does not require the subjective interpretation of crack initiation stress by the user.

### **3.4. Crack-initiation stress for Äspö Diorite**

The various methods described previously and capable of determining the crack-initiation stress were applied to laboratory test results obtained using modern testing equipment illustrated in Figure 3.11. The purpose was to establish if the various strain-based methods provided similar results.

The Swedish Nuclear Fuel and Waste management Co. owns and operates the Äspö Hard Rock Laboratory (HRL) located near Oskarshamn in Southern Sweden. Äspö HRL has been in operation since 1995 and has excavated tunnel access to a depth of 450 m. The rock type encountered at the Äspö HRL is called Äspö Diorite. Äspö Diorite is grey to reddish grey, medium grained, low ( $\approx 0.4\%$ ) porosity igneous rock. The Äspö Diorite has a density of  $2740 \text{ kg/m}^3$  and consists of  $19\%(\pm 4.5)$  quartz,  $8\%(\pm 4)$  K-feldspar and  $73\%(\pm 6)$  Plagioclase (Janson et al., 2007). The potassium feldspars (K-feldspar) are sparsely distributed as large crystals, often reaching 10 mm. Figure 3.12 shows a typical example of Äspö Diorite that was used for laboratory testing.

A total of 10 specimens were tested in uniaxial compression tests by SP Technical Research Institute of Sweden. The specimens were prepared according to ASTM 4543-01 and stored from 21 to 24 days in water prior to carrying out the uniaxial compression testing in a servo-controlled testing machine (Glamheden et al., 2010). The axial load was determined by a load cell with maximum capacity of 1.5 MN. The axial and lateral deformation measurements of the specimens were conducted with miniature LVDTs with relative error of 0.6% in 1 mm for axial deformation and 1.3% in 3 mm for the radial deformation measurement. The loading rate was set to a circumferential strain rate of  $-0.025\%/min$  and increased after reaching the post-failure region (Glamheden et al. 2010). While the complete stress-strain response into the post peak region was obtained, only the stress-strain results up to the peak strength are discussed here.

Table 3.1 lists the Young's Modulus ( $E$ ), Poisson's Ratio ( $\nu$ ) and the Uniaxial Compressive Strength (UCS) for each specimen and the stress-strain curves of each test have been presented in Appendix 1. The mean, standard deviation (StDev) and coefficient of variation (CoV) expressed as percentage of each parameter is also provided. The UCS for the ten samples ranged from 171 to 242 MPa, with a mean value of 227 MPa, a standard deviation of 31.3 MPa and a coefficient of variation of 13.8 %.

The crack initiation (CI) stress values were determined for each of the ten specimens using the six methods described previously. Again the mean, StDev and CoV were determined and these results are also summarized in Table 3.1. While the mean CI values from the six methods only ranged from 105 to 111 MPa, the CoV ranged from 16.5 to 22.4 %. Inspection of the results in Table 3.1 shows that regardless of the method used to determine the crack-initiation stress, the results appear surprisingly consistent. A statistical methodology referred to as the Analysis of Variance (ANOVA), was carried out in order to evaluate if the mean values from the 6 CI methods statistically differ. ANOVA is a statistical method to test the variation in an experimental outcome when there are more than two groups. In our case we are testing if the results from the 6 methods (groups) are all alike or not. One approach is to compare the means obtained from each method, using the F-ratio in ANOVA, which is the ratio of the variation between the methods to the variation within the method. In the ANOVA F-test, when the calculated F-ratio is less than the critical F-ratio, there is no statistical difference in the results. A detailed discussion of the ANOVA methodology is beyond the scope of this paper and interested readers are referred to Walpole (2002). For our dataset (6 methods with 10 samples) F-critical is 2.39, while the F-ratio is 0.26. The ANOVA results indicate that none of the 6 methods have a significant statistical advantage over the other. Hence choosing a particular method to establish the crack-initiation stress is one of convenience.

**Table 3.1: Comparison of results from different strain-based methods available for determining the crack-initiation stress of Äspö Diorite.**

Sample ID	E (GPa)	$\nu$	UCS (MPa)	Crack Initiation Stress (MPa)									
				Brace <sup>a</sup> (1966)	Lajtai (1974)	Stacey (1981)	Martin <sup>b</sup> (1993)	Diederichs (2007)	LSR (MPa)	Mean (MPa)	StDev (MPa)	CoV (%)	CI / UCS
46G02-02	79	0.18	171	74	74	74	71	70	78	74	2.4	3.3	0.46
46G02-03	80	0.25	238	118	122	118	115	111	118	117	3.1	2.7	0.50
46G02-04	77	0.25	242	122	115	116	117	100	119	115	6.5	5.7	0.49
46G05-01	74	0.28	203	115	119	117	97	110	101	107	9.1	8.5	0.50
48G02-01	77	0.29	224	108	112	114	96	98	116	108	7.2	6.7	0.52
48G02-02	75	0.31	224	107	113	105	117	115	115	112	4.2	3.7	0.51
51G01-01	72	0.27	218	109	117	117	102	103	108	109	5.5	5.1	0.50
54G01-02	73	0.29	294	157	118	118	150	146	164	142	19.7	13.9	0.56
54G02-01	78	0.26	237	118	132	114	116	113	113	117	6.2	5.3	0.48
54G06-01	72	0.24	218	76	73	74	71	88	76	76	5.1	6.7	0.35
Mean	76	0.26	227	110	110	107	105	105	111				0.49
StDev	2.9	0.04	31.3	23.5	19.8	17.6	23.6	19.7	24.5				0.05
CoV (%)	3.8	13.8	13.8	21.3	18.1	16.5	22.4	18.7	22.1				11.3

<sup>a</sup>Brace et al (1966)

<sup>b</sup>Martin and Chandler (1994)

### 3.5. Discussion

One of the notable findings from the evaluation discussed in the previous section is that regardless of the method, the crack-initiation stress is consistently lower than the peak uniaxial compressive strength.

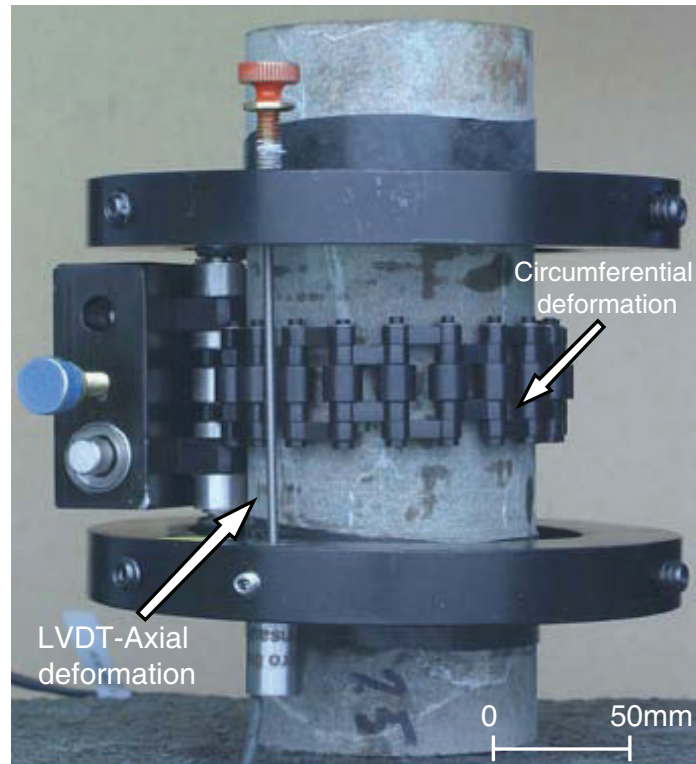


**Figure 3.11: Example of the measurement system; LVDTs and chain used to measure the axial and circumferential deformation, respectively. Photo provided by SKB.**

Figure 3.13 shows the uniaxial compressive strength versus the crack-initiation stress determined using the Lateral Strain Response Method. Also shown in Figure 3.13 is the linear least squares fit to the 10 data points which suggest that the crack-initiation stress for Äspö diorite occurs at approximately 0.49 of the uniaxial compressive strength.

Andersson et al. (2009) conducted an in-situ experiment (APSE) to investigate the onset of spalling (cracking) in a fractured Äspö diorite rock mass. They used mechanical and thermal loading to gradually increase the boundary stresses around 1.8-m-diameter mechanically excavated holes until spalling occurred. Spalling was recorded using displacement and acoustic emission monitoring.



**Figure 3.12: Sample of Äspö Diorite used to compare the crack-initiation stress using various methods. The specimen is mostly composed of Plagioclase, Oligoclase (in orange) and Anorthite (dark brown). Quartz grains are rarely observable as light coloured mineral while K-feldspars are not obvious in the specimen.**

Andersson et al. (2009) concluded that spalling initiated when the stress magnitudes ranged between 114 to 133 MPa with a mean value of 124.6 MPa. The ten samples of Äspö diorite used in the previous section were taken from a borehole drilled parallel and in close proximity to APSE experiment. When compared to the laboratory mean uniaxial compressive strength (227 MPa), the in-situ spalling strength can be expressed as 0.55 of the uniaxial compressive strength. This value and the range are also shown in Figure 3.13. As concluded by Andersson et al. (2009) and shown in Figure 3.13 it would appear that the crack initiation stress determined from unconfined laboratory compression tests provides an estimate for the in-situ spalling strength.

Read (2004) compiled the experience obtained while excavating various shaped tunnels in Lac du Bonnet granite at AECL's underground Research Laboratory.

Read concluded that regardless of the tunnel shape or tunnel direction, the compressive stress at the in-situ initiation of spalling on the tunnel wall was about 50 to 60% of the uniaxial compression strength. Martin et al. (1999) examined spalling in tunnels in rock types with uniaxial compressive strength that ranged from 36 to 350 MPa. They concluded that the initiation of spalling occurred when the maximum tangential boundary stress exceeded approximately  $0.40 \pm 0.1$  of the uniaxial compressive strength. Hence the experience from carefully controlled in-situ experiments and observations made while tunnelling all suggest that the spalling strength cannot be estimated from the peak uniaxial compressive strength. While more in-situ experiments are needed in different rock types there is sufficient evidence to warrant using the crack-initiation stress in laboratory uniaxial compression as an estimate for the in-situ spalling strength.

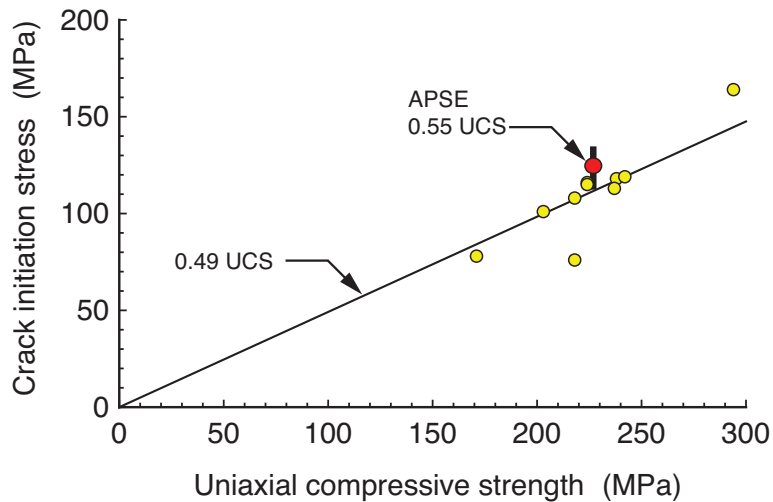


**Figure 3.13: Relation between the uniaxial compressive strength (UCS) and the crack-initiation stress for Äspö diorite measured by LSR method. Also shown is the stress associated with onset of in-situ cracking (APSE) for Äspö diorite determined by Andersson et al. (2009)**

### **3.6. Conclusion**

Five strain based methods were reviewed for establishing the onset of cracking in laboratory compression tests on low porosity rocks. These methods utilized the laboratory locally measured axial and/or lateral strains. Identifying the stress level associated with crack initiation using these five methods relied on user judgment. A new method was introduced called the Lateral Strain Response (LSR), which relies only on the lateral strain response and removes the user judgment in selecting crack initiation stress on strain curves. A statistical evaluation of the results from the application of all six methods to 10 samples of Äspö Diorite showed that any of the strain methods provided statistically similar results.

Crack initiation in Äspö Diorite begins at stress levels well below the peak strength. Comparison of the stress magnitudes required to initiate spalling in Äspö diorite in large scale in-situ experiments showed that the laboratory crack-initiation stress provided an estimate for the onset of spalling. Given the importance of establishing laboratory testing procedures that can be used for estimating in-situ strength, it is proposed that the ISRM Suggested Methods develop standardized procedures for establishing crack initiation from laboratory stress-strain data.

*Acknowledgements* We would like to acknowledge the financial contribution of Swedish Nuclear Fuel and Waste Management Company through the DECOVALEX Project. The authors would like to thank Lars Jacobsson (SP Sweden) for providing the stress-strain data for Äspö Diorite.

## References

- Andersson, J.C., and Martin, C.D., 2009, The Äspö pillar stability experiment: Part I—Experiment design: *International Journal of Rock Mechanics and Mining Sciences*, v. 46, no. 5, p. 865-878.
- Bieniawski, Z.T., 1967a, Mechanism of brittle fracture of rock: Part II—experimental studies: *International Journal of Rock Mechanics and Mining Sciences & Geomechanics Abstracts*, v. 4, no. 4, p. 407-408, IN13-IN14, 409-418, IN15-IN18, 419-423.
- Bieniawski, Z.T., 1967b, Mechanism of brittle fracture of rock: Part I—theory of the fracture process: *International Journal of Rock Mechanics and Mining Sciences & Geomechanics Abstracts*, v. 4, no. 4, p. 395-404, IN11-IN12, 405-406.
- Bieniawski, Z.T., and Bernede, M.J., 1979, Suggested methods for determining the uniaxial compressive strength and deformability of rock materials: Part 1. Suggested method for determining deformability of rock materials in uniaxial compression: *International Journal of Rock Mechanics and Mining Sciences & Geomechanics Abstracts*, v. 16, no. 2, p. 138-140
- Brace, W.F., Paulding, B., and Scholz, C., 1966, Dilatancy in the fracture of crystalline rocks: *Journal of Geophysical Research*, v. 71, p. 3939-3953.
- Brown, E.T., editor, 1981, *Rock characterization, Testing and monitoring, ISRM suggested methods*: Oxford, Pergamon Press.
- Cook, N.G.W., 1963, The basic mechanics of rockbursts: *Journal of the South African Institute of Mining and Metallurgy*, no. 63, p. 71-81.
- Diederichs, M.S., 2007, The 2003 Canadian Geotechnical Colloquium: Mechanistic interpretation and practical application of damage and spalling

- prediction criteria for deep tunneling: *Canadian Geotechnical Journal*, v. 44, p. 1082-1116.
- Diederichs, M.S., Kaiser, P.K., and Eberhardt, E., 2004, Damage initiation and propagation in hard rock during tunnelling and the influence of near-face stress rotation: *International Journal of Rock Mechanics and Mining Sciences*, v. 41, no. 5, p. 785-812.
- Eberhardt, E., Stead, D., Stimpson, B., and Read, R.S., 1998, Identifying crack initiation and propagation thresholds in brittle rock: *Canadian Geotechnical Journal*, v. 35, no. 2, p. 222-233.
- Fairhurst, C., and Cook, N.G.W., 1966, The phenomenon of rock splitting parallel to direction of maximum compression in the neighborhood of a surface, *in* 1st congress of the international society of rock mechanics: Lisbon, p. 687-692.
- Glamheden, R., Fälth, B., Jacobsson, L., Harrström, J., Berglund, G., and Bergkvist, L., 2010, Counterforce applied to prevent spalling: Technical Report, TR-10-37.
- Griffith, A.A., 1921, The Phenomena of Rupture and Flow in Solids: *Philosophical Transactions of the Royal Society of London. Series A, Containing Papers of a Mathematical or Physical Character*, v. 221, p. 163-198.
- Griffith, A.A., 1924, Theory of rupture, *in* *Proceedings of the First International Congress of Applied Mechanics*: Delft, p. 55-63.
- Hallbauer, D.K., Wagner, H., and Cook, N.G.W., 1973, Some observations concerning the microscopic and mechanical behaviour of quartzite specimens in stiff, triaxial compression tests: *International Journal of Rock Mechanics and Mining Sciences & Geomechanics Abstracts*, v. 10, no. 6, p. 713-726.

- Hardy, H.R., 1981, Applications of acoustic emission techniques to rock and rock structures: a state of the art review. *in* Drnevich and Gray, ed., Acoustic Emission in Geotechnical Engineering Practice, ASTM STP750, ASTM, p.4-92.
- Hoek, E., and Brown, E.T., 1980, Empirical strength criterion for rock masses: *Journal of the Geotechnical Engineering Division*, v. 106, no. 9, p. 1013-1035.
- Janson, T., Ljunggren, B., and Bergman, T., 2007, Modal analysis on rock mechanical specimens. Specimen from borehole KLX03, KLX04, KQ0065G, KF0066A and KF0069A. Oskarshamn site investigation: SKB P-07-03.
- Lajtai, E.Z., 1974, Brittle fracture in compression: *International Journal of Fracture*, v. 10, no. 4, p. 525-536.
- Lockner, D., 1993, The role of acoustic emission in the study of rock fracture: *International Journal of Rock Mechanics and Mining Sciences & Geomechanics Abstracts*, v. 30, no. 7, p. 883-899.
- Martin, C.D., and Chandler, N.A., 1994, The progressive fracture of Lac du Bonnet granite: *International Journal of Rock Mechanics and Mining Sciences & Geomechanics Abstracts*, v. 31, no. 6, p. 643-659.
- Martin, C.D., and Christiansson, R., 2009, Estimating the potential for spalling around a deep nuclear waste repository in crystalline rock: *International Journal of Rock Mechanics and Mining Sciences*, v. 46, no. 2, p. 219-228.
- Martin, C.D., Kaiser, P.K., and McCreath, D.R., 1999, Hoek-Brown parameters for predicting the depth of brittle failure around tunnels: *Canadian Geotechnical Journal*, v. 36, no. 1, p. 136-151.
- Moore, D.E., and Lockner, D.A., 1995, The role of microcracking in shear-fracture propagation in granite: *Journal of Structural Geology*, v. 17, no. 1, p. 95-114.

- Murrell, S., 1963, A criterion for brittle fracture of rocks and concrete under triaxial stress, and the effect of pore pressure on the criterion, *in* 5th U.S. Symp. on Rock Mechanics, Pergamon Press, p. 577.
- Read, R.S., 2004, 20 years of excavation response studies at AECL's Underground Research Laboratory: *International Journal of Rock Mechanics and Mining Sciences*, v. 41, no. 8, p. 1251-1275.
- Rojat, F., Labiouse, V., Kaiser, P.K., and Descoedres, F., 2009, *Brittle Rock Failure in the Steg Lateral Adit of the Lötschberg Base Tunnel*, Springer Wien 42, 341 p.
- Stacey, T.R., 1981, A simple extension strain criterion for fracture of brittle rock: *International Journal of Rock Mechanics and Mining Sciences & Geomechanics Abstracts*, v. 18, no. 6, p. 469-474.
- Thompson, B., Young, R., and Lockner, D., 2006, *Fracture in Westerly Granite under AE Feedback and Constant Strain Rate Loading: Nucleation, Quasi-static Propagation, and the Transition to Unstable Fracture Propagation*, Birkhäuser Basel 163, 995 p.
- Walpole, R.E., 2002, *Probability & Statistics for Engineers and Scientists: Upper Saddle River, NJ*, Prentice Hall.

# Chapter 4. Crack initiation stress in low porosity crystalline and sedimentary rocks<sup>6</sup>

## 4.1. Introduction

It is well known that the operational strengths of soils and rocks that are back calculated from case histories seldom match laboratory peak strength values. The reasons put forward for this discrepancy vary from (1) rate effects, i.e., loading rate in the laboratory is different from that in situ (Lavrov, 2001), (2) scale effects, i.e., the strength in-situ decreases with increasing scale, with the lab strength representing the maximum strength (Hoek and Brown, 1980), and (3) process effects, i.e., the laboratory sample is tested using loading conditions that do not reflect the loading process followed in-situ (Holcomb, 1993). In brittle rock, the failure process in laboratory samples is a progressive process requiring the initiation, growth and coalescence of cracks (Lockner, 1993; Thompson et al., 2006). This process has also been observed in-situ around underground excavations using microseismic monitoring systems (Collins and Young, 2000). Several researchers have suggested that the crack initiation observed in laboratory compression tests provides a good estimate of the operational spalling strength observed in hard brittle rocks around underground openings (Martin, 1997; Andersson and Martin, 2009; Martin and Christiansson, 2009; Rojat et al., 2009; Diederichs, 2007). More recently Damjanac and Fairhurst (2010) suggested that crack initiation may also be used as a lower bound estimate for the long-term strength threshold of crystalline rocks. Other researchers suggest that crack

---

<sup>6</sup> A version of this chapter has been submitted as a paper to the journal of Engineering Geology

initiation related to the Kaiser effect can be used to establish the in-situ state of stress. Hence there is ample evidence that crack initiation in compression testing may be an important parameter.

The early work of Brace et al. (1966) showed that crack initiation in laboratory samples was coincident with dilatancy measured using volumetric strain and that the crack initiation for granite, marble and aplite occurred between 0.3 and 0.7 of the peak strength. Brace et al. (1966) also compiled results for Dolomite, Soapstone, Diabase, Olivine Basalt, Quartzite and Concrete, and found similar crack initiation values ranging from 0.35 to 0.6 of the peak strength. The ratio of crack initiation stress to peak strength appeared narrowly constrained despite the range in rock types. Despite this early work determination of crack initiation from laboratory tests are seldom reported in the literature. In this paper we examine crack initiation in uniaxial compression and triaxial compressions tests in igneous, metamorphic and sedimentary rocks. A total of 336 tests were evaluated and used to examine the effect of mineralogy, anisotropy, grain size and confinement on crack initiation. The Griffith criterion is often considered as a crack initiation criterion (Hoek and Bieniawski, 1966). The tensile strength measured on a suite of Lac du Bonnet samples is used to examine if the Griffith or Hoek-Brown Criteria can be used to predict crack initiation over a confining stress ranging up to 60 MPa.

## **4.2. Sample description**

### ***4.2.1. Igneous rocks***

The igneous samples were obtained by the Swedish Nuclear Fuel and Waste Management Co. (SKB) during their site investigation of the Forsmark and Laxemar-Simpevarp area between 2002 and 2007. All samples were obtained using triple tube core barrels, which produced a 50.6-mm-diameter core. The Forsmark site is located within the municipality of Östhammar about 150 km north of Stockholm, Sweden (Stephen, 2010) while Laxemar-Simpevarp is

situated in Småland in the south-eastern part of Sweden and 230 km south of Stockholm.

Both sites are located in geology that is considered typical of the Precambrian Scandinavian Shield. In summary, Forsmark site rock types are meta-intrusive bodies that are located at the south-western part of Fennoscandian Shield. The bedrock is classified into four rock units based on their mineralogy, grain size and relative age that ranged from meta-granite or meta-granodiorite to tonalite. More detail description of the bedrock geology can be found in Stephen et al. (2007).

The bedrock at the Laxemar-Simpevarp site was dated at 1.8-1.9 Ga (Wahlgren, 2010). The petrology includes intrusive rocks of quartz monzodiorite, granodiorite or granite with a range of grain size and texture. The dominant rock types are medium-grained porphyritic Ävrö granite and medium grained equigranular quartz monzodiorite (Wahlgren, 2010). The modal analysis of the samples with measured uniaxial compressive strength data have been used for classification according to Quartz-Alkali Feldspar-Plagioclase (QAP) diagram. (Streckeisen, 1976) and presented in Figure 4.1. Based on grain size, almost all the samples that are used in this study are from fine grained to medium grained, Table 4.1.

The next group of samples were obtained from the site investigations for the Deep Underground Science and Engineering Laboratory (DUSEL) at the former Homestake mine in northern Black Hills of South Dakota, USA. The unconfined compression tests were done on the samples of 50mm in diameter that represent two types of rocks, fine grained amphibolite and rhyolite.

**Table 4.1: Grain size classification system of igneous rock samples (Strahle, 2001)**

Class	Grain Size (mm)
Very fine grained	0.05-0.5
Fine grained	0.5-1
Fine to medium grained	1-1.5
Medium grained	1.5-3
Medium to coarse grained	3-5
Coarse grained	>5

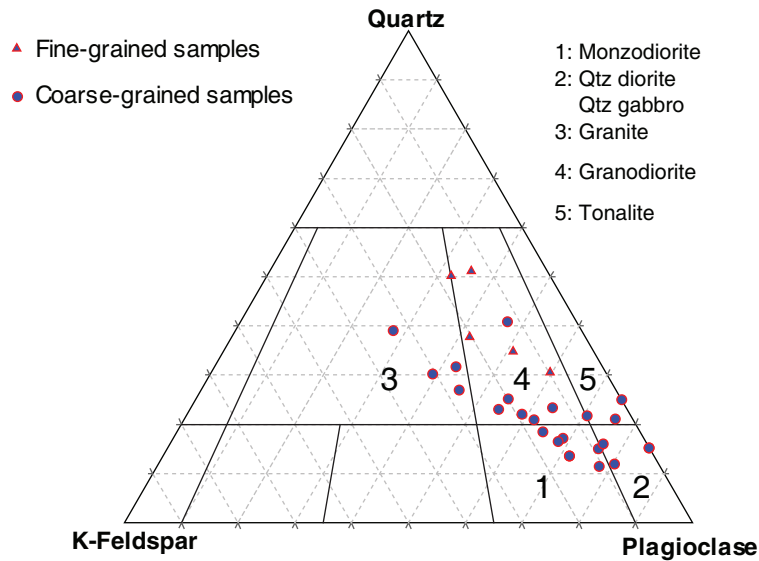


**Figure 4.1: Classification of igneous samples based on modal analysis**

The grain size data of rhyolite samples based on visual examination are considered as very fine grained which is consistent with common geological description of rhyolite (RESPEC Co, 2010). An overview of geological description of available igneous specimens is presented in Table 4.2.

#### **4.2.2. Sedimentary Rocks**

The sedimentary samples have been obtained by Nuclear Waste Management Organization (NWMO) during their site investigations for a low- to intermediate-level radioactive waste Deep Geological Repository, known as Bruce site, located near Tiverton, Ontario, Canada. The 75 mm-diameter samples were obtained from the Paleozoic stratigraphy typical of southern Ontario (Frizzel et al., 2008). The samples in this paper range in lithology from shale to limestone/dolomite with various amounts of clay (mainly illite) and carbonate. The samples are very fine to fine grained according to Schandl (2009). The mineralogical descriptions of the sedimentary specimens are presented in Table 4.3. Samples were jacketed with heat-shrink tubing before the sample preparation to minimize the change in water content (Gorski et al., 2009a).

**Table 4.2: Geological description of igneous specimens**

Igneous rocks-Forsmark site, Sweden				
Rock type	Grain size	Number of specimens	Mineralogy <sup>7</sup>	Photo of specimens (width=50mm)
Pegmatite	Medium grained	12	Qtz: 34%±4; K-Fel: 31%±10; Pl: 31%±7; Bio: 2%±2; Other: 2%	
Modal analysis from (Stephen et al., 2007) Image taken from (Jacobsson, 2006a)				
Granodiorite	Fine grained	14	Qtz: 30%±8; K-Fel: 12%±3; Pl: 43%±7; Bio: 8%±3; Other: 7%	
Modal analysis from (Stephen et al., 2007) Image taken from (Jacobsson, 2004b)				
Granodiorite	Medium grained	10	Qtz: 32%±18; K-Fel: 12%±5; Pl: 41%±16; Bio: 9%±5; Other: 6%	
Modal analysis from (Adl-Zarrabi, 2006) Image taken from (Jacobsson, 2006a)				
Tonalite	Fine grained	9	Qtz: 23%±8; K-Fel: 5%±3; Pl: 49%±6; Bio: 10%±4; Other: 13%	
Modal analysis from (Stephen et al., 2007) Image taken from (Jacobsson, 2004b)				
Granite	Fine grained	19	Qtz: 37%±5; K-Fel: 32%±9; Pl: 26%±4; Bio: 4%±3; Other: 1%	
Modal analysis from (Stephen et al., 2007) Image taken from (Jacobsson, 2004c)				
Granite	Medium grained	29	Qtz: 36%±6; K-Fel: 23%±6; Pl: 34%±5; Bio: 6%±2; Other: 1%	
Modal analysis from (Stephen et al., 2007) Image taken from (Jacobsson, 2004b)				

<sup>7</sup> Qtz: Quartz; K-Fel: K-Feldspar; Pl: Plagioclase; Bio: Biotite; Amph: Amphibole

**Table 4.2. continued**

Igneous rocks- Laxemar site, Sweden				
Rock type	Grain size	Number of specimen	Mineralogy (%)	Photo of sample (width=50mm)
Quartz monzodiorite	Fine grained	5	Qtz: 13%±3; K-Fel:11%±5; Pl: 47%±5; Bio: 14%±4; Other: 15%	
Modal analysis from (Wahlgren et al., 2008) Image taken from (Jacobsson, 2005)				
Quartz monzodiorite	Medium grained	27	Qtz: 13%±3; K-Fel:11%±5; Pl: 47%±5; Bio: 14%±4; Other: 15%	
Modal analysis from (Wahlgren et al., 2008) Image taken from (Jacobsson, 2007)				
Granite (Ävrö)	Medium grained	59	Qtz: 22%±6; K-Fel:20%±7; Pl: 44%±8; Bio: 9%±3; Other: 5%	
Modal analysis from (Wahlgren et al., 2008) Image taken from (Jacobsson, 2006b)				
Diorite	Fine grained	6	Qtz:7%±5; K-Fel:11%±6; Pl: 51%±9; Bio: 15%±8; Other: 16%	
Modal analysis from (Wahlgren et al., 2008) Image taken from (Jacobsson, 2006b)				
Diorite	Medium grained	11	Qtz: 4%±1; K-Fel: 0% Pl: 47%±5; Bio: 11%±4; Amph: 30%±5; Other: 8%;	
Modal analysis from (Wahlgren et al., 2008) Image taken from (Jacobsson, 2006b)				
Igneous rocks- Homestake site, USA				
Rhyolite	Very fine grained	5	Not Available	
Image taken from (RESPEC Co, 2010)				

**Table 4.3: Geological description of sedimentary rock specimens**

Sedimentary Rocks-Bruce site, Canada				
Rock type	Grain size	Number of specimen	Mineralogy	Photo of sample (width=50mm)
Anhydrite/ Gypsum	Fine to medium	2	Anhydrite: 85%	
Modal analysis from (Schandl, 2009) Image taken from (Gorski et al., 2009b)				
Argillaceous limestone	Fine to medium	21	Carbonate: 74%±21; Clay:12%±8	
Modal analysis from (Schandl, 2009) Image taken from (Gorski et al., 2009b)				
Calcareous shale	Very fine	4	Carbonate: 46%±19 Clay: 37%±17	
Modal analysis from (Schandl, 2009) Image taken from (RESPEC Co, 2010)				
Siltstone/ shale	Very fine	6	Carbonate: 17%±14 Clay: 71%±12	Photo Unavailable
Modal analysis from (Schandl, 2009)				

#### 4.2.3. Metamorphic Rocks

In addition to Homestake amphibolite specimens, which were described in Section 2.1, other metamorphic specimens that have been used were obtained by Posiva Oy during the site investigation at the Olkiluoto site in Finland, Posiva. The Olkiluoto site is located on the Gulf of Bothnia coast in the municipality of Eurakoki in western Finland within the Fennoscandian Shield. The study area is within Precambrian crystalline rocks of Fennoscandian Shield known as Svecofennian domain (Saari, 2008). The lithology of Olkiluoto is divided into two groups: (1) high-grade metamorphic rocks that are classified according to their major mineral composition, texture and migmatitic structure that was metamorphosed at 1.8 Ga, and (2) igneous rocks which are mostly diabase dykes (Lahti et al., 2010). The 57-mm diameter samples belong to the first group and

include migmatite gneisses, quartz gneisses and mica gneiss. The modal analysis of the metamorphic specimens is presented in Table 4.4.

### 4.3. Testing Methodology

#### 4.3.1. Testing Procedure

The uniaxial compressive strength of almost all samples was measured according to ISRM Suggested Methods (Brown, 1981). The igneous rock samples from Sweden were stored in water 20 to 60 days prior to performing the test. The axial load was recorded by a load cells and the axial and circumferential deformations were recorded by strain monitoring systems (Jacobsson, 2006a; Figure 4.2). All tests were data logged and these stress-strain responses were used for the results discussed in this paper.

**Table 4.4: Modal analysis of metamorphic specimen**

Metamorphic rocks-Forsmark site, Sweden				
Rock type	Grain size	Number of specimen	Mineralogy	Photo of sample (width=50mm)
Metagranite	Medium grained	32	Qtz: 32%±3; K-Fel: 28%±8; Pl: 34%±2; Bio: 4%±2; Other: 2%±1	
Modal analysis from (Peterson et al., 2004) Image taken from (Jacobsson, 2004a)				
Metamorphic rocks-Olkilouto site, Finland				
Mica gneiss	Medium grained	53	Qtz: 34%±10; K-Fel: 11%±7; Pl: 17%±6; Bio: 26%±8; Other: 12%±8	
Modal analysis from (Kärki and Paulamäki, 2006) Image taken from (Eloranta, 2006)				
Metamorphic rocks-Homestake site, USA				
Amphibolite	-	6	Not available	
Image taken from (RESPEC Co, 2010)				

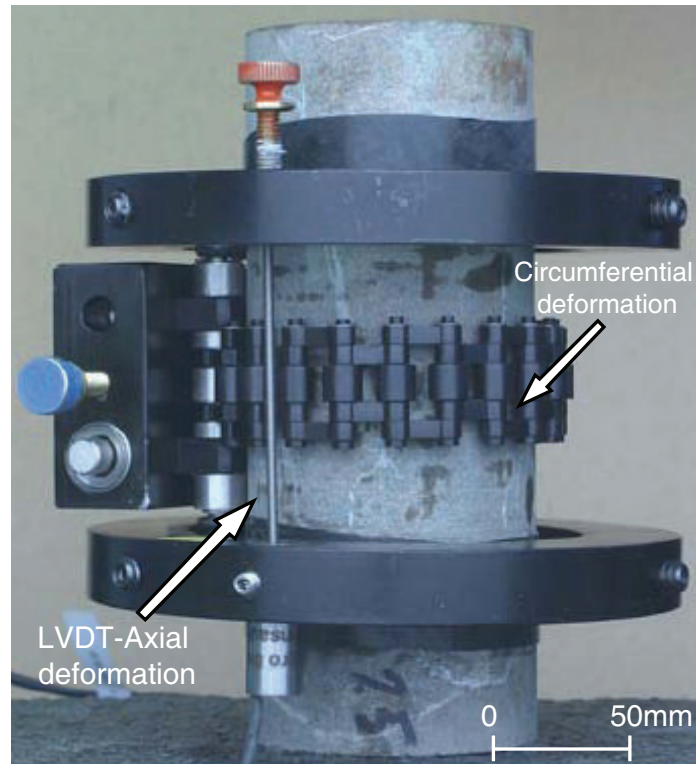


**Figure 4.2: Example of the measurement system; LVDTs and chain used to measure the axial and circumferential deformation, respectively. Photo provided by SKB**

#### ***4.3.2. Crack initiation stress measurement***

Brace et al. (1966) and Bieniawski (1967) demonstrated that the stress-strain response in both unconfined and confined tests for low porosity rocks displays four important inflections: (1) crack closure, observed in the axial strain; (2) crack initiation, observed in the lateral strain; (3) Unstable crack growth, observed in the volumetric strain; and (4) peak, observed in the axial strain (see Figure 4.3).

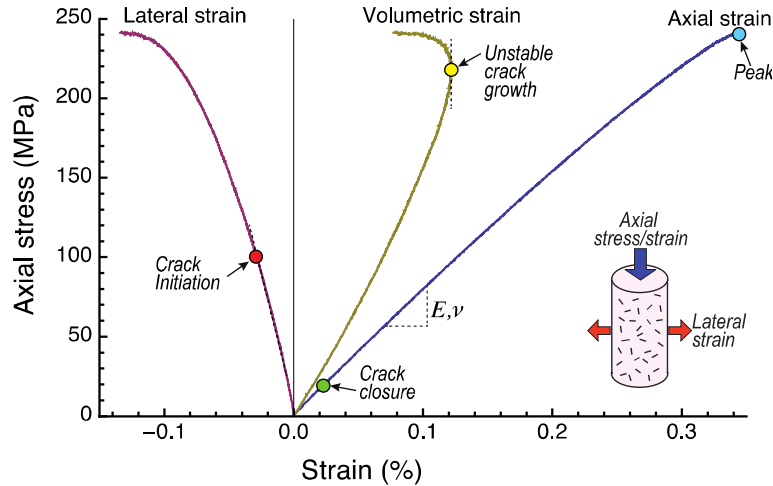


**Figure 4.3: Typical stress–strain response recorded in a uniaxial compressive test**

The methods that researchers have used to establish the load associated with the onset of crack initiation during laboratory compression have relied primarily on the measured strains.

The methods utilized either the volumetric strain or the lateral strain, and have been modified by researchers and at times augmented by acoustic emission techniques. These methods were reviewed by Nicksiar and Martin (2012) who showed, using 10 samples of Äspö Diorite, that any of the strain methods provided statistically accurate results. In this research, a technique described by Nicksiar and Martin (2012) that relies on the Lateral Strain Response (LSR) is used to calculate crack initiation stress.

#### **4.3.3. Grouping of samples**

To assess the effect of rock characteristics on crack initiation, 474 uniaxial compressive strength tests were selected including 241 igneous, 71 sedimentary and 162 metamorphic rock specimens. The distribution of UCS stress for different rock types is presented in Figure 4.4.

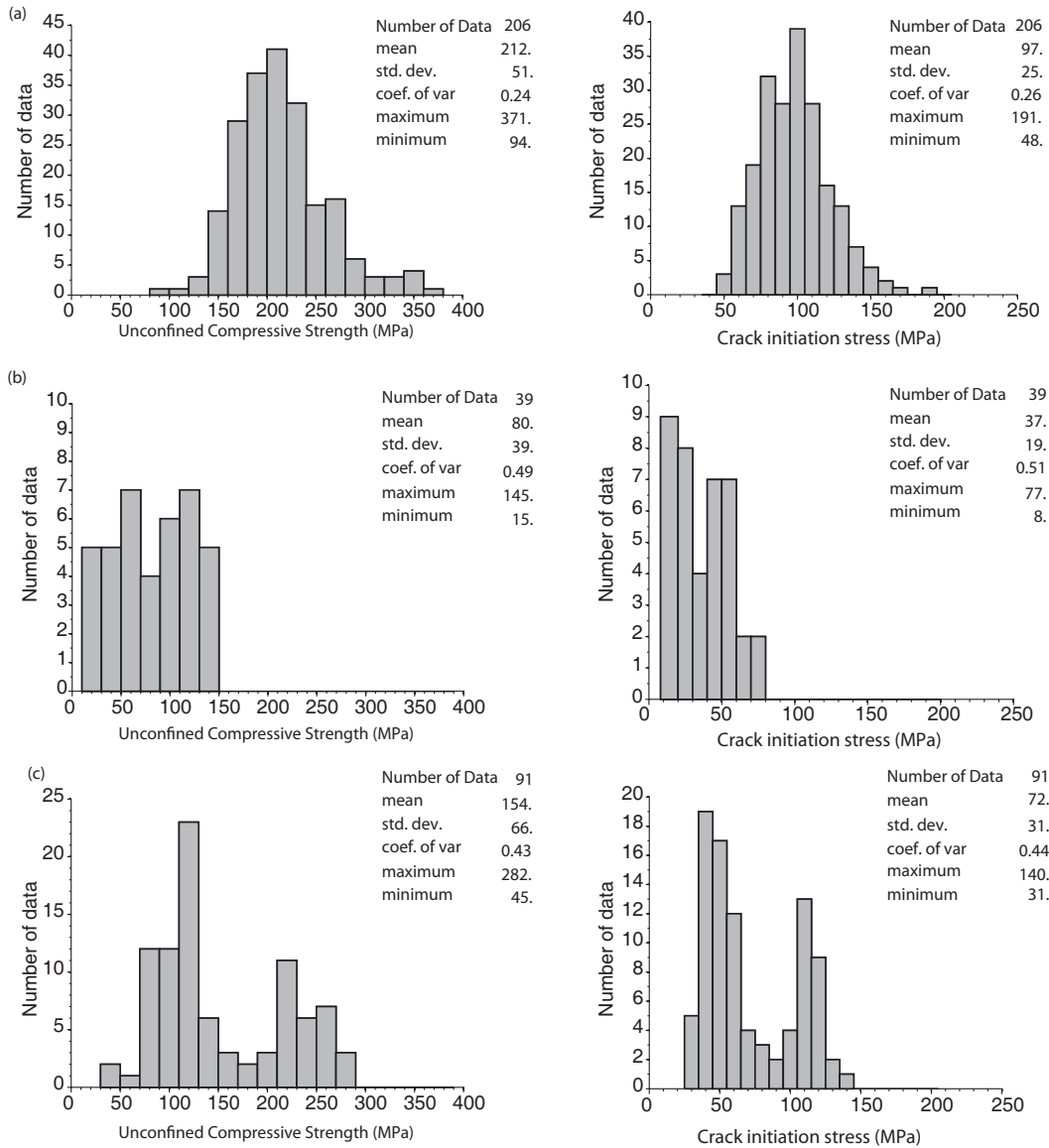


**Figure 4.4: Statistical distribution of unconfined compressive strength and crack initiation stress in (a) igneous, (b) sedimentary and (c) metamorphic rocks**

In this paper, the effect of material properties on brittle behaviour of rocks has been investigated. Therefore, the mineral compositions and average grain size are correlated to crack initiation and peak stress.

## 4.4. Effect of material properties on crack initiation stress

### 4.4.1. Mineral composition

The effect of mineralogy on the samples with known modal analysis has been studied. Among the available data, 201 igneous and 31 sedimentary specimens were selected. Igneous rocks consist of 53 fine-grained and 148 medium-grained samples. The sedimentary rocks petrology ranges from shale to limestone with clay and carbonate content and an average grain size of less than 0.3mm. The distributions of crack initiation and peak stress of the igneous and sedimentary samples are summarized in Figure 4.5.

Spearman rank correlation provides a criterion to show the relationship between two sets of data by ranking the variables and can be calculated as:

$$\rho = 1 - \frac{6\sum d_i^2}{(n^3 - n)} \quad (4.1)$$

where  $d$  is the difference between the rank orders and  $n$  is the sample size

The value of  $\rho$  ranges from 1 to -1 indicating the strong positive and strong negative correlation, respectively. The value of 0 indicates no correlation. A detailed discussion of Spearman rank correlation can be found in Muijs (2004). The Spearman correlation coefficient is applied to the igneous rock data to assess the correlation between mineralogy, crack-initiation stress and peak stress (Table 4.5)

The results in Table 4.5 indicate that in igneous rocks, quartz and K-Feldspars content, have a positive correlation to both crack initiation and peak stress while the Plagioclase shows a negative correlation. The dependency of brittle failure stress levels to mineralogy is more pronounced in medium grained specimens. Moreover, the results show that the crack initiation stress increases as the grain size is decreased. The same results obtained for the peak stress in accordance with

the grain size. However, it should be noted that, since the variation of quartz, plagioclase and K-Feldspar contents are related, interpretation of the statistical analysis has been associated with some uncertainties.

The effect of mineralogy on sedimentary samples is investigated by comparing the crack initiation and peak stress changes corresponding to the clay-carbonate content. The results are summarized in Figure 4.6 which indicates the positive relation between the stress levels and carbonate content.

#### ***4.4.2. Effect of directional heterogeneity***

The effect of directional anisotropy on tensile strength, crack initiation and peak stress has been studied for Olkiluoto veined gneiss. Veined gneiss is a migmatitic gneiss which shows a distinct linear structure containing elongated leucosome veins and banded palaeosome that can show an intense shear deformation (Andersson et al., 2007). During metamorphism, in situ partial melting forms migmatite. Migmatites can be defined as coarse grained, heterogeneous rocks which are characterized by discontinuous intervals of melt-driven light coloured, granitoid material, leucosome (Barker, 1998).

**Table 4.5: Spearman rank correlation coefficient between mineralogy and brittle failure parameters of fine and medium grained igneous rocks**

	Fine grained specimens			Medium grained specimens		
	Quartz	Plagioclase	K-Feldspar	Quartz	Plagioclase	K-Feldspar
Crack initiation						
stress	0.50	-0.55	0.74	0.62	-0.81	0.48
Peak stress	0.45	-0.52	0.83	0.66	-0.79	0.38

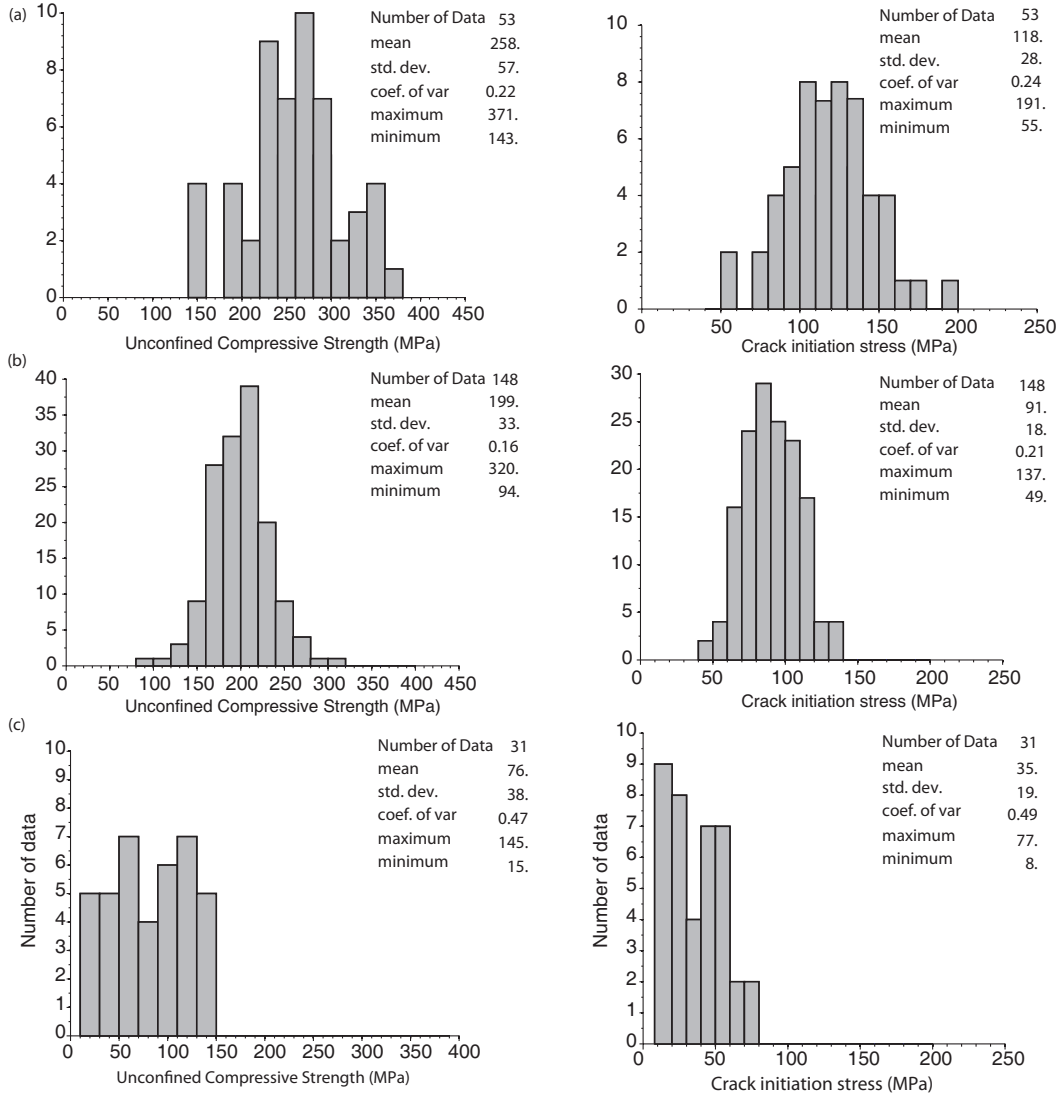


**Figure 4.5: Statistical distribution of unconfined compressive strength and crack initiation stress of (a) fine grained igneous; (b) medium grained igneous and (c) sedimentary samples**

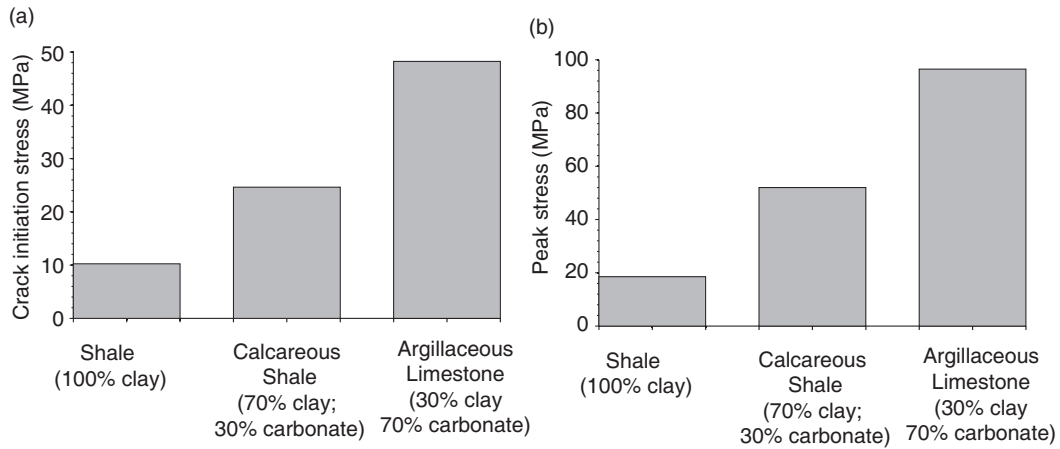


**Figure 4.6: Crack initiation and peak stress in sedimentary rocks with different clay-carbonate content**

The tensile strength results are obtained from Brazilian tests. Crack initiation stress and peak stress are measured from uniaxial compressive stress-strain curves which are inferred from Andersson et al. (2007; Figure 4.7). The crack initiation stress for veined gneiss was measured using crack volumetric strain method (Martin and Chandler, 1994).

Foliation and natural preferential orientation of the grains can reduce the strength of rocks by introducing weakness planes and microcracks in one or more directions. In Figure 4.7, the trend of tensile strength, crack initiation and peak stress are similar. However, the sensitivity of peak stress to foliation dip angle is more pronounced relative to other stress levels. It can be also inferred from Figure 4.7 that the average peak stress is largest when the foliation is in the range of 0 to 20 degrees relative to the axial stress.

Although the crack initiation stress and tensile strength decrease when the angle between foliation and axial stress reaches  $45^\circ$ , the reduction in peak stress is more obvious. This is explained by the failure mode in the stages of failure and crack initiation.

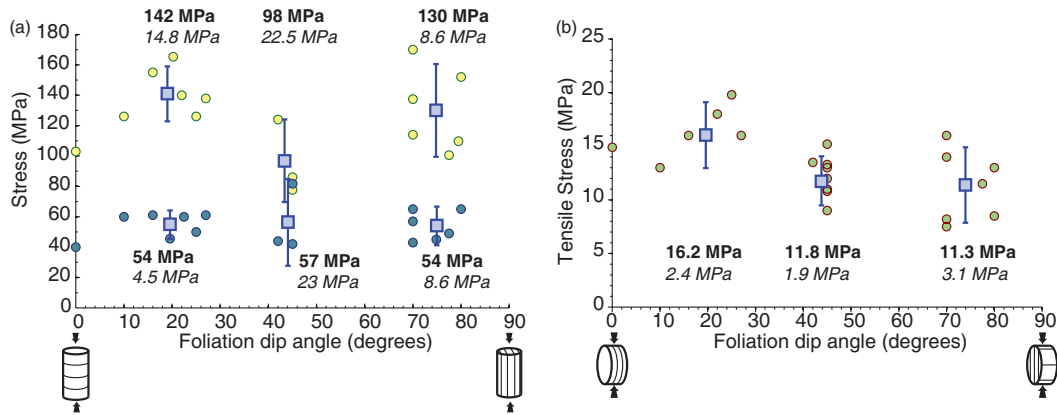


**Figure 4.7: Effect of directional anisotropy on (a) crack initiation and peak stress and (b) tensile strength. Peak (light colour) and crack initiation stress (dark colour) are measured from UCS stress-strain curve. Average stress values (in bold) and standard deviation**

Crack initiation stress is known to be a tensile mechanism whereas at peak stress, the shear mechanism is also present. When the anisotropy reaches to 40-45°, the shear stress acting on the planes of weakness reaches a maximum and facilitates the process of failure under the peak load.

## 4.5. Crack initiation for different loading paths

### 4.5.1. Uniaxial compression

The effect of material properties on crack initiation stress has been discussed in Section 4. Those results showed that, the mineralogy has the same influence on crack initiation and peak stress in both igneous and sedimentary rocks. Brace et al. (1966) found the normalized value of crack initiation to peak stress is 0.5 for granite, 0.45 for marble and 0.45 for aplite. It was also observed by Martin and Chandler (1994) that cracking in Lac du Bonnet granite initiated when the load first exceeds about 0.4 of the peak strength. The variation of crack initiation to peak stress for different rock types is compiled in Figure 4.8. The results indicate that the crack initiation stress ratio in different rock types ranges from 0.42 to 0.47 regardless of rock properties.

#### ***4.5.2. Triaxial compression***

Ashby and Sammis (1990) noted that the cracking associated with brittle failure is inhibited when the confining stress increases. Ashby and Sammis concluded that in high confinement, the crack propagation is replaced by plastic creep. In this work, the effect of confinement on crack initiation stress has been studied on 61 igneous and 40 metamorphic samples.

The geological and mechanical properties of igneous and metamorphic samples were reviewed in Section 4.2. Lac du Bonnet granite data used in this paper was acquired from medium-grained pink granite of Lac du Bonnet Batholith, Manitoba as part of the nuclear fuel waste disposal test facility at the Underground Research Laboratory (URL). In order to measure crack initiation stress, strain gauges were used at the middle of all specimens to record the deformations. Lau and Gorski (1992) used axial stress-lateral strain curve to measure crack initiation stress which was previously introduced by Lajtai (1974).

The triaxial tests for the igneous samples used a confinement ranging from 2 to 50 MPa following Fairhurst and Hudson (1999). The confining stress for metamorphic samples was in the range of 0.5-15 MPa with a constant axial loading rate of 0.75 MPa.sec<sup>-1</sup> (Eloranta, 2006). The confining stress for the Lac du Bonnet samples ranged from 0-60 MPa with the axial loading rate of 0.75 MPa.sec<sup>-1</sup> (Lau and Gorski, 1992). In the igneous and metamorphic rock specimens, the crack initiation stress was measured using the crack volumetric strain method (Martin and Chandler, 1994).

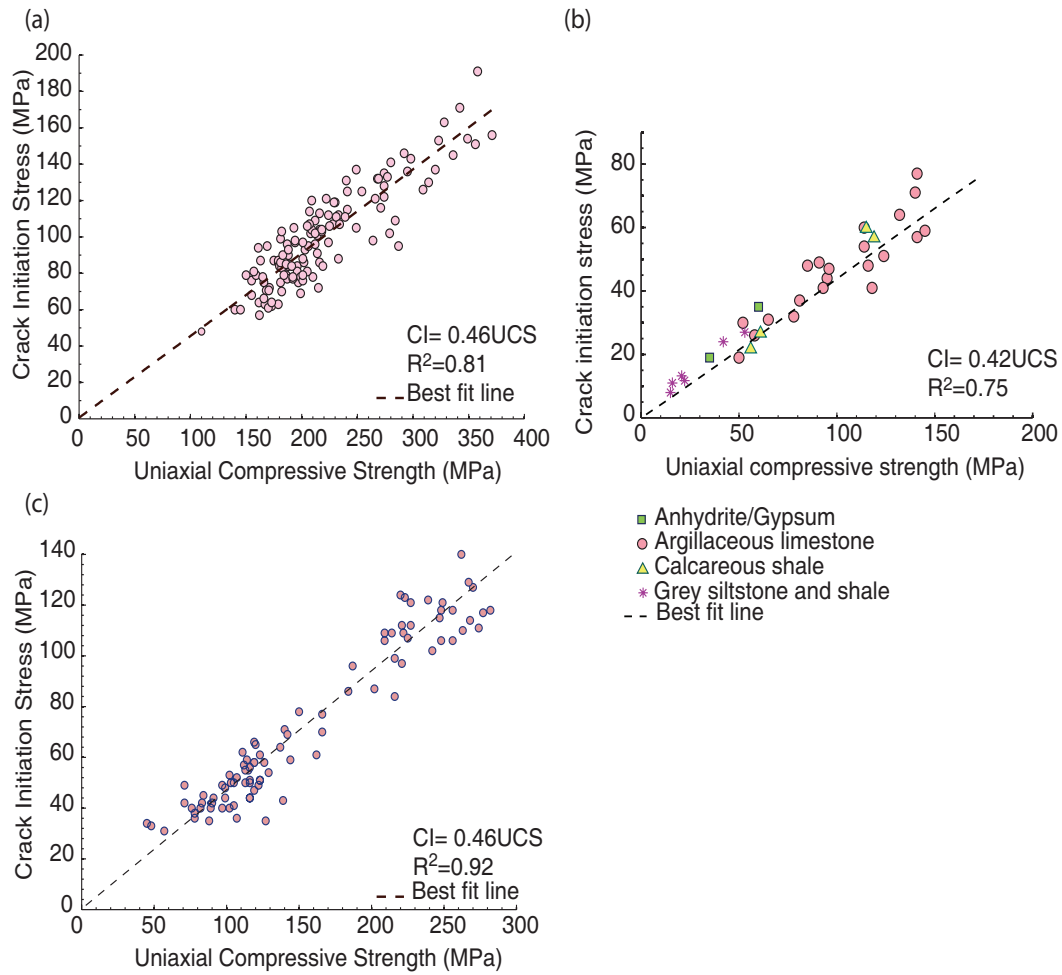


**Figure 4.8: The relationship between crack initiation and peak stress in different rock types: (a) Igneous; (b) sedimentary and (c) metamorphic rocks**

The relationship between crack initiation and peak stress for different confinements in triaxial compression is summarized in Figure 4.9. It can be inferred from Figure 4.9 that the crack initiation stress ratios for all confinements are in the range of 0.50-0.54. The variation of crack initiation to peak stress, was also examined using the deviatoric stress, i.e. subtracting confining stress from CI and peak stress. Those results gave similar ratios with the average crack initiation stress ratio reduced from 0.53 to 0.51.

### 4.5.3. Tensile loading

*Relationship between Brazilian and direct tensile strength:*

The tensile strength of rock is found from Brazilian tensile (BT) and direct tension (DT) tests. The DT test is more difficult to perform, as it requires shaping of the core to resemble a “dog-bone”, to obtain a uniform stress distribution at the centre of the core. It is generally assumed that the tensile strength obtained from DT tests is less than that obtained from the BT test. In this section, the BT and DT tests are compared.

Brazilian samples of Lac du Bonnet granite were taken from both ends of “dog-bone” samples used to measure the direct tensile strength. Hence, there were two Brazilian samples for each direct tension sample. This approach minimizes the scatter associated with sample variability.

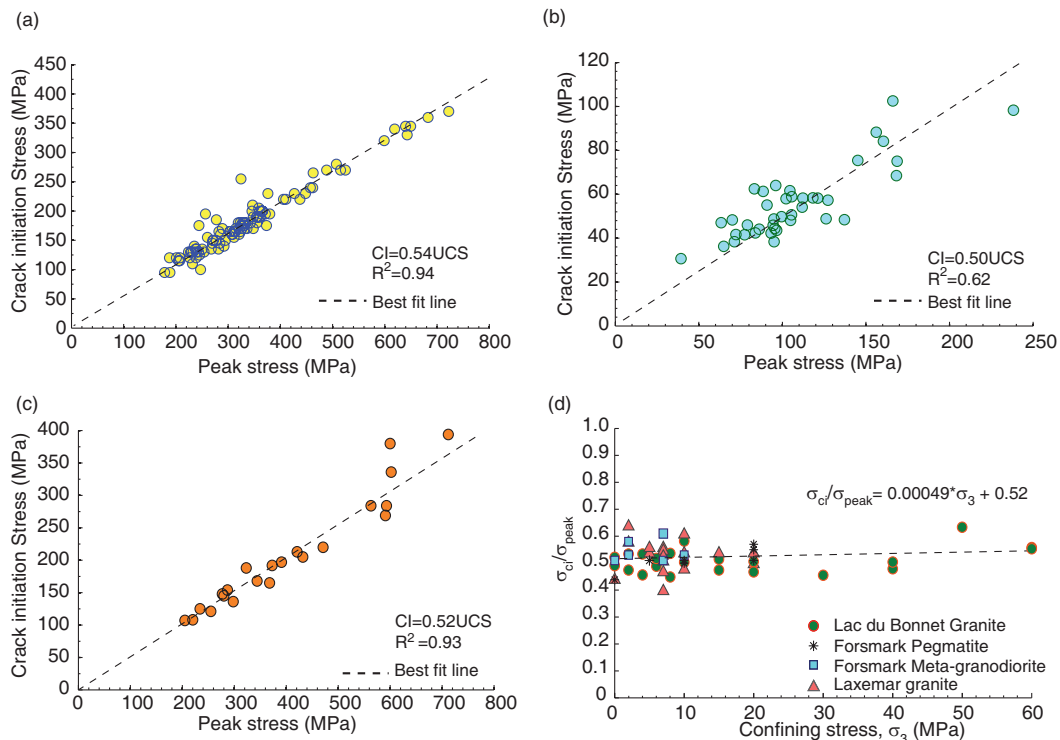


**Figure 4.9: Relationship between crack initiation and peak stress in (a) igneous rocks, (b) metamorphic rocks, (c) Lac du Bonnet granite and (d) crack initiation stress ratios in triaxial compression**

A summary of the test results is given in Figure 4.10. The mean Brazilian and direct tensile strengths were 8.8 MPa and 6.9 MPa, respectively. This suggests that the direct tensile strength is approximately 0.78 of the Brazilian tensile strength.

Additional laboratory tensile tests were compiled to determine if the ratio observed in Figure 4.10 was generally applicable to other data sets. Figure 4.11 shows the results compiled for various crystalline rocks. The ratio in Figure 4.11 ranges from an average of 0.75 for 10 samples of medium-grained Lac du Bonnet granite (LdB disturbed) to 0.58 for 20 samples of fine-grained Forsmark granite. The 18 mica gneiss samples from Olkiluoto, Finland, have an average ratio of 0.67 and show the greatest variability, likely related to the mica fabric in the samples. The variability in the ratios for Lac du Bonnet (LdB) granite reflects varying amounts of microcracking (see Martin and Stimpson, 1994). These microcracks not only affect the ratio of tensile strength but also the tensile strength itself, particularly the direct tensile strength. For example, the samples of LdB granite that have the least amount of microcracks have a direct tensile strength of 6.9 MPa, while the samples with the greatest amount of microcracks have a direct tensile strength of only 1.47 MPa. The linear trend line of 0.78 BT represents the ratio for the samples with the least amount of microcracking.

#### *Direct tension and Crack initiation stress*

The Brazilian tensile strength data are available for 41 igneous samples and 23 metamorphic samples with known unconfined compressive strength. Igneous samples are 50mm in diameter and 26mm long. The testing procedure was according to D3967-95a (ASTM, 1996). Metamorphic samples were loaded between two concave steel plates with the surface radius of 1.5 times the specimen radius (Eloranta, 2006). The specimens were 60 mm in diameter and 30 mm long and the two flat steel jaws, 3.5 mm wide, applied the load.

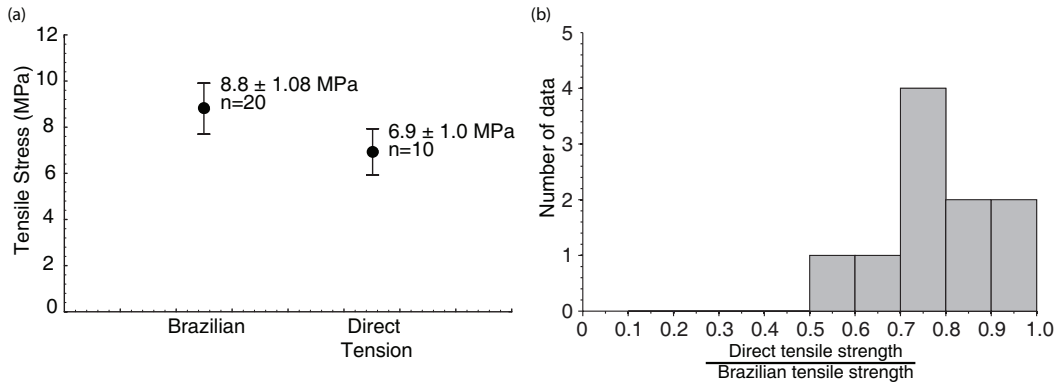


**Figure 4.10: (a) Comparison of the mean Brazilian tensile strength of 20 samples and the mean tensile strength obtained from 10 Direct Tension tests; (b) Statistical distribution of direct to Brazilian tensile strength ratio for 10 available samples**

The scatter plots of the Brazilian tensile strength relative to crack initiation stress are summarized in Figure 4.12. Also shown in Figure 4.12 is the distribution of crack initiation stress to Direct tensile strength ratio (CI/DT), where the Direct tensile strength is estimated from the Brazilian strength results. Figure 4.12 illustrates that the mean values for the ratio of the crack initiation stress to Direct Tensile strength for each rock type range from 8 for mica gneiss to 9 for metagranodiorite.

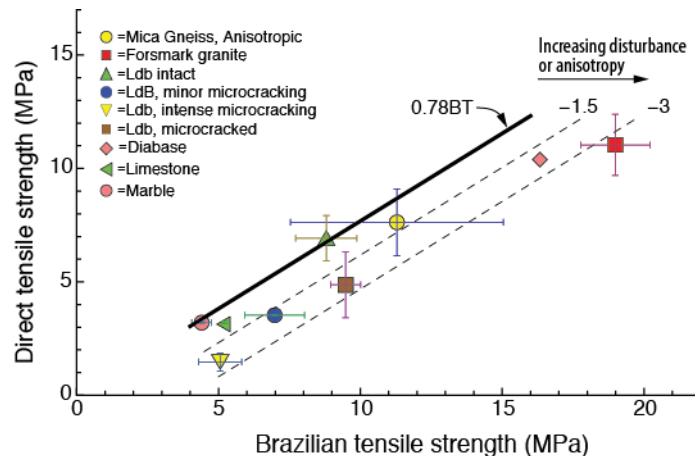


**Figure 4.11: Relationship between Brazilian and “dog-bone” Direct Tension tensile strength for various crystalline rocks: Olkiluoto Mica Gneiss, Forsmark granite, Lac du Bonnet granite (Ldb), Diabase and Marble. Error bars represent standard deviation**

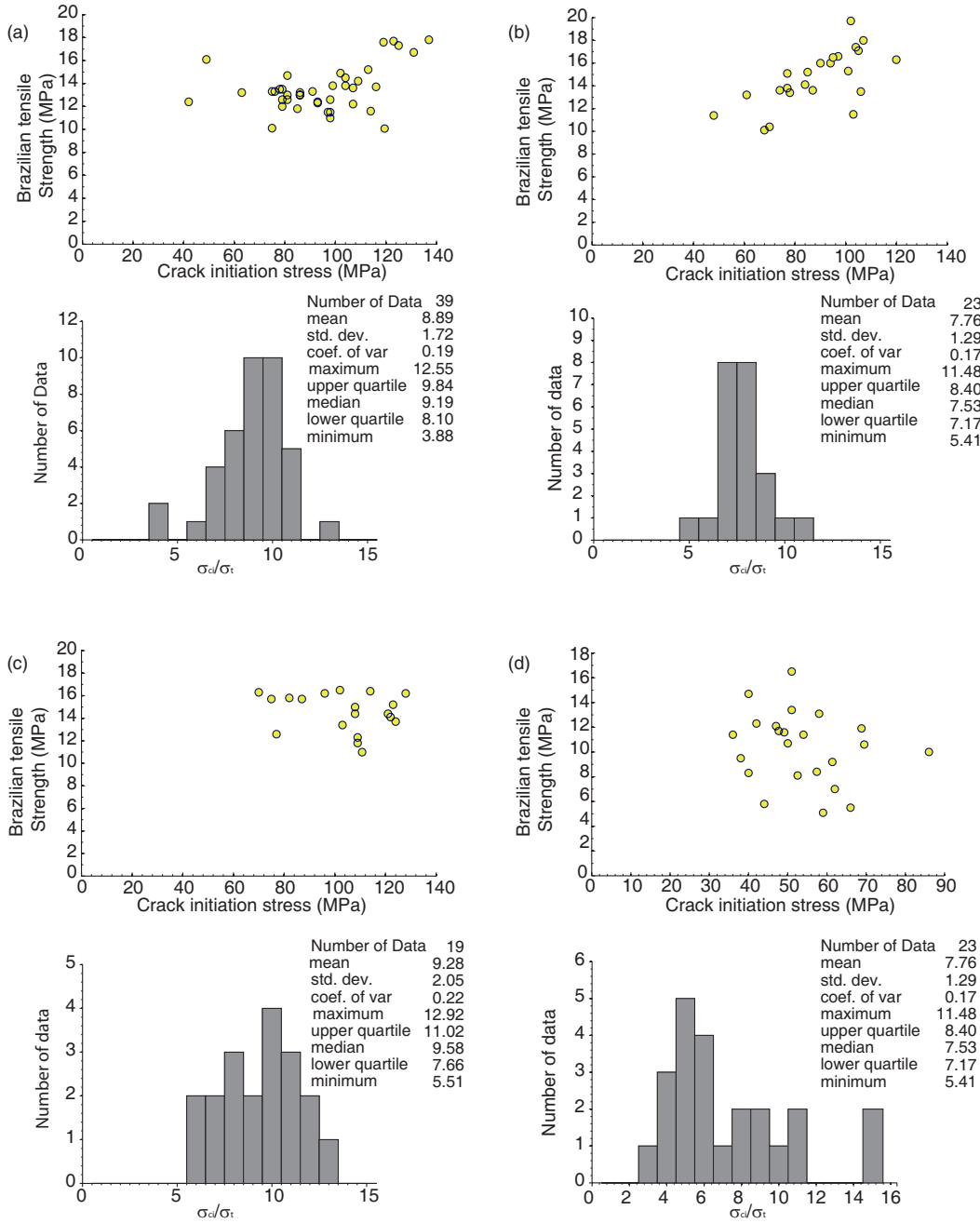


Figure 4.12: Statistical distribution of crack initiation to tensile strength ratio of (a) Laxemar granite, (b) Laxemar quartz monzodiorite, (c) Forsmark metagranodiorite and (d) Olkiluoto mica gneiss. The Direct tensile strength values in the histograms are calculated using the relationship given in Figure 4.11.

#### 4.6. Estimation of crack initiation in triaxial compression

In 1921, Griffith used a constant tensile stress loading system to support his energy theory for tensile rupture of brittle solids. Griffith (1924) using elliptical open cracks noted that in compression the local stress on the boundary of the open inclined crack near the tip is still tensile. Griffith (1924) proposed that initiation of failure in compression could be expressed in terms of principal stresses ( $\sigma_1$  and  $\sigma_3$ ) and uniaxial tensile strength ( $T$ , expressed as a negative value) as:

$$\sigma_1 = \sigma_3 + 4T \pm 4\sqrt{T\sigma_3 + T^2} \quad \text{if } \sigma_1 + 3\sigma_3 \geq 0 \quad (4.2a)$$

and

$$\sigma_3 = T \quad \text{if } \sigma_1 + 3\sigma_3 < 0 \quad (4.2b)$$

In uniaxial compressive loading, where  $\sigma_3=0$ , Equation 4.2a states that the uniaxial compressive strength (UCS) is 8 times the tensile strength. Although the Griffith energy theory led to the development of fracture mechanics for materials loaded in tension, the theory is not widely used for predicting the rupture of rocks loaded in compression. However, as noted by Hoek (1968), the original Griffith Criterion in compression may provide a practical approximation to fracture initiation.

The crack initiation stresses of four igneous rock types tested over confining stresses ranging from 0 to 60 MPa were compared to the Griffith Criterion given by Equation 4.2. Figure 4.13 shows the four igneous rock types and measured crack initiation. The Griffith Criterion was estimated using the Brazilian tensile strength: Lac du Bonnet granite (8.8MPa), granite (10.5MPa), meta-granodiorite (11.2 MPa) and quartz monzodiorite (11.3 MPa). The Brazilian tensile strength was used, rather than the direct tensile strength because as shown in Figure 4.11,

the stress and hence the energy required to develop tensile cracks in compression is greater than the energy required to develop tensile cracks when subjected to direct tensile loading. Hence for predicting crack initiation in compression, the Brazilian tensile strength appears more appropriate. Examination of Figure 4.13 suggests that the Griffith Criterion generally underestimates the crack initiation stress and this difference increases as the confining stress increases, over the confining stresses measured.

Martin and Christianson (2009) examined a number of in situ experiments in igneous rocks and concluded that the in-situ spalling strength, in the absence of field data, could be approximated using the crack initiation stress from laboratory uniaxial compressive strength tests. In their analysis to establish the risk of spalling, the crack initiation stress was simply used as a strength indicator. More recently, Diederichs et al. (2010) suggested a spalling prediction criterion based on the generalized Hoek-Brown failure envelope, given by (Hoek et al 2002):

$$\sigma_1' = \sigma_3' + UCS \left( m \frac{\sigma_3'}{UCS} + s \right)^a \quad (4.3)$$

Diederichs et al. (2010) suggested that peak spalling prediction criterion could be approximated using the following parameters:

$$a = 0.25 \quad s = (CI/UCS)^{1/a} \quad m = s(UCS/|T|) \quad (4.4)$$

where  $a$ ,  $s$  and  $m$  are Hoek-Brown failure criterion parameters, and  $CI$ ,  $UCS$  and  $T$  are crack initiation stress, unconfined and the tensile strength, respectively. Figure 4.13 compares the Hoek-Brown spalling criterion using the parameters in Equation 4.4 with the Crack Initiation laboratory data. Reasonable agreement was obtained if the  $a$  parameter was changed from a constant value of 0.25 to the Crack Initiation Ratio ( $CIR$ ) for confined tests. Based on these findings the Spalling parameters for igneous rocks can be expressed as

$$a = CIR \quad s = (CI/UCS)^{1/a} \quad m = s(UCS/|T_{BR}|) \quad (4.5)$$

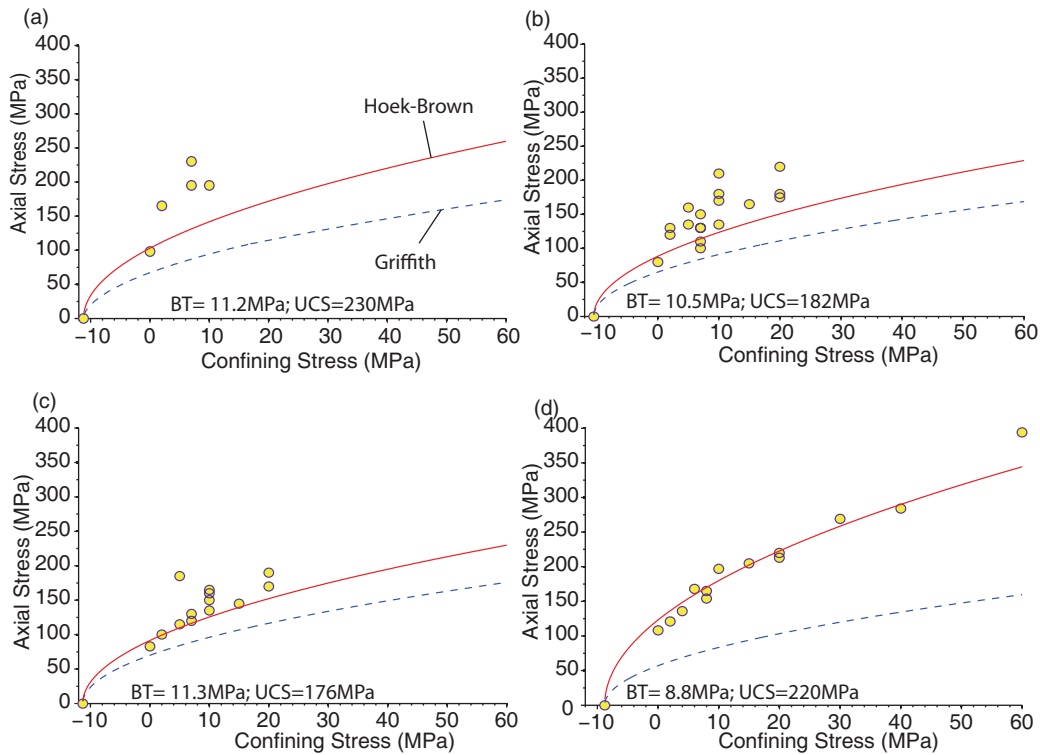


**Figure 4.13: Crack initiation stress from lab measurement, Griffith and Generalized Hoek-Brown failure criteria. (a) metagranodiorite; (b) granite; (c) quartz monzodiorite and (d) Lac du Bonnet granite**

In Figure 4.9, the *CIR* ranged from 0.5 to 0.54, with a mean value of 0.52, and provided much better agreement with the laboratory data. While this test comparison is limited to igneous rocks, the results are encouraging and other rock types are currently being evaluated.

## 4.7. Conclusion

In this paper, the effects of geology and loading conditions on crack initiation stress have been examined using a data base of 336 samples.

In igneous rocks with different mineralogy, the crack initiation stress is positively correlated to quartz and negatively correlated to plagioclase content. Moreover, crack initiation stress in igneous rocks increases as the grain size decreases. In sedimentary rocks, cracks are initiated at higher stress level when the carbonate is increased relative to the clay content.

In high-grade metamorphic rocks, directional anisotropy can also affect the rock strength. The results confirmed the sensitivity of peak stress to the direction of foliation due to the shearing mechanism associated with failure. Because crack initiation occurs due to tensile and extensile rupture, the crack initiation stress is not influenced by this anisotropy.

The means of ratios of crack initiation to peak stress in some igneous, sedimentary and metamorphic rocks, regardless of the mineralogy and grain size, was found to range from 0.42 to 0.47 in uniaxial compression. In triaxial compression, the crack initiation stress ratio ranges from 0.50-0.54. A comparison of the direct tensile strength with the Brazilian tensile strength was carried out for igneous rocks. The results indicate that direct tension tensile strength is 0.78 times the Brazilian tensile strength.

Finally, the Griffith and Hoek-Brown spalling parameters are compared with the crack initiation results from uniaxial and triaxial compression tests. Although the Griffith Criterion is in reasonable agreement with the crack initiation stress in uniaxial compression, it underestimates cracks initiation in triaxial compression. The crack initiation parameters for the Hoek-Brown spalling criterion for igneous rocks can be expressed in terms of the CI stress ratio and the tensile strength.

#### Acknowledgements

The authors wish to acknowledge the support of the Natural Science and Engineering Research Council of Canada, the Swedish Nuclear Fuel and Waste Management Co, and the Nuclear Waste Management Organization, Toronto.

## 4.8. References

- Adl-Zarrabi, B., 2006, Forsmark Site investigation- Borehole KFM01A, KFM01C, KFM01D, KFM04A, KFM05A, KFM06A and KFM09A: Thermal properties of rocks using calorimeter and TPS method, and mineralogical composition by modal analysis: P-06-233.
- Andersson, J., Ahokas, H., Hudson, J. A., Koskinen, L., Luukkonen, A., Löfman, J., Keto, V., Pitkänen, P., Mattila, J., Ikonen, Ari T. K., Ylä-Mella, M., 2007, Olkiluoto Site Description 2006: Posiva 2007-03.
- Andersson, J.C., and Martin, C.D., 2009, The Äspö pillar stability experiment: Part I—Experiment design: *International Journal of Rock Mechanics and Mining Sciences*, v. 46, no. 5, p. 865-878.
- Ashby, M.F., and Sammis, C.G., 1990, The damage mechanics of brittle solids in compression: *Pure and applied geophysics*, v. 133, no. 3, p. 489-521.
- ASTM, 1996, Standard test method for splitting tensile strength of intact rock core specimens: D3967-95a.
- Barker, A.J., 1998, *Introduction to metamorphic texture*: Cheltenham, United Kingdom, Stanley Thornes Ltd, 264 p.
- Bieniawski, Z.T., 1967, Mechanism of brittle fracture of rock: Part I—theory of the fracture process: *International Journal of Rock Mechanics and Mining Sciences & Geomechanics Abstracts*, v. 4, no. 4, p. 395-404, IN11-IN12, 405-406.
- Brace, W.F., Paulding, B., and Scholz, C., 1966, Dilatancy in the fracture of crystalline rocks: *Journal of Geophysical Research*, v. 71, p. 3939-3953.

- Brown, E.T., editor, 1981, Rock characterization, Testing and monitoring, ISRM suggested methods: Oxford, Pergamon Press.
- Collins, D.S., and Paul Young, R., 2000, Lithological controls on seismicity in granitic rocks: Bulletin of the Seismological Society of America, v. 90, no. 3, p. 709-723.
- Damjanac, B., and Fairhurst, C., 2010, Evidence for a Long-Term Strength Threshold in Crystalline Rock: Rock Mechanics and Rock Engineering, p. 1-19.
- Diederichs, M.S., 2007, The 2003 Canadian Geotechnical Colloquium: Mechanistic interpretation and practical application of damage and spalling prediction criteria for deep tunneling: Canadian Geotechnical Journal, v. 44, p. 1082-1116.
- Diederichs, M.S., Carter, T., Martin, C.D., 2010, Practical rock spall prediction in tunnel, *in* World Tunnelling Congress, Vancouver, Canada
- Eloranta, P., 2006, Laboratory Testing of Gneissic Rocks in Olkiluoto Borehole OL-KR24: Working report: 2006-80.
- Fairhurst, C., and Hudson, J.A., 1999, Draft ISRM suggested method for the complete stress-strain curve for intact rock in uniaxial compression: International Journal of Rock Mechanics and Mining Sciences, v. 36, no. 3, p. 279-289.
- Frizzel, R., Cotesta, L., and Usher, S., 2008, OPG's deep geologic repository for low & intermediate level waste: Phase I- Regional geology, Southern Ontario: OPG 00216-REP-01300-00007-R00.
- Gorski, B., Anderson, T., and Conlon, B., 2009a, Laboratory Geomechanical Strength Testing of DGR-1 & DGR-2 Core: TR-07-03.

- Gorski, B., Anderson, T., and Conlon, B., 2009b, Laboratory geomechanical strength testing of DGR-3 and DGR-4 core: TR-08-24.
- Griffith, A.A., 1921, The Phenomena of Rupture and Flow in Solids: Philosophical Transactions of the Royal Society of London. Series A, v. 221, p. 163-198.
- Griffith, A.A., 1924, Theory of rupture, *in* Proceedings of the First International Congress of Applied Mechanics: Delft, p. 55-63.
- Hoek, E., 1968, Brittle failure of rock, *in* Rock Mechanics in Engineering Practice: eds K.G. Stagg and O.C. Zienkiewicz, 99-124. London: Wiley
- Hoek, E., and Bieniawski, Z.T., 1966, Fracture propagation mechanism in hard rock, *in* First congress of the international society of rock mechanics, p. 243-249.
- Hoek, E., and Brown, E.T., 1980, Underground excavations in rocks: London, Institution of Mining and Metallurgy.
- Holcomb, D.J., 1993, General theory of the Kaiser effect: International Journal of Rock Mechanics and Mining Sciences & Geomechanics Abstracts, v. 30, no. 7, p. 929-935.
- Jacobsson, L., 2007, Oskarshamn site investigation- Borehole KLX16A: Uniaxial compression test of intact rock: P-07-143.
- Jacobsson, L., 2006a, Forsmark site investigation: Borehole KFM09A-Uniaxial compression test of intact rock: P-06-27.
- Jacobsson, L., 2006b, Oskarshamn site investigation- Borehole KLX10: Uniaxial compression test of intact rock: P-06-37.

- Jacobsson, L., 2005, Oskarshamn site investigation- Borehole KLX03A: Uniaxial compression test of intact rock: P-05-90.
- Jacobsson, L., 2004a, Forsmark site investigation- Borehole KFM02A: Uniaxial compression test of intact rock: P-04-224.
- Jacobsson, L., 2004b, Forsmark site investigation- Borehole KFM03A: Uniaxial compression test of intact rock: P-04-225.
- Jacobsson, L., 2004c, Forsmark site investigation- Borehole KFM04A: Uniaxial compression test of intact rock: P-04-226.
- Kärki, A., and Paulamäki, S., 2006, Petrology of Olkiluoto: Posiva 2006-02.
- Lahti, M., Engström, J., Mattila, J., et al., 2010, Geological Model of the Olkiluoto Site: 2010-70.
- Lajtai, E.Z., 1974, Brittle fracture in compression: *International Journal of Fracture*, v. 10, no. 4, p. 525-536.
- Lau, J.S.O., and Gorski, B., 1992, Uniaxial and triaxial compression tests on URL rock samples from boreholes 207-045-GC3 and 209-069-PH3: Divisional Report MRL 92-025(TR).
- Lavrov, A., 2001, Kaiser effect observation in brittle rock cyclically loaded with different loading rates: *Mechanics of Materials*, v. 33, no. 11, p. 669-677.
- Lockner, D., 1993, The role of acoustic emission in the study of rock fracture: *International Journal of Rock Mechanics and Mining Sciences & Geomechanics Abstracts*, v. 30, no. 7, p. 883-899.
- Martin, C.D., 1997, Seventeen Canadian Geotechnical Colloquium: the effect of cohesion loss and stress path on brittle rock strength: *Canadian Geotechnical Journal*, v. 34, p. 698-725.

- Martin, C.D., and Chandler, N.A., 1994, The progressive fracture of Lac du Bonnet granite: *International Journal of Rock Mechanics and Mining Sciences & Geomechanics Abstracts*, v. 31, no. 6, p. 643-659.
- Martin, C.D., and Christiansson, R., 2009, Estimating the potential for spalling around a deep nuclear waste repository in crystalline rock: *International Journal of Rock Mechanics and Mining Sciences*, v. 46, no. 2, p. 219-228.
- Martin, C.D., and Stimpson, B., 1994, The effect of sample disturbance on laboratory properties of Lac du Bonnet granite: *Canadian Geotechnical Journal*, v. 31, no. 5, p. 692-702.
- Muijs, D., 2004, Bivariate analysis: looking at the relationship between two variables. *in* *Doing Quantitative Research in Education with SPSS*: London, UK, SAGE Publications Ltd.
- Nicksiar, M., and Martin, C. D. (2012). "Evaluation of Methods for Determining Crack Initiation in Compression Tests on Low-Porosity Rocks." *Rock Mechanics and Rock Engineering*, 45(4), 607-617.
- Peterson, J., Berglund, J., Danielsson, P., et al., 2004, Forsmark site investigation: Petrography, geochemistry, petrophysics and fracture mineralogy of boreholes KFM01A, KFM02A and KFM03A+B: P-04-103.
- RESPEC Co, 2010, Laboratory testing of amphibolite and rhyolite from 4850 level of DUSEL facility: RSI-2100.
- Rojat, F., Labiouse, V., Kaiser, P.K., and Descoeurdes, F., 2009, *Brittle Rock Failure in the Steg Lateral Adit of the Lötschberg Base Tunnel*, Springer Wien 42, 341 p.
- Saari, J., 2008, *Seismicity in the Olkiluoto Area: 2008-04*.
- Schandl, E., 2009, *Petrography of DGR-1 and DGR-2 cores: TR-07-12*.

- Stephen, M.B., 2010, Forsmark site investigation: Bedrock geology- overview and excursion guide: R-10-04.
- Stephen, M.B., Fox, A., La Pointe, P., Simenov, A., Isaksson, H., Hermanson, J., and Ohman, J., 2007, Geology Forsmark- Site descriptive modelling Forsmark stage 2.2: R-07-45.
- Strahle, A., 2001, Definition och beskrivning av parametrar för geologisk, geofysisk och bergmekanisk kartering av berg: R-01-19.
- Streckeisen, A., 1976, To each plutonic rock its proper name: Earth-Science Reviews, v. 12, no. 1, p. 1-33.
- Thompson, B., Young, R., and Lockner, D., 2006, Fracture in Westerly Granite under AE Feedback and Constant Strain Rate Loading: Nucleation, Quasi-static Propagation, and the Transition to Unstable Fracture Propagation, Birkhäuser Basel 163, 995 p.
- Wahlgren, C., 2010, Oskarshamn site investigation: Bedrock geology-overview and extrusion guide: R-10-05.
- Wahlgren, C., Curtis, P., Hermanson, J., Forsberg, O., Ohman, J., Fox, A., and La Pointe, P., 2008, Geology Laxemar: Site descriptive modelling SDM-Site Laxemar: R-08-54.

# Chapter 5. Factors affecting crack initiation in low porosity crystalline rocks<sup>8</sup>

## 5.1. Introduction

It is well known that the microstructure of a rock should be taken into account when determining its compressive strength. To minimize its influence on the test results, the ISRM “Suggested Methods for Determining the Uniaxial Compressive Strength and Deformability of Rock Materials states that the test specimen shall be right cylinders having a height to diameter ratio of 2.5-3.0 and a diameter preferably of not less than 54 mm.” The method then states that the diameter of the specimen should be greater than 10 times the largest mineral grain in the rock (Brown 1981). Presumably the latter requirement ensures that the right-cylinder sample statistically captures the flaws that are typically associated with grain boundaries. The effect of flaw size on compressive strength was examined by Cook (1963). Using the energy approach of Griffith (1921, 1924), Cook (1963) showed that the compressive strength was proportional to the flaw size and as the flaw size increased the compressive strength decreases. The effect of grain size on the strength of rocks has been studied using anhydrite, dolomite and granite by Skinner (1959), Olsson (1974) and Prikryl (2001), respectively. These authors found that as the grain size increased the uniaxial compressive strength decreases, supporting the theory proposed by Cook (1963) and the requirements of the ISRM Suggested Methods, assuming that the grain boundary can be considered as a flaw. While, it appears that the compressive strength is influenced by grain size, there are few studies on the effect of grain size on other stress levels during laboratory compression testing.

---

<sup>8</sup> A version of this chapter has been submitted as a Paper to the journal of Rock Mechanics and Rock Engineering

Brace (1964) and Bieniawski (1967) using laboratory tests that monitored the local axial and lateral strains carried out detailed analyses of the stress-strain response as the compression load was applied. They clearly showed that microcrack growth is initiated at stress magnitudes well below the peak compressive strength. The early work of Brace (1964) showed that in laboratory samples loaded in compression, dilatancy occurred at approximately 50% of the peak compressive load. This dilatancy stress, which today is referred to as the crack initiation (CI) stress, was found by Brace (1964) to range between 1/3 and 2/3 of the peak strength for a wide range of rock types. More recently Nicksiar and Martin (Submitted) showed that crack initiation was observed in all 376 samples of low porosity rocks tested in compression.

**Figure 5.1: Crack initiation (CI) stress versus uniaxial compressive strength (UCS) for low porosity igneous, sedimentary and metamorphic rocks. Regression line and its 95% confidence interval are shown as solid and dashed line, respectively**

Figure 5.1 shows a summary of the igneous, sedimentary and metamorphic rock data used by Nicksiar and Martin (Submitted) in their study. As shown in Figure 5.1 the relationship of the crack initiation stress to the uniaxial compressive strength (UCS) is linear, despite the wide range of UCS values from 15 MPa to 370 MPa. If grain size affects the peak strength, as discussed above, then it is also likely that grain size should affect the crack initiation stress.

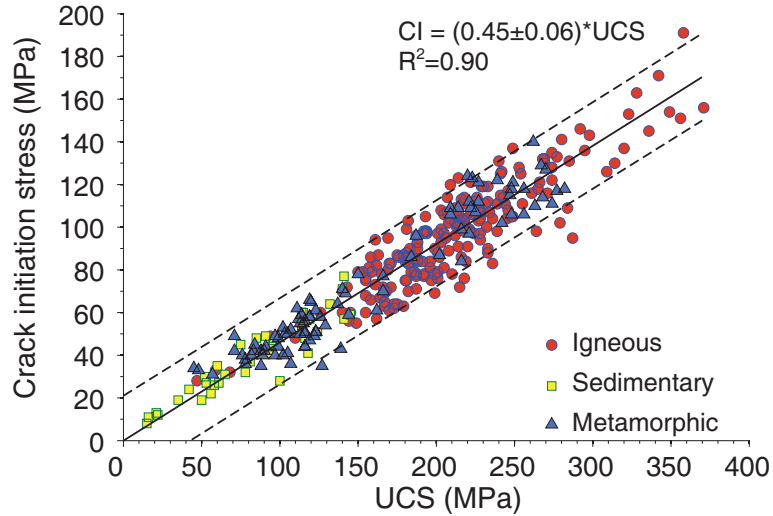


**Figure 5.1: Crack initiation (CI) stress versus uniaxial compressive strength (UCS) for low porosity igneous, sedimentary and metamorphic rocks. Regression line and its 95% confidence interval are shown as solid and dashed line, respectively**

The rocks used to establish Figure 5.1, had grain sizes ranging from microns to centimetres. Despite this orders of magnitude range in grain size, the crack initiation stress to uniaxial compressive strength ratio (CIR) remained well constrained at approximately  $0.45 \pm 0.06$ , supporting the early findings of Brace (1964). It would appear that grain size might not be a significant factor in controlling CIR. Similarly the effect of material and geometry heterogeneities would also appear not to significantly impact CIR. In this study, a grain-based discrete element numerical model is used to examine the effect of grain size, material and geometry heterogeneities on crack initiation stress and CIR. The work of Stacey (1981), Read et al. (1998), Martin et al. (1999), Read (2004), Diederichs (2007), Andersson et al. (2009), and Martin and Christiansson (2009) showed that crack initiation stress from laboratory tests is a relevant parameter when evaluating the potential for spalling around underground openings. Hence if this laboratory parameter is needed for assessing the stability of underground openings, it is important to understand the factors that affect its magnitude.

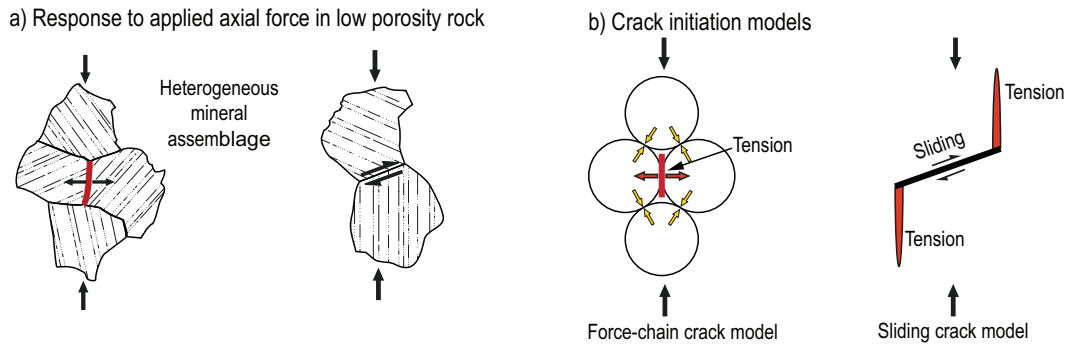
## **5.2. Crack initiation models in compression loading**

The cracking of mineral grains associated with axial compressive loading has been studied extensively over the past several decades. One of the consistent findings from such studies is that the majority of the cracks are oriented within  $\pm 15^\circ$  from the loading direction (Brace et al. 1966, Hallbauer et al. 1973; Lajtai 1974). There are two basic models to explain this observation (see Figure 5.2): (1) the Sliding-crack model (Nemat-Nasser and Horii 1982, Nemat-Nasser and Obata 1988, Ashby and Hallam (Née Cooksley) 1986), and (2) the Force-chain crack model (Potyondy and Cundall 2004, Cho et al. 2007). Inspection of the models in **Error! Reference source not found.** illustrates an important fundamental difference in the concepts used by the two models. With the Sliding-crack model, a suitably oriented weak plane must exist and sliding along this weak plane must occur before the local tensile stresses are adequate to initiate and grow the axially aligned fractures. The Force-chain crack model however, does not require this weak plane to exist or the initial sliding to occur. The heterogeneous nature of the mineral assemblage in low porosity rocks is adequate in the Force-chain crack model to create local tensile stresses that are sufficient to form the cracks. Clearly, these two models represent very different fundamental concepts for cracking in low porosity rocks. The Sliding-crack model implies that in compressive loading, rock is weaker in shear than in tension since sliding must occur first before tensile cracking can occur. The Force-chain crack model however implies that rock is weakest in tension, and as shown by Potyondy and Cundall (2004) and Cho et al. (2007), once a sufficient number of tensile cracks form, a macroscopic shear fracture will naturally develop.

To investigate which crack model in Figure 5.2 is more applicable for describing crack initiation observed in low porosity rocks, a sample of Lac du Bonnet granite was subjected to a number of monotonically load-unload cycles (Figure 5.3a). The axial stress was increased from an initial 175 MPa to 198 MPa using 4 load steps with approximately 10 cycles for each load step (Figure 5.3b).

This test followed the procedure given by Martin and Chandler (1994) where interpreted axial and lateral strains provided the permanent axial and lateral strain with each cycle. The uniaxial compressive strength of Lac du Bonnet granite is

approximately 220 MPa, and the crack initiation stress is approximately 120 MPa (Lau and Chandler 2004). Hence the initial load step of 175 MPa is well above the crack initiation stress.



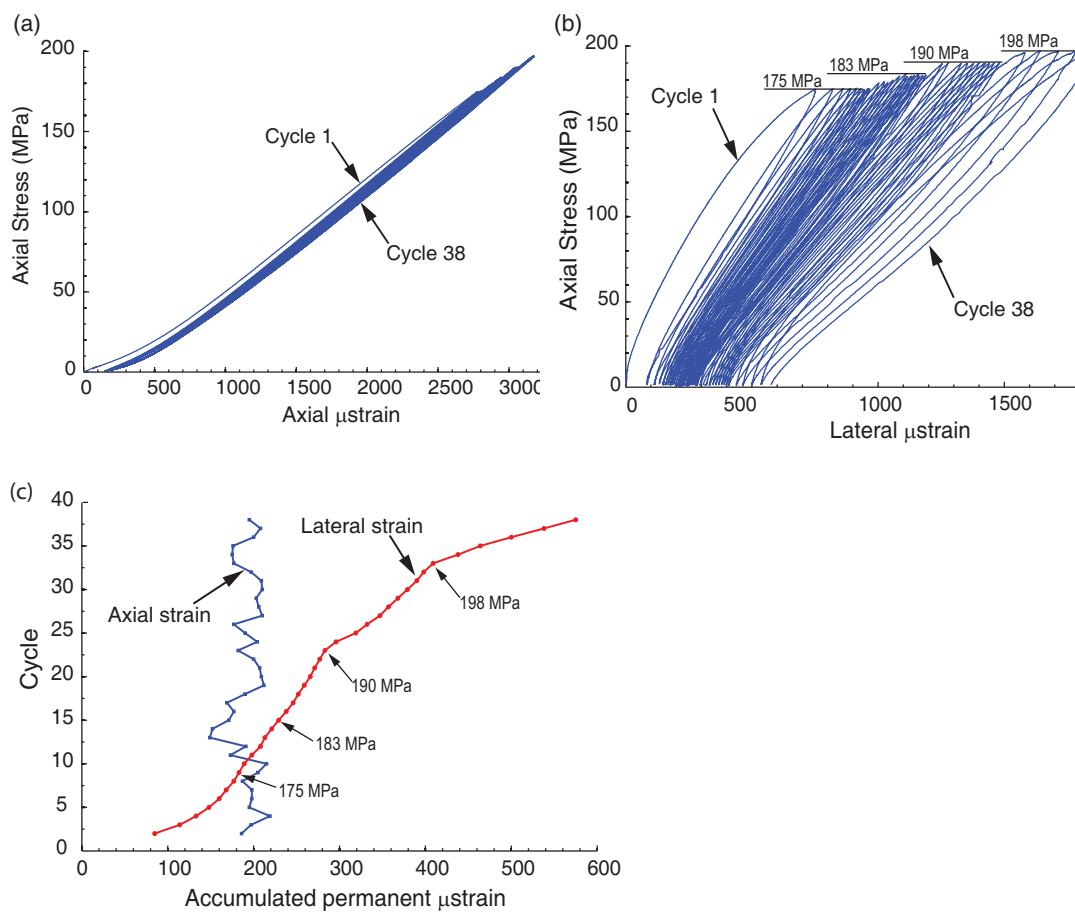
**Figure 5.2: Two models commonly used to explain crack initiation observed in laboratory tests.**

Figure 5.3c shows the accumulated permanent axial and lateral strain for each cycle. The accumulated axial strain shows essentially no increase for all 38 cycles despite the load increasing from 175 MPa to 198 MPa. This is consistent with the axial stress versus axial strain response shown in Figure 5.3a. The accumulated permanent lateral strain in Figure 5.3b however shows a gradual increase in strain with each cycle. Figure 5.3c also shows that the accumulated lateral strain increases as the load is increased, particularly when the load step exceeds 190 MPa. These results show that the permanent damage in the sample is only a function of lateral strain, regardless of the applied load.

Inspection of the initial stress-strain response in Figure 5.3a shows that the sample tested contains initial cracks, indicated by the nonlinear stress strain response in the early stages of loading. As noted by Martin and Stimpson (1994), this is a common phenomenon in low porosity rocks, and is attributed to naturally occurring and/or stress-induced microcracking. It is likely that slip could occur along some of these cracks, assuming they were optimally oriented. Despite the presence of these micro-cracks, which may be adequate to cause the nonlinear

axial strain response, there is no evidence that axial slip occurs. Thus the sliding-crack model, which would require permanent axial strains is not supported by this data and hence not linked to crack initiation.

Bieniawski (1967) was one of the early researchers to suggest that the long-term strength of rock was the stress associated with volumetric strain reversal and coined the term “unstable fracture propagation” (unstable crack growth in Figure 5.4a). This inflection point in the stress-strain curve marks the beginning of significant increase in crack density (Hallbauer et al. 1973).



**Figure 5.3: Comparison of measured axial and lateral strain in a uniaxial compression tests subjected to 38 load-unload cycles. (a) Axial strain for 38 load-unload cycles; (b) Lateral strain for 38 load-unload cycles; and (c) Permanent axial and lateral strain for 38 load-unload cycles**

Two load cycles were examined to assess the crack model likely associated with the unstable crack growth. The 183 MPa and 190 MPa load cycles were chosen as the formation of unstable crack growth initiated in the 183 MPa cycle and significantly propagated in the 190 MPa cycle (Figure 5.4a). The volumetric strain plots in Figure 5.4a have been purposely offset to clearly show both graphs. This offset does not affect the axial stress of 179 MPa associated with the unstable crack growth. The axial strain and lateral strain for the 190 MPa volumetric strain in Figure 5.4a were analyzed separately to determine the incremental slope of axial strain and lateral strain response. The slope was determined by carrying out a linear least squares fit and the results are shown in Figure 5.4b. It is clear from Figure 5.4b that there is no change in the axial strain response even at the initiation of the unstable crack growth and beyond. However, the lateral strain shows a marked change in response in the region of the stress associated with unstable crack growth. The slope of the lateral strain plot in Figure 5.4b suggests that unstable crack growth initiated before the stress associated with volumetric strain reversal at an axial stress of 175 MPa. Again the data suggest that the Force-chain crack model better describes the damage mechanism associated with the initiation and propagation of unstable crack growth than the Sliding-crack model.

The measured stress-strain response of laboratory samples subjected to compressive loading suggests that the Sliding-crack model is not an appropriate modelling approach for simulating early stage cracking in low porosity rocks. The measured stress-strain response of the onset of crack initiation to beyond unstable crack growth supports the concepts introduced by the Force-chain crack model, i.e., mineral heterogeneity alone is adequate to create tensile stresses sufficient to initiate cracking.

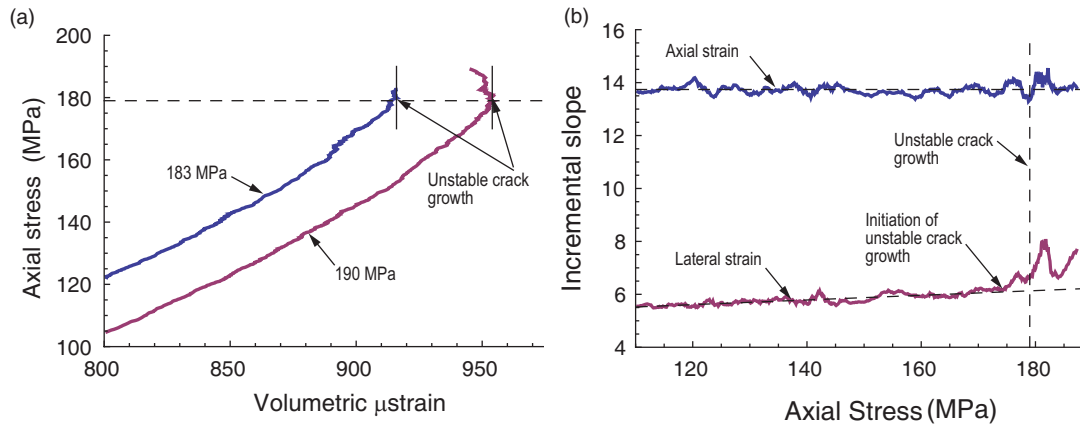


**Figure 5.4: Comparison of volumetric strain reversal when applied stress is 183 MPa and 190 MPa, and slope of the axial and lateral strain for 190 MPa. (a) Volumetric strain reversal (b) Slope of axial and lateral strain for 190 MPa**

### 5.3. UDEC modeling of brittle failure in intact rocks

In 1979, Cundall and Strack (1979) proposed a Discrete Element Method for modelling discrete spheres of random size. This approach was used by Potyondy et al. (1996) to develop the Bonded Particle Method (BPM) for modelling of intact rock. In the BPM, the intact behaviour is calculated by the mechanical response of distinct circular discs or spheres, which incorporates the elements of the force-chain contact model. Cho et al. (2007) showed that the proposed BPM by Potyondy et al. (1996) could not capture the stress-strain response of intact rock without modification. They used a clumping technique to represent the polygonal structure/geometry commonly found in rocks and showed that with this polygonal structure the BPM could capture the behaviour of intact rock in compression. Since 2007, Lan et al. (2010) showed that an efficient means of representing the polygonal structure of intact mineral assemblages could be achieved using the discrete element formulation in the Universal Distinct Element Code (UDEC, Cundall 1980). In UDEC, a Voronoi tessellation approach is used to partition the domain into polygons of pre-defined edge length and size distribution. These polygons represent individual mineral grains. Unlike the BPM, in UDEC the mineral grains represented by the individual polygons cannot break, i.e., all rupture must follow polygonal boundaries. This UDEC limitation has

implications for the post-peak response but as noted by Tapponnier and Brace (1976) the pre-peak response is dominated by grain-boundary cracking.

The UDEC methodology of force interaction of the blocks and the contacts is the same as with the BPM method, except that the contacts are not *point contact* but both *point and area contacts*. The force-displacement of the contacts is determined by normal and shear stiffness along the contact. The contact tensile strength, cohesion and friction are defined according to the selected constitutive contact model and the contact fails in tension or shear when the stress exceeds the contacts' strength.

### **5.3.1. Model setup**

The primary focus of the UDEC modelling is to establish the effect of the various input parameters on crack initiation during compressive loading. In UDEC, the initiation of microcracks occurs due to the rupture along the polygon boundaries and hence tracking the rupture of these grain boundaries can be used to identify the onset of cracking (Lan et al. 2010). The laboratory properties of a medium-grained granite were used to calibrate the model, however, an exact match to the peak stress-strain response is not necessary due to the comparative nature of this study for crack initiation. In most models, one property was changed while other properties are held constant in order to find the effect of the changed parameter on the crack initiation stress.

The UDEC models are 51mm x128mm and all models are bounded at the top and bottom by the steel loading platens. The Voronoi tessellation is then applied to discretize the model into finite difference zone representing the mineral grains based on the target grain size (see Appendix 3). The mechanical behaviour of the model is controlled by parameters that can be divided into two groups (Christianson et al. 2006):

1. parameters that control the sample's unconfined compressive strength: cohesion and friction angle
2. parameters that control the sample's elastic constants: bulk and shear modulus of the grains as well as normal and shear stiffness of the polygonal contacts

The load is applied to the sample by uniform velocity in y-direction over the top platen with the bottom platen remaining fixed. Cundall and Strack (1979) examined the effect of various loading rates and recommended a loading rate that keeps the internal unbalanced forces low compared to the contact forces. The velocity of  $2 \times 10^{-2}$  m/s, meets Cundall's recommendation for the sample size used.

A sampling area (51mm x 10mm) at the middle of the sample where the stress distribution is expected to be relatively uniform was used to simulate strain gauges in laboratory testing (Figure 5.5). The lateral and axial strains are calculated using the average displacement in x and y directions at several locations in this sampling area to monitor the sample response. The stress-strain response of the blocks and contacts are calculated using UDEC built-in commands.

### ***5.3.2. Block constitutive model***

Crack initiation in laboratory samples occurs well before peak stress is obtained. At these low loads cracking is expected to occur along the grain boundaries as the mineral grains deform elastically. Consequently, an *elastic* constitutive block model is used to track the behaviour of the grains. In the *elastic* constitutive model, the required parameters are density, bulk and shear modulus. The overall elastic constants of the model-sample will be the average values of its rock forming minerals calibrated to the laboratory results.

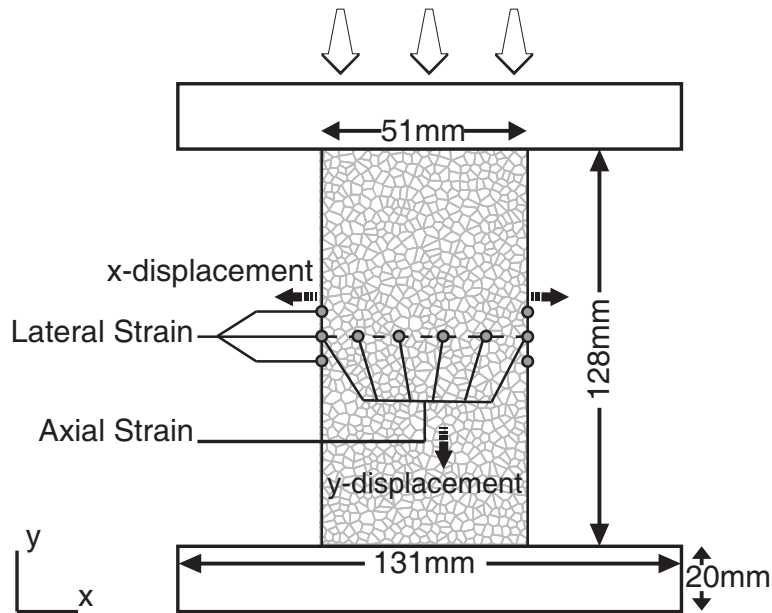


**Figure 5.5:** Axial and lateral strains are recorded at the locations shown to monitor the sample response

### 5.3.3. Contact constitutive model

The contact behaviour used a *Coulomb slip model with residual strength properties*. The initial contact cohesion and friction values were based on those values reported in laboratory tests reports (Glamheden et al. 2007). The contacts are assumed to instantly lose their cohesion and friction to their residual values once failure occurs.

The normal and shear stiffness values for the contacts were obtained by calibrating to the laboratory test results. Different contact shear to normal stiffness ratios have been reported by several authors using different DEM methods. Diederichs et al. (2004) used the ratio of 0.4 for Lac du Bonnet granite in BPM model. Lan et al. (2010) used the ratio of 0.67 for Lac du Bonnet in their UDEC model. In this study, the contact shear stiffness was set to 0.6 of the normal stiffness. Table 5.1 gives the contact and block properties used to establish the macroscale response of the UDEC sample.

## 5.4. Crack initiation stress

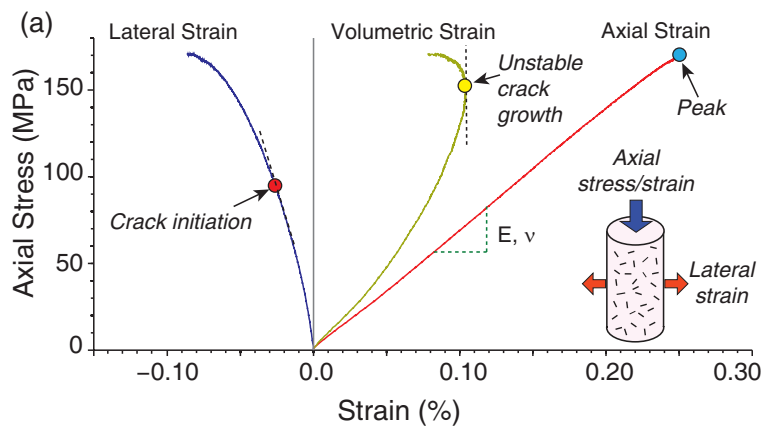
Crack initiation in laboratory compression tests is noted as the first stage of stress-induced damage in low-porosity rocks (Figure 5.6a). Nicksiar and Martin (2012) reviewed the various methods that have been proposed for identifying crack initiation and concluded that statistically, all methods identify acceptable crack-initiation values. The Lateral Strain Response (LSR) method was proposed by Nicksiar and Martin (2012) for laboratory stress-strain results and was found to be a relatively robust method that only relied on the lateral strain response. In numerical models, tracking the rupture of the grain contacts can identify crack initiation.

**Table 5.1: Material Properties used in the UDEC models. The bulk and shear modulus as well as normal and shear stiffness are changed in the mineral based models.**

<b>Contact Properties</b>							
Normal stiffness (GPa/m)	Shear stiffness (GPa/m)	Cohesion (MPa)	Friction angle (deg)	Tensile strength (MPa)	Dilation angle (deg)	Residual cohesion (MPa)	Residual friction (deg)
43428	26056	42	57.5	18	0	2	30
<b>Block Properties</b>							
Bulk Modulus (GPa)	Shear Modulus (GPa)	Density (kg/m <sup>3</sup> )					
45	30	2630					
<b>Platen Properties</b>							
Bulk Modulus (GPa)	Shear Modulus (GPa)	Density (kg/m <sup>3</sup> )					
160	79	7750					

Diederichs et al. (2004) used changes in Poisson's ratio to identify the initiation of the cracking in their BPM modelling of Lac du Bonnet granite and found that this approach gave similar results to laboratory tests.

In order to detect crack initiation in the UDEC models two methods have been used: (a) Poisson's ratio changes (Diederichs et al. 2004) and (b) Lateral Strain Response (LSR, Nicksiar and Martin 2012). In addition to these methods, the rupture of grain contacts (cracks) was also tracked. Since each UDEC sample may have a unique number of polygons, the number of cracks was normalized to the total number of grain boundaries.



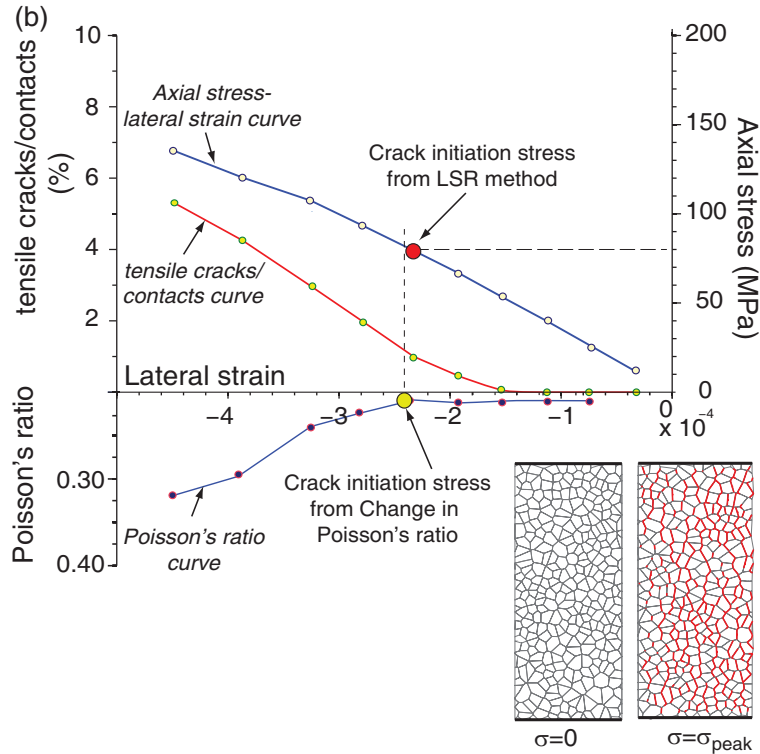


**Figure 5.6: Comparison of the crack initiation stress in a laboratory compression test and the methods used to establish crack initiation stress in the UDEC Model. (a) Stress strain response and crack initiation in a laboratory test; (b) Crack initiation in the UDEC model**

## 5.5. Modelling approach used to assess the effect of heterogeneity

The objective of the study was to establish the effect of heterogeneity caused by: (1) grain size distribution; (2) average grain size and (3) mineralogy, on initiation of cracking in the numerical samples. A total of 20 models were evaluated and crack initiation and peak stress were recorded for each model.

## 5.6. Grain size distribution

The first group of models evaluated the effect of grain size distribution. In these models, the average grain size resembles fine-medium to medium grained granite (1-2mm) and the random seed number for the Voronoi tessellation for all three models remained constant to generate a similar distribution of grains. The sorting

coefficient ( $S_o$ ) introduced by Trask (1932) has been used to describe the degree of uniformity in the grain size distribution. The coefficient is defined as:

$$S_o = \sqrt{Q_{25\%} / Q_{75\%}} \quad (5.1)$$

where  $Q_{25\%}$  and  $Q_{75\%}$  corresponds to the diameter which 25% and 75% of the grains are coarser than this diameter on the grain size cumulative frequency plot. As the sorting coefficient approaches 1, the grain size distribution becomes more uniform. Four models were generated with  $S_o$  values ranging from 1.03 to 1.5 and these are illustrated in Figure 5.7. While the models with  $S_o$  1.03 to 1.14 were created using the built in functionality within UDEC 5.0, the model with  $S_o=1.5$  was created using the methodology described by Lan et al. (2010). The grain size distribution for each model was calculated using the MATLAB image processing tools

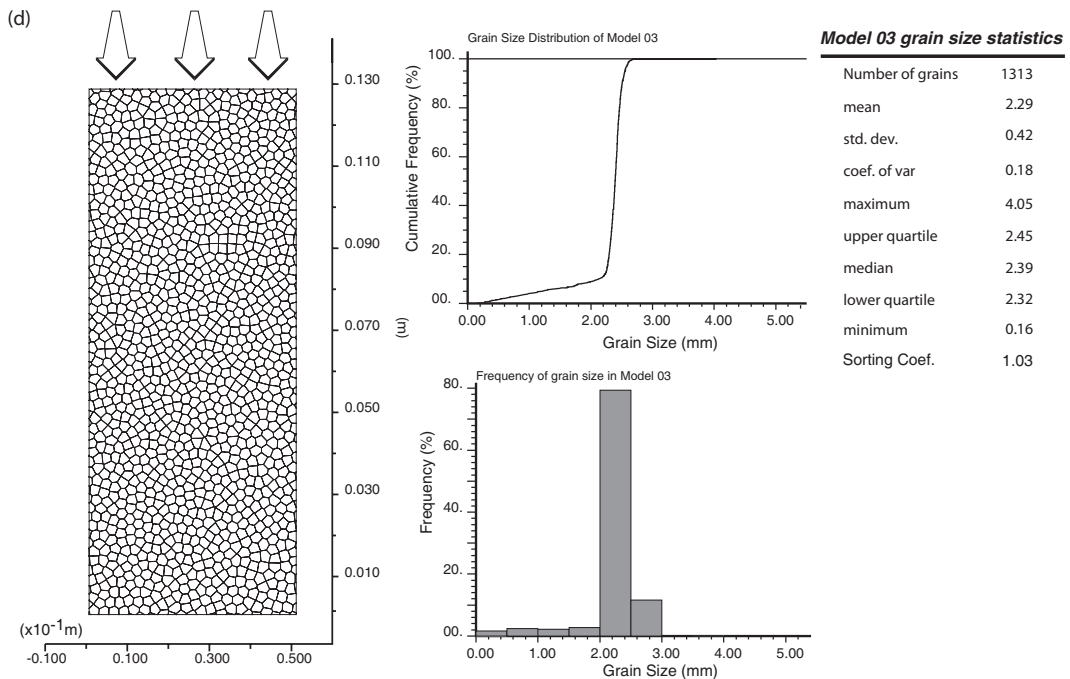
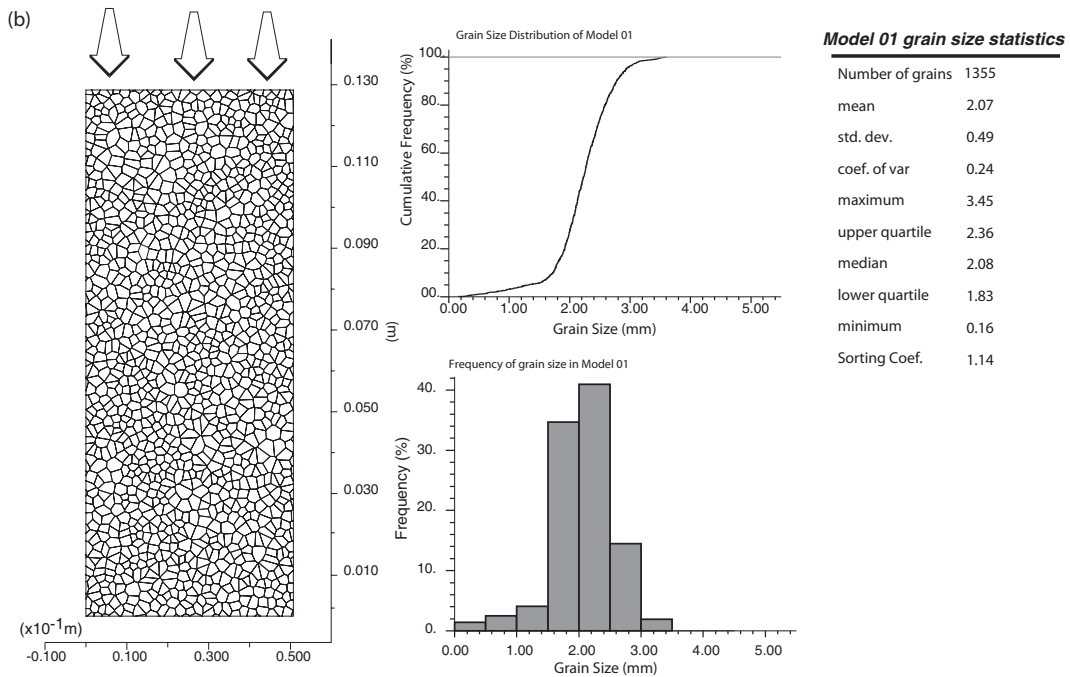
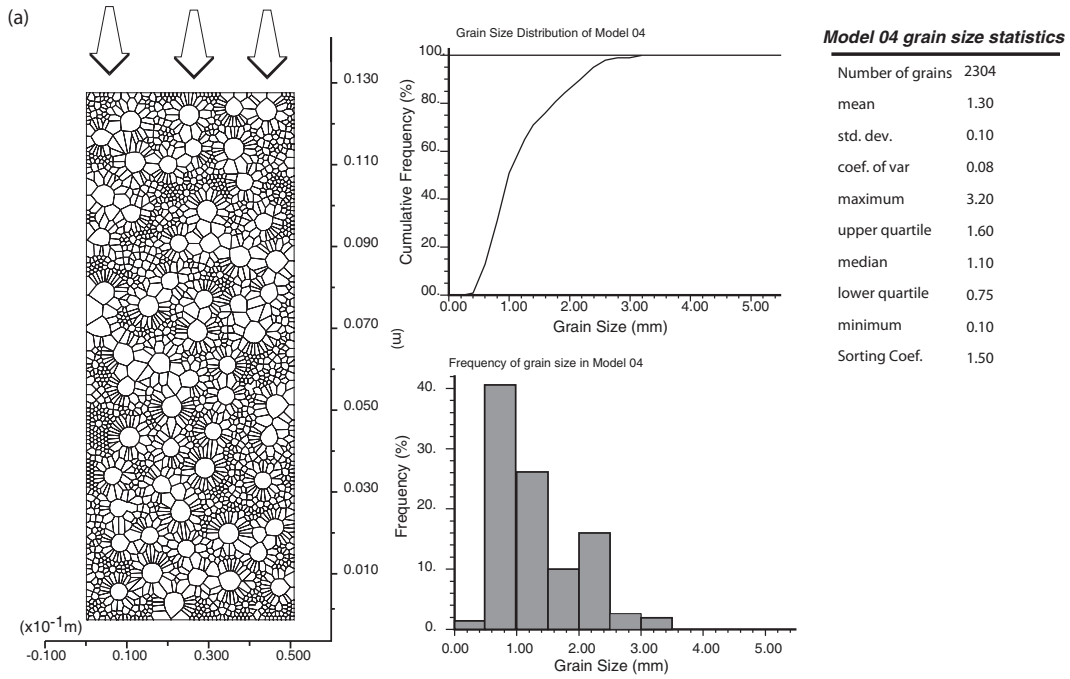
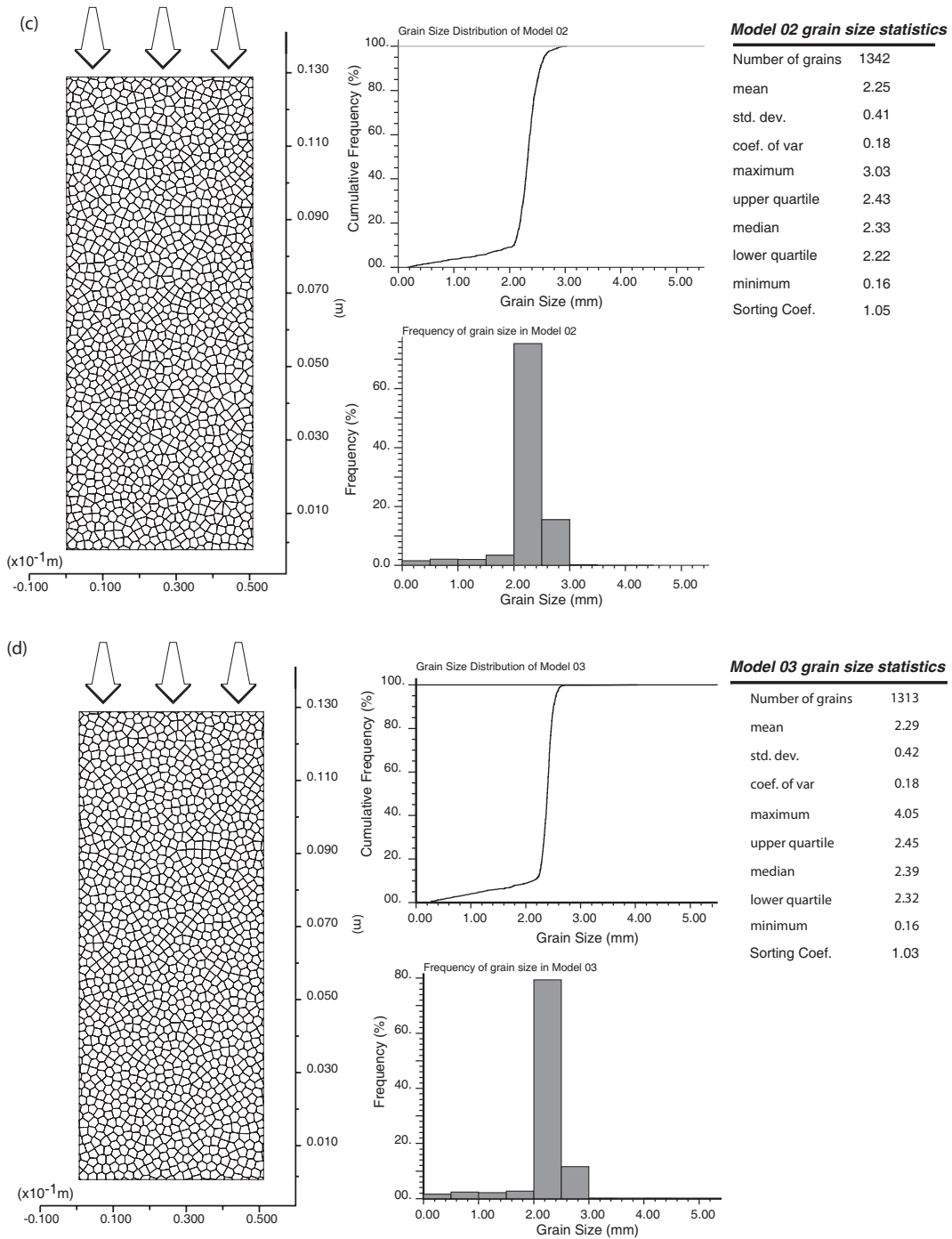


Figure 5.7. These models represent grain size distributions ranging from uniform ( $S_o=1.03$ ) to heterogeneous ( $S_o=1.5$ ).





**Figure 5.7: Grain size distribution of the models with different sorting coefficient. The uniformity of the grain size increases from (a) to (d)**

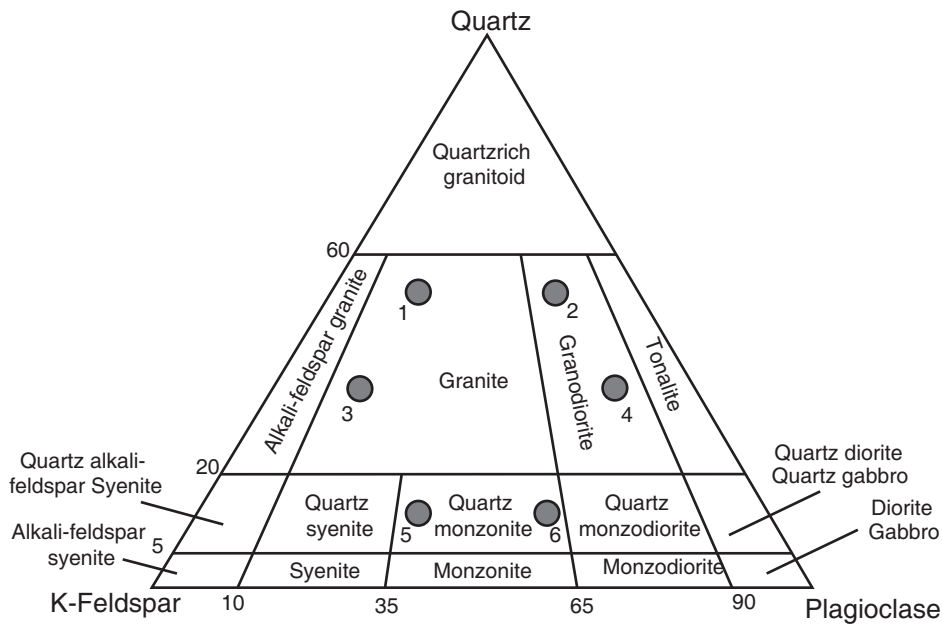
## 5.7. Grain size

Three numerical samples each with different average grain size and uniform grain size distribution ( $S_o = 1.03$ ) were used to examine the effect of grain size on crack initiation. Three models with fine (0.75mm), fine to medium (1.5mm) and medium grained (2.25mm) specimens were designed with  $S_o$  equals to 1.03. The computational time required to complete each model increased dramatically as the average grain size decreased. Despite this increase in run times the overall dimensions of the models were unchanged.

## 5.8. Mineralogy

The last group of numerical models examined the effect of mineralogy. All the previous models have been created using the grain properties mentioned in Table 5.1. In the next groups of models, the properties of different igneous rock forming minerals, i.e. quartz, K-feldspar and plagioclase, were assigned randomly to the grains according to a target rock composition (Figure 5.8) using the mineral properties given in Table 5.2. All the geometric parameters are kept constant using the same uniform grain size distribution ( $S_o = 1.03$ ) and the average grain size of 2.25 mm (medium grain size). The mineral heterogeneity was applied to the models in several steps:

1. The location of each grain's centroid was measured using MATLAB image processing tool.
2. The mineral types were assigned randomly to meet the mineral content percentages shown in Figure 5.8.
3. The mineral properties were imported into the UDEC model via a FISH code that reads the location data file from Step 2 (see Appendix 3).



	Model 1	Model 2	Model 3	Model 4	Model 5	Model 6
Quartz (%)	55	55	35	35	10	10
Plagioclase (%)	10	35	10	55	35	55
K-Feldspar (%)	35	10	55	10	55	35

**Figure 5.8: Location of 6 mineral-based models on Quartz–K-feldspar–Plagioclase diagram**

The contact properties were assigned according to the neighbouring material types. The contact stiffness values were calculated according to Hooke’s law by defining the equivalent stiffness of a contact between two grains as illustrated in Figure 5.9 using the properties presented in Table 5.3.

There is no clear methodology for estimating the stiffness of the contact properties for two adjoining mineral grains. In order to have a reasonable estimate of grain contact normal and shear stiffness, two separate UDEC models have been created representing rocks that are composed of specific minerals. For this example, the unconfined compression test results for syenite and diorite were used. These two samples represent rock types with more than 90% K-feldspar and Plagioclase, respectively. The normal and shear stiffness of the contacts between the minerals were adjusted until the elastic Young’s modulus and Poisson’s ratio and peak uniaxial strength of the UDEC specimen matched the laboratory data

(Table 5.4). Normal and shear stiffness of quartz were later calibrated from the medium grained granite properties (Table 5.1) knowing the contact stiffness of plagioclase and K-feldspar.

**Table 5.2: Elastic properties of igneous rock forming minerals (Bass 1995)**

Grain type	Density ( $\text{kgm}^{-3}$ )	Shear Modulus (GPa)	Bulk Modulus (GPa)
Quartz	2650	44.0	37.0
Plagioclase	2630	29.3	50.8
K-feldspar	2560	27.2	53.7

**Table 5.3: Contact normal and shear stiffness based on Hooke's law for different minerals (Units are in GPa/m)**

Grain Type	Quartz	Plagioclase	K-Feldspar
Quartz	$k_n=43428$ $k_s=26057$	$k_n=37939$ $k_s=22763$	$k_n=26146$ $k_s=15687$
Plagioclase	$k_n=37939$ $k_s=22763$	$k_n=32450$ $k_s=19548$	$k_n=20657$ $k_s=12444$
K-Feldspar	$k_n=26146$ $k_s=15687$	$k_n=20657$ $k_s=12444$	$k_n=8865$ $k_s=5349$

**Table 5.4: Modeling properties of Syenite and Gabbro**

Rock Type	UCS Sample		UDEC model	
	E (GPa), $\nu$	Peak stress (MPa)	E (GPa), $\nu$	Peak stress (MPa)
Syenite <sup>a</sup>	51, 0.27 <sup>b</sup>	222.6	60, 0.24	241
Diorite <sup>c</sup>	92, 0.24	210.0	102, 0.24	234

a- Lan et al. (2010); Jian-An and Sijing (1985)

b- Poisson's ratio from D'yachkova A. Ya. et al. (1966)

c- Shimada et al. (1983)

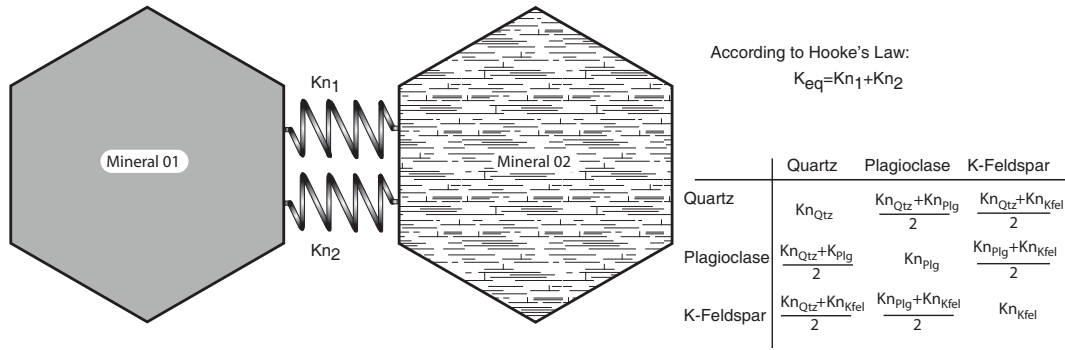


Figure 5.9: Equivalent mineral stiffness based on Hooke's law

## 5.9. Results and discussion

### 5.9.1. Crack initiation mechanism

The two cracking models proposed in Section 5.2 and illustrated in Figure 5.2 rely on either tensile failure or sliding (shear) failure. In laboratory compression testing, crack initiation (tensile) is recorded early in the loading process when the applied stress reaches approximately 0.4 to 0.5 of the peak stress while the opportunity for crack sliding occurs when the applied stress reaches approximately 0.7 to 0.8 of the peak stress (Bieniawski 1967, Hallbauer et al. 1973). The Force-chain model in Figure 5.2 will cause cracking, provided that the normal stress acting on the crack surface is equal to its tensile strength. However, the Sliding-crack model will be valid when the shear stress on the crack surface is equal to the shear strength of the cracks ( $\tau$ ) defined as:

$$\tau = C + \sigma_n \tan \phi \quad (5.2)$$

where  $C$  and  $\phi$  are cohesion and internal friction angle and  $\sigma_n$  is the normal stress acting on the crack surface.

The four models with  $S_o$  equal to 1.5, 1.14, 1.05 and 1.03 were analyzed to assess the mode of rupture (tensile or sliding) as cracking occurs during the loading process. The number of shear and tensile cracks were determined for every 5000 time steps in the UDEC model which equates to approximately a 0.07 increment

of the peak strength. Figure 5.10 shows the number of cracks in the sample volume normalized to the number of grain contacts for each loading increment versus the applied stress normalized to the peak strength. Figure 5.10 illustrates that all the cracking observed in the early stages of loading is tensile cracking. The more uniform grain size distributions with  $S_o$  ranging from 1.14 to 1.03 showed no shear cracking until the loads exceeded 0.7 of the peak strength while the heterogeneous sample with  $S_o=1.5$  showed shear cracking initiating at approximately 0.6 of the peak strength. There are only tensile cracks associated with the laboratory crack initiation (CI). However for the laboratory crack damage (CD) both shear and tensile cracks are associated with this stress threshold and for  $S_o$  ranging from 1.14 to 1.03, the number of shear cracks are significantly greater than the number of tensile cracks as the peak strength is approached.

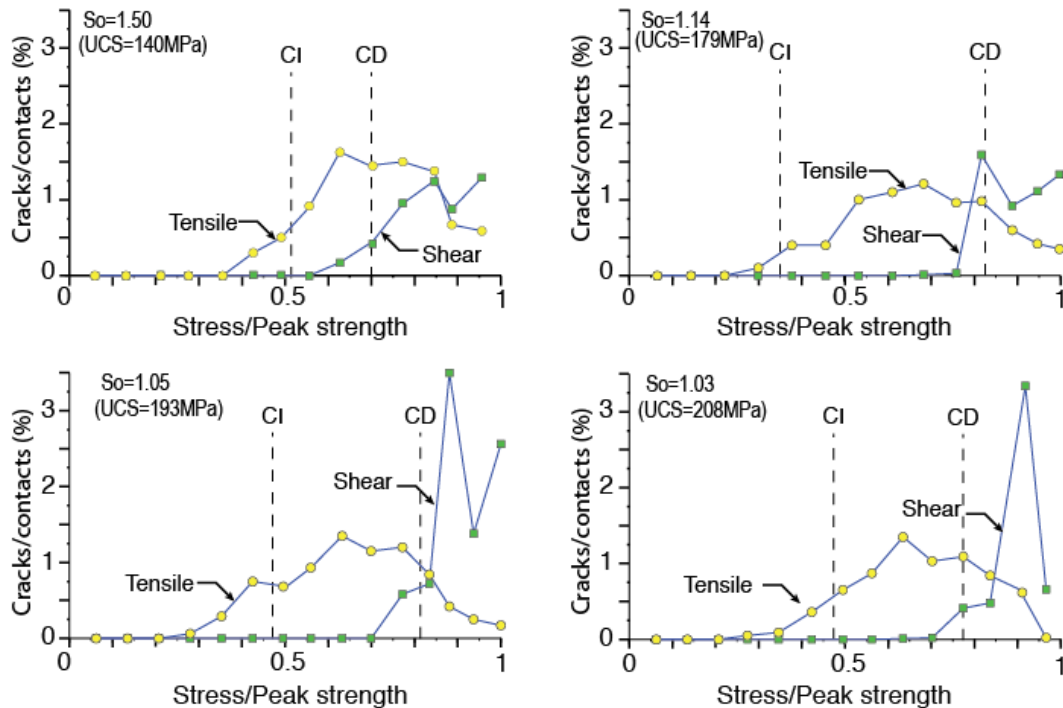


**Figure 5.10: Relationship between the quantity of tensile and shear cracks, expressed as a percentage of the total contacts, for each approximate 0.07 load increment. The applied stress is normalized to the peak strength. CI refers to crack initiation and CD refers to crack damage (unstable crack growth) obtained by strain-based methods.**

All four models support the notion that tensile cracks are a precursor to the macro scale failure process but near the peak strength both shear and tensile cracks contribute to the failure process.

In addition to the crack type, the direction of the crack is also an indicator of the loading model that is causing the cracking. It is generally reported that the orientation of the majority of stress-induced cracks observed in laboratory tests are oriented in the direction of the applied load (Lajtai 1998). The directions of the cracks were recorded in the four models and these directions are summarized in Figure 5.11 and Table 5.5.

The results clearly illustrate that the majority of the cracks are within  $\pm 10^\circ$  of the applied axial stress and that the mean orientation is within  $\pm 1^\circ$  of the applied stress. These orientations are approximately parallel to the applied stress also support the notion that the Force-Chain model, resulting in the generation of tensile cracking, is the dominant mode of cracking during all stages of compressive loading.

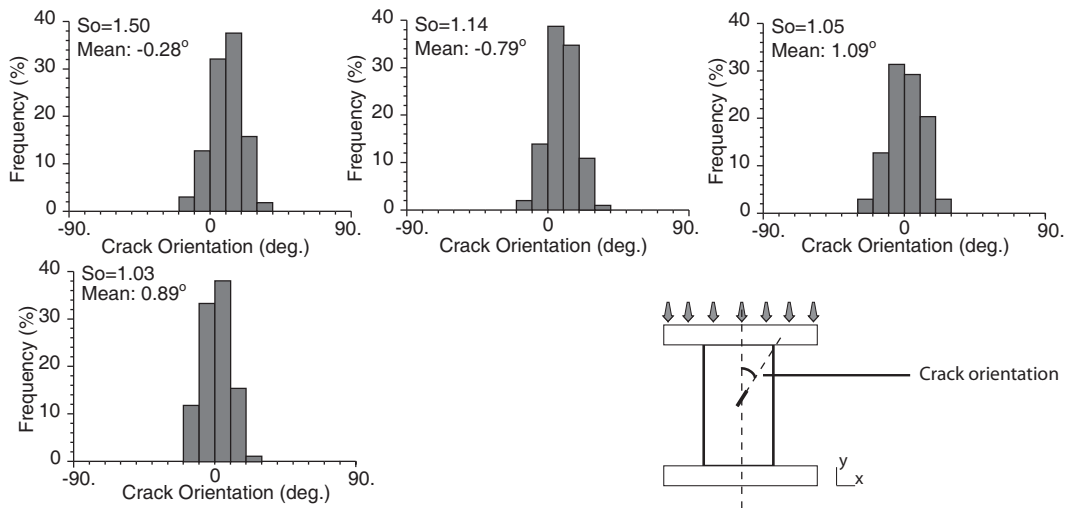


**Figure 5.11: The direction of cracks measured in the four models (So=1.5, 1.14, 1.05 and 1.03)**

### 5.9.2. Effect of heterogeneity induced by grain size distribution

The effect of the heterogeneity, i.e., the grain size distributions illustrated in Figure 5.7, on the Crack initiation stress and peak strength is summarized in Figure 5.12 and Table 5.6. According to Table 5.6, the peak uniaxial strength ranges from 140 to 208 MPa as the grain size distribution varies from heterogeneous to uniform, respectively.

This 32% increase in peak strength as the heterogeneity decreases, is also accompanied by an increase in the stress required for crack initiation from 72 to 101 MPa. In essence both the crack initiation and peak stress increases as the sample grain size distribution becomes more uniform. Consequently, the crack initiation ratio of CI to peak stress shows only minor variation: 0.51, 0.45, 0.47 and 0.49, as the heterogeneity decreases.

**Table 5.5: Crack orientation in models with different attributes. Crack orientations are measured relative to the load direction**

<b>Avg. grain size=1-2mm</b>					
<b>Models with different <math>S_o</math></b>					
$S_o=1.50$	$S_o=1.14$	$S_o=1.05$	$S_o=1.03$		
-0.28°	-0.79°	1.09°	0.89°		
<b>Sorting Coefficient = 1.03</b>					
<b>Models with average grain size</b>					
0.75mm	1.15mm	2.25mm			
0.14°	-0.65°	0.89°			
<b>Sorting Coefficient= 1.14; Avg. grain size=2.25mm</b>					
<b>Models with different mineralogy (Qtz/Pl/K-fel %)</b>					
55/10/35	55/35/10	35/10/55	35/55/10	10/35/55	10/55/35
-0.91°	-0.72°	-1.00°	-0.23°	0.38°	-0.41°
<b>Sorting Coefficient= 1.03; Avg. grain size=2.25mm</b>					
<b>Models with different mineralogy (Qtz/Pl/K-fel %)</b>					
55/10/35	55/35/10	35/10/55	35/55/10	10/35/55	10/55/35
0.27°	1.79°	-0.61°	-0.82°	0.75°	0.28°

### 5.9.3. Effect of grain size

It is often reported that the strength of intact rock is a function of grain size (Brace 1961; Fredrich et al. 1990). The three models with average grain size of fine (0.75mm), fine to medium (1.5mm) and medium grained (2.25mm) and constant grain size distribution ( $S_o=1.03$ ) gave peak uniaxial strengths of 203, 200, and 208 MPa (Figure 5.13 and Table 5.7).

The results suggest that grain size has no effect on the peak uniaxial strength provided the grain-size distribution is held uniform ( $S_o=1.03$ ). The crack initiation stresses were also found to be relatively insensitive to grain size, ranging from 97 MPa for fine grain, 94 MPa for fine-medium grain to 101 MPa for medium grain (Table 5.7).

The values given in Table 5.7 give ratios of CI to peak strength of 0.48, 0.47 and 0.49 for fine, fine to medium, and medium grained, respectively. Based on these results, it appears that the peak strength and crack initiation stress is independent of average grain size for a rock with a uniform grain size distribution and constant mineralogy.

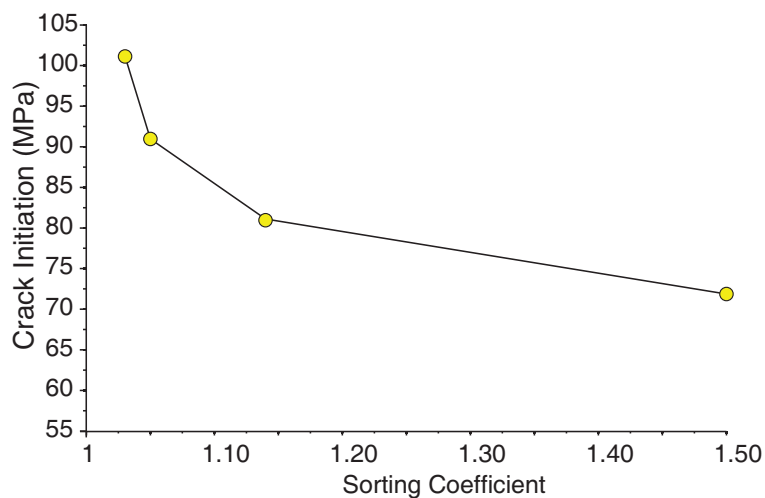


**Figure 5.12: Crack initiation stress as a function of peak stress in models with different grain size distribution**

**Table 5.6: Crack initiation stress peak stress in models with different grain size distribution.**

$S_o$	CI- Poisson's ratio (MPa)	CI- LSR (MPa)	UCS (MPa)	Average CI (MPa) % normalized cracks	CI / UCS
1.50	71	73	140	72, 0.9%	0.51
1.14	82	80	179	81, 1.2%	0.45
1.05	102	82	193	91, 1.4%	0.47
1.03	105	97	208	101, 0.8%	0.49

#### ***5.9.4. Effect of mineralogy***

**5.10. The effect of mineralogy on crack initiation stress was examined using uniform ( $S_o=1.03$ ) and non-uniform ( $S_o=1.14$ ) grain size distribution. It should be emphasized that the effect of mineralogy was evaluated using variation in the elastic constants for each mineral grain. Figure 5.14 and Summary**

The results from the numerical grain-based models have provided insights into the mechanism associated with the laboratory findings by Nicksiar and Martin (2012) and summarized in Figure 5.1.

For the low porosity rocks simulated, tensile cracking is the dominant mode of damage that occurs as compressive loads are applied to a heterogeneous assemblage of mineral grains. Figure 5.15 summarizes the results from the 20 grain-based models. For the range of factors investigated in these models, the heterogeneity created by grain size distributions has the greatest impact on peak strength and crack initiation stress. However, despite the range in peak strength and crack initiation stress, the ratio of crack initiation stress to peak uniaxial strength is relatively well constrained.

Table 5.8 summarizes the results from the UDEC models and illustrates that the peak uniaxial strength is a function of the quartz content with the strength increasing as the quartz content increases. This is not surprising as quartz, while a common mineral, is one of the toughest and strongest minerals and as noted by

Lajtai (1998) “the quartz framework gives the high strength to granites”. This trend is also observed in the stress required for crack initiation, i.e. the higher the quartz content the higher stress required for crack initiation, provided that the grain size distribution is uniform ( $S_o=1.03$ ).

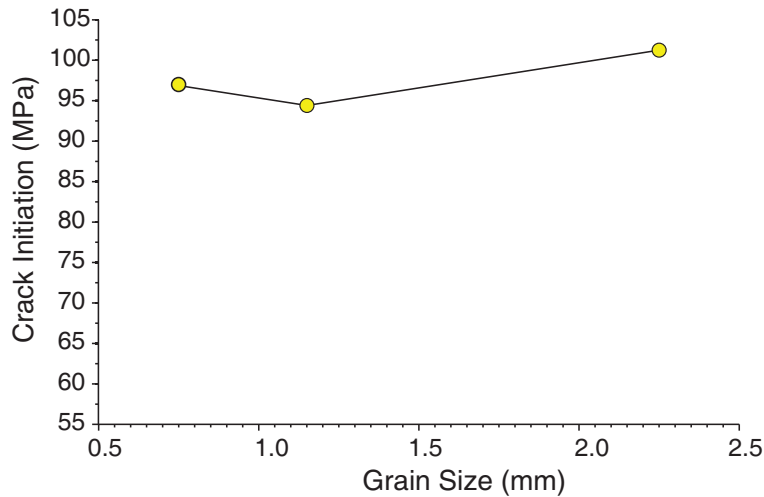


**Figure 5.13: Crack initiation stress as a function of average grain size when  $S_o=1.03$**

**Table 5.7: Crack initiation stress and peak stress in models with different average grain size when  $S_o=1.03$ .**

Average grain size	CI - Poisson's ratio (MPa)	CI- LSR (MPa)	UCS (MPa)	Average CI (MPa) and normalized % cracks	CI/UCS
Fine (0.75mm)	101	93	203	97, 0.8%	0.48
Fine to medium (1.5mm)	92	95	200	94, 0.7%	0.47
Medium (2.25mm)	105	97	208	101, 1.0%	0.49

When the grain size distribution is more heterogeneous ( $S_o=1.14$ ) these trends are less obvious suggesting that grain size distribution is likely more relevant than the proportions of an individual mineral.

**5.11. The crack initiation ratios for models with different mineralogy and various grain size distributions are also summarized in Summary**

The results from the numerical grain-based models have provided insights into the mechanism associated with the laboratory findings by Nicksiar and Martin (2012) and summarized in Figure 5.1.

For the low porosity rocks simulated, tensile cracking is the dominant mode of damage that occurs as compressive loads are applied to a heterogeneous assemblage of mineral grains. Figure 5.15 summarizes the results from the 20 grain-based models. For the range of factors investigated in these models, the heterogeneity created by grain size distributions has the greatest impact on peak strength and crack initiation stress. However, despite the range in peak strength and crack initiation stress, the ratio of crack initiation stress to peak uniaxial strength is relatively well constrained.

Table 5.8. In models with uniform grain size distribution, the crack initiation stress ratio is ranging from 0.41 to 0.47 (average of  $0.44 \pm 0.03$ ). On the other hand, in models with non-uniform grain size distribution, the crack initiation stress ratio ranges from 0.37 to 0.47 (average of  $0.41 \pm 0.03$ ).

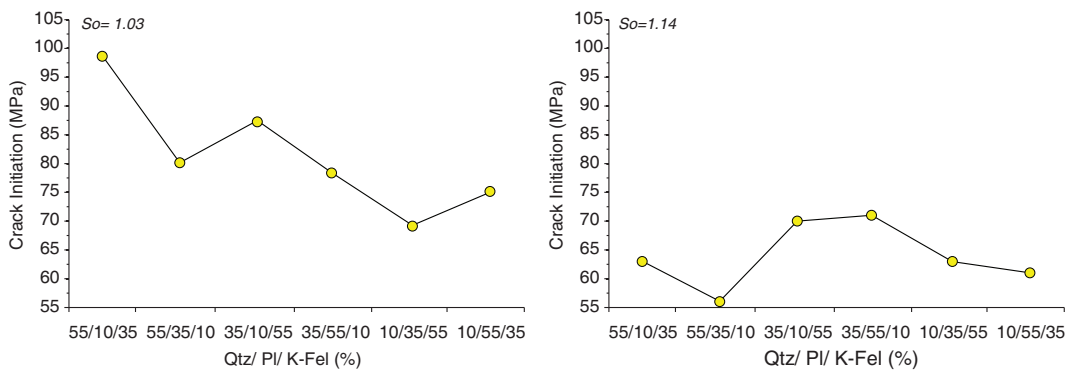


**Figure 5.14: Crack initiation stress and peak stress in models with different mineralogy and grain size distributions.**

## 5.12. Summary

The results from the numerical grain-based models have provided insights into the mechanism associated with the laboratory findings by Nicksiar and Martin (2012) and summarized in Figure 5.1.

For the low porosity rocks simulated, tensile cracking is the dominant mode of damage that occurs as compressive loads are applied to a heterogeneous assemblage of mineral grains. Figure 5.15 summarizes the results from the 20 grain-based models. For the range of factors investigated in these models, the heterogeneity created by grain size distributions has the greatest impact on peak strength and crack initiation stress. However, despite the range in peak strength and crack initiation stress, the ratio of crack initiation stress to peak uniaxial strength is relatively well constrained.

**Table 5.8: Crack initiation stress and peak stress in models with different mineralogy and grain size distributions.**

Model (Qtz/Pl/K-Fel)	CI- Poisson's ratio (MPa)	CI-LSR (MPa)	UCS (MPa)	Average CI and % normalized cracks	CI/ UCS
So=1.03					
(55/10/35)	93	102	207	98, 1.7%	0.47
(55/35/10)	72	87	195	80, 1.2%	0.41
(35/10/55)	79	95	206	87, 1.0%	0.42
(35/55/10)	75	81	179	78, 1.2%	0.44
(10/35/55)	65	72	159	69, 1.5%	0.43
(10/55/35)	76	74	161	75, 0.9%	0.47
So=1.14					
(55/10/35)	63	63	158	63, 1.1%	0.40
(55/35/10)	54	58	139	56, 1.2%	0.40
(35/10/55)	75	64	167	70, 1.0%	0.42
(35/55/10)	74	67	174	71, 1.2%	0.41
(10/35/55)	64	61	133	63, 1.3%	0.47
(10/55/35)	64	57	163	61, 1.5%	0.37

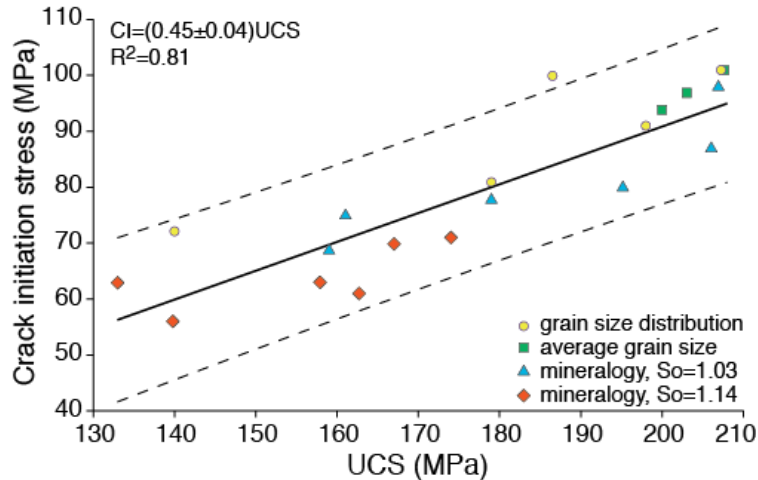


**Figure 5.15: Relation between crack initiation stress (CI) and peak uniaxial compressive strength (UCS) found in the grain-based numerical models**

### 5.13. Conclusion

Crack initiation in uniaxial compressive loading of rock occurs well before the peak strength is reached. The factors that may influence the onset of cracking and possible initiating mechanisms were explored using a discrete element numerical approach. The numerical approach was based on grain-based model that utilized a voronoi tessellation scheme to represent low porosity crystalline rocks such as granite. This approach enabled complete tracking of the failure process along the mineral grain boundaries.

The two general mechanisms proposed for crack initiation observed in laboratory compression tests are: (1) Sliding (shear) crack model and (2) Force-chain (tensile) crack model. The numerical models showed that crack initiation is a phenomenon associated with tensile cracking. This tensile cracking dominates at the early stages of loading. Shear cracking was only observed after crack initiation occurred and in most of the models was only prominent near the peak strength.

The effect of grain-size distribution (sorting coefficient ranging from 1.5 to 1.03), grain size (ranging from 0.75 mm to 2.25 mm), and the heterogeneities of different mineral grains (quartz, K-Feldspar, plagioclase) were examined. Modelling revealed that the grain size distribution had the most significant effect

on peak strength and crack initiation stress. The peak strength ranges from 140 to 208 MPa as the grain size distribution varies from heterogeneous to uniform, respectively. However, the ratio of crack initiation to peak stress showed only minor variation, as the heterogeneity decreases. Grain size was found to have no effect on peak strength in the models provided the grain size distribution was not changed. The other factors investigated had only minor effects on crack initiation and peak strength, and crack initiation ratio. The findings from these investigations suggest that crack initiation is a consequence of the heterogeneity of the materials and that the geometrical heterogeneity has the greatest influence. The findings also help to explain why the ratio of crack initiation stress to peak strength in laboratory compression tests is usually found to be approximately  $0.45 \pm 0.05$  for a wide range of low porosity rocks.

The application of our two dimensional models has limitations. Moreover, all of our models were constructed to simulate granite-like rocks. Future research should examine, using a three dimensional model, the effect of heterogeneity on other rock types, including those with porosities higher than that found in our granite-like rock.

#### Acknowledgements

We would like to acknowledge the financial contribution of Swedish Nuclear Fuel and Waste Management Company through the DECOVALEX Project and the Synthetic Rock Project. The authors would like to thank Dr. Erik Eberhardt (University of British Columbia) for providing the stress-strain data of Lac du Bonnet granite and Yun Lu (University of Alberta) for his help creating some of the models.

## 5.14. References

- Andersson, J. C., Martin, C. D., and Stille, H. (2009). "The Äspö Pillar Stability Experiment: Part II—Rock mass response to coupled excavation-induced and thermal-induced stresses." *Int.J.Rock Mech.Min.Sci.*, 46(5), 879-895.
- Ashby, M. F., and Hallam (Née Cooksley), S. D. (1986). "The failure of brittle solids containing small cracks under compressive stress states." *Acta Metallurgica*, 34(3), 497-510.
- Bass, D. J. (1995). "Elasticity of minerals, glasses and melts." *Mineral Physics and Crystallography, Reference Shelf 2*, T. J. Ahrens, ed., AGU, Washington, D. C., 45-63.
- Bieniawski, Z. T. (1967). "Mechanism of brittle fracture of rock: Part I—theory of the fracture process." *International Journal of Rock Mechanics and Mining Sciences & Geomechanics Abstracts*, 4(4), 395-404, IN11-IN12, 405-406.
- Brace, W. F. (1964). "Brittle Fracture of Rock." *State of Stress in the Earth's Crust*, W. R. Judd, ed., Elsevier, New York, 111-181.
- Brace, W. F. (1961). "Dependence of fracture strength of rocks on grain size." *Bull. Miner. Inds. Exp. Stn. Penn. St. Univ.*, 76 99-103.
- Brace, W. F., Paulding, B., and Scholz, C. (1966). "Dilatancy in the fracture of crystalline rocks." *Journal of Geophysical Research*, 71 3939-3953.
- Brown, E. T. (1981). "Rock characterization, Testing and monitoring, ISRM suggested methods." .
- Cho, N., Martin, C. D., and Segol, D. C. (2007). "A clumped particle model for rock." *Int.J.Rock Mech.Min.Sci.*, 44(7), 997-1010.

- Christianson, M., Board, M., and Rigby, D. (2006). "UDEC simulation of triaxial testing of lithophysal tuff." *Golden Rocks 2006, The 41st U.S. Symposium on Rock Mechanics (USRMS)*, 06-968-06-976.
- Cook, N. G. W. (1963). "The basic mechanics of rockbursts." *Journal of the South African Institute of Mining and Metallurgy*, (63), 71-81.
- Cundall, P. A. (1980). "UDEC - A Generalised Distinct Element Program for Modelling Jointed Rock." *Rep. No. ADA087610*, Peter Cundall Associates, European Research Office, U.S. Army Corps of Engineers, .
- Cundall, P. A., and Strack, D. L. O. (1979). "A discrete numerical model for granular assemblies." *Geotechnique*, 29(1), 47-65.
- Diederichs, M. S. (2007). "The 2003 Canadian Geotechnical Colloquium: Mechanistic interpretation and practical application of damage and spalling prediction criteria for deep tunneling." *Canadian Geotechnical Journal*, 44 1082-1116.
- Diederichs, M. S., Kaiser, P. K., and Eberhardt, E. (2004). "Damage initiation and propagation in hard rock during tunnelling and the influence of near-face stress rotation." *Int.J.Rock Mech.Min.Sci.*, 41(5), 785-812.
- D'yachkova A. Ya., Gorbenko, V. S., and Kudryavtseva, M. N. (1966). "Elastic properties of alkali syenites from the October Massif." National Aeronautics and space administration, Washington, D.C.
- Fredrich, J. T., Evans, B., and Wong, T. (1990). "Effect of size on brittle and semi-brittle strength: Implication for micromechanical modelling of fracture in compression." *Journal of Geophysical Research*, 95 10907-10920.
- Glamheden, R., Fredriksson, A., Roshoff, K., Karlsson, J., Hakami, H., and Christiansson, R. (2007). "Rock Mechanics Forsmark, Site descriptive

- modelling, Forsmark stage 2.2." *Rep. No. R-07-31*, Swedish Nuclear Fuel and Waste Management Co., Stockholm, Sweden.
- Griffith, A. A. (1921). "The Phenomena of Rupture and Flow in Solids." *Philosophical Transactions of the Royal Society of London. Series A, Containing Papers of a Mathematical Or Physical Character*, 221 163-198.
- Griffith, A. A. (1924). "Theory of rupture." *Proceedings of the First International Congress of Applied Mechanics*, 55-63.
- Hallbauer, D. K., Wagner, H., and Cook, N. G. W. (1973). "Some observations concerning the microscopic and mechanical behaviour of quartzite specimens in stiff, triaxial compression tests." *International Journal of Rock Mechanics and Mining Sciences & Geomechanics Abstracts*, 10(6), 713-726.
- Jian-An, H., and Sijing, W. (1985). "An experimental investigation concerning the comprehensive fracture toughness of some brittle rocks." *International Journal of Rock Mechanics and Mining Sciences & Geomechanics Abstracts*, 22(2), 99-104.
- Lajtai, E. Z. (1998). "Microscopic fracture process in a granite." *Rock Mechanics and Rock Engineering*, 31(4), 237-250.
- Lajtai, E. Z. (1974). "Brittle fracture in compression." *International Journal of Fracture*, 10(4), 525-536.
- Lan, H., Martin, C. D., and Hu, B. (2010). "Effect of heterogeneity of brittle rock on micromechanical extensile behavior during compression loading." *Journal of Geophysical Research*, 115.
- Lau, J. S. O., and Chandler, N. A. (2004). "Innovative laboratory testing." *International Journal of Rock Mechanics and Mining Sciences*, 41(8), 1427-1445.

- Martin, C. D., and Chandler, N. A. (1994). "The progressive fracture of Lac du Bonnet granite." *International Journal of Rock Mechanics and Mining Sciences & Geomechanics Abstracts*, 31(6), 643-659.
- Martin, C. D., and Christiansson, R. (2009). "Estimating the potential for spalling around a deep nuclear waste repository in crystalline rock." *Int.J.Rock Mech.Min.Sci.*, 46(2), 219-228.
- Martin, C. D., Kaiser, P. K., and McCreath, D. R. (1999). "Hoek-Brown parameters for predicting the depth of brittle failure around tunnels." *Canadian Geotechnical Journal*, 36(1), 136-151.
- Martin, C. D., and Stimpson, B. (1994). "The effect of sample disturbance on laboratory properties of Lac du Bonnet granite." *Canadian Geotechnical Journal*, 31(5), 692-702.
- Nemat-Nasser, S., and Horii, H. (1982). "Compression-Induced Nonplanar Crack Extension With Application to Splitting, Exfoliation, and Rockburst." - *J. Geophys. Res.*, 87(B8), 6805-6821.
- Nemat-Nasser, S., and Obata, M. (1988). "A micromodel of dilatancy in materials." *Transactions of the ASME Journal of Applied Mechanics*, 55 24-35.
- Nicksiar, M., and Martin, C. D. (Submitted). "Crack initiation stress in low porosity crystalline and sedimentary rocks." *Engineering Geology*, .
- Nicksiar, M., and Martin, C. D. (2012). "Evaluation of Methods for Determining Crack Initiation in Compression Tests on Low-Porosity Rocks." *Rock Mechanics and Rock Engineering*, 45(4), 607-617.
- Olsson, W. A. (1974). "Grain Size Dependence of Yield Stress in Marble." *J. Geophys. Res.*, 79(32), 4859-4862.

- Potyondy, D., and Cundall, P. A. (2004). "A bonded-particle model of rock." *International Journal of Rock Mechanics and Mining Sciences*, 41(8), 1329-1364.
- Potyondy, D., Cundall, P. A., and Lee, C. (1996). "Modeling rock using bonded assemblies of circular particles." *Rock Mechanics tools and techniques*, 1937-1944.
- Prikryl, R. (2001). "Some microstructural aspects of strength variation in rocks." *Int.J.Rock Mech.Min.Sci.*, 38(5), 671-682.
- Read, R. S. (2004). "20 years of excavation response studies at AECL's Underground Research Laboratory." *Int.J.Rock Mech.Min.Sci.*, 41(8), 1251-1275.
- Read, R. S., Chandler, N. A., and Dzik, E. J. (1998). "In situ strength criteria for tunnel design in highly-stressed rock masses." *Int.J.Rock Mech.Min.Sci.*, 35(3), 261-278.
- Shimada, M., Cho, A., and Yukutake, H. (1983). "Fracture strength of dry silicate rocks at high confining pressures and activity of acoustic emission." *Tectonophysics*, 96(1-2), 159-172.
- Skinner, W. J. (1959). "Experiments on the compressive strength of anhydrite." *Engineer*, 207 255-259.
- Stacey, T. R. (1981). "A simple extension strain criterion for fracture of brittle rock." *International Journal of Rock Mechanics and Mining Sciences & Geomechanics Abstracts*, 18(6), 469-474.
- Tapponnier, P., and Brace, W. F. (1976). "Development of stress-induced microcracks in Westerly Granite." *International Journal of Rock Mechanics and Mining Sciences & Geomechanics Abstracts*, 13(4), 103-112.

Trask, P. D. (1932). *Origin and environment of source sediments of petroleum*.  
Gulf Pub., Houston.

## Chapter 6. Conclusion

The stress at which cracks are initiated in compression laboratory testing, commonly referred to as crack initiation stress (CI), has been studied in this research. Crack initiation has gained prominence in the past 20 years, as various studies have shown that it can be used for estimating the in-situ spalling strength of crystalline rock masses. In order to measure crack initiation stress in laboratory tests, different methodologies have been proposed by various researchers. While crack initiation is only observed in the lateral strain gauge, some of the methods proposed use both the lateral and axial strain gauges or require the calculation a crack volume. For many of these methods, this has lead to user-dependency in determining CI. In order to eliminate this user-dependency in establishing CI, a new method was developed which is based only on the measured Lateral Strain Response (LSR). In the LSR method, the recorded lateral strain is subtracted from a reference line to produce a lateral strain versus axial stress relationship. Crack initiation stress is defined as the maximum value in LSR-Axial stress curve which can be programmed using mathematical software such as Matlab. This approach removes the user-dependency in determining CI.

In order to quantify the robustness of LSR method, 10 samples of Äspö diorite were examined using six well-established methods for determining the Crack Initiation Stress. The methods used the stress-strain data obtained from modern laboratory uniaxial compression tests. Äspö diorite was selected due to low pre-existing damage that removes the associated errors in some methods. The results have been compared using a statistical approach, Analysis of Variance (ANOVA).

Study of all six methods indicates that LSR method is statistically in agreement to other methods.

Several studies have suggested that crack initiation is a material property. The relation between material properties such as grain size, grain size distribution and mineralogy with crack initiation stress was studied in this research both statistically and numerically to assess the factors that influence CI. Moreover, the effect of confinement on CI stress is also investigated.

The effect of mineralogy on CI stress was investigated for igneous rocks. The results show that CI is positively correlated to quartz content while it has a negative correlation to the plagioclase. Further research proves the CI value in igneous rocks is mostly related to the hardest minerals present. Study of sedimentary specimens loaded under uniaxial compression confirms these findings due to a positive correlation between CI and carbonate content compared to the negative correlation between CI and clay content. Moreover, the CI increases as the average grain size decreases.

Other geological properties, such as directional anisotropy can also affect brittle behaviour of the samples. The effect of foliation on tensile, crack initiation and peak strength of metamorphic specimens have been reviewed. The study of high grade metamorphic rocks that possess a strong foliation indicates the sensitivity of peak strength to direction of foliation relative to the direction of maximum load. However, the tensile and CI stress remains almost constant. These results can be described by the cracking mechanism associated with these stress values. In CI, the new cracks (rupture along the grain boundaries) are formed in the induced tensile stress regime similar to the failure of the sample due to tension. However, the sample failure at the peak stress is due to shearing.

The analysis of crack initiation and peak stress in different rock types also shows the constant relation between CI and UCS. The crack initiation stress to peak stress ratio in lab specimen for different rock types has been found to be 0.42-0.47

in uniaxial compression. In the presence of confinement, i.e. triaxial compression, the crack initiation stress ratio increases to 0.50-0.54 suggesting that confining stress suppresses crack initiation.

The Griffith criterion is usually referred to as a crack initiation criterion rather than a rock failure criterion. However, it was found that the Griffith criterion underestimated CI in triaxial compression.

The Crack Initiation findings in the laboratory test results in this study were examined in more detail using a grain-based numerical model. In this numerical modelling, the effect of geometrical and mineral heterogeneity is studied. These numerical models were used to examine the effects of grain size distribution, average grain size and heterogeneities due to mineralogy. The results clearly showed that the crack initiation stress is mostly affected by grain size distribution. Moreover, the constant crack initiation to peak stress ratio reveal the dependency of both crack initiation and peak stress to the material properties.

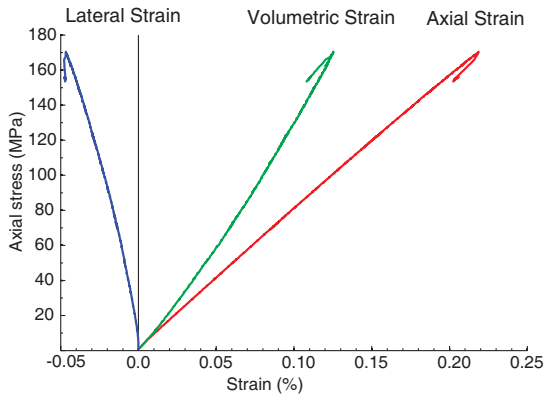
The crack initiation stress in this thesis was analyzed using a grain based modelling methodology that utilizes the two-dimensional discrete element code UDEC. The capability of UDEC in modelling brittle failure of intact rock is found to be satisfactory. However, by introducing the improvement of discrete element codes in 3D, the brittle failure of intact sample can be modelled in more detail. Besides, the effect of porosity on crack initiation or anisotropy within the mineral grains can be modelled in the future with having improved codes.

Two general mechanisms for cracking during unconfined compression loading have been studied using the grain-based numerical models. These mechanisms are: (1) sliding crack model (cracking due to shearing) and (2) force-chain crack model (cracking due to tension). The numerical models and laboratory uniaxial cyclic loading reveal that the crack initiation is a tensile mechanism at the early stages of loading. Shear cracking was only observed after crack initiation and became a prominent cracking mechanism near the peak strength.

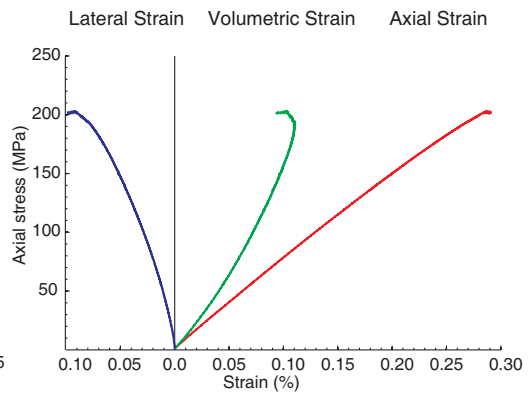
Crack initiation stress in this research was examined for low porosity crystalline rocks. The effect of porosity, or in general terms, crack initiation in porous material should be examined in the future studies.

# Appendix 1

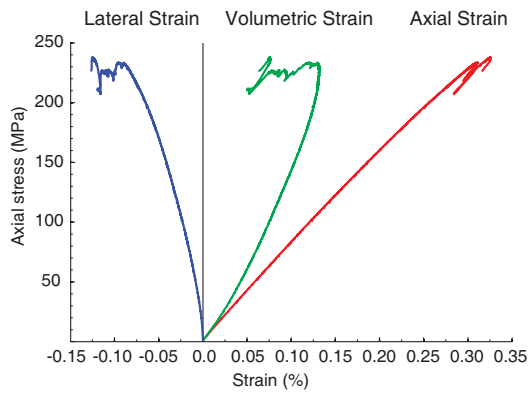
Specimen ID: 46G02-02



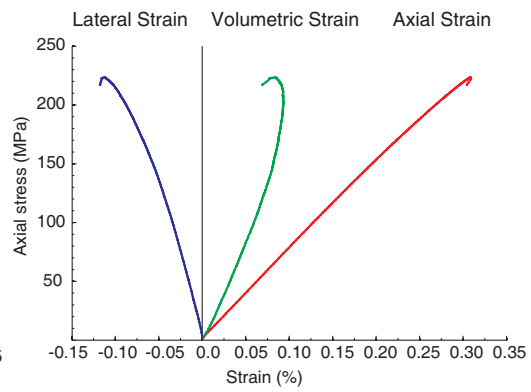
Specimen ID: 46G05-01



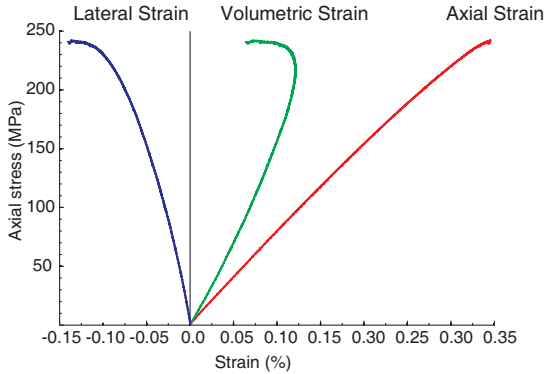
Specimen ID: 46G02-03



Specimen ID: 48G01-01



Specimen ID: 46G02-04



Specimen ID: 48G02-02

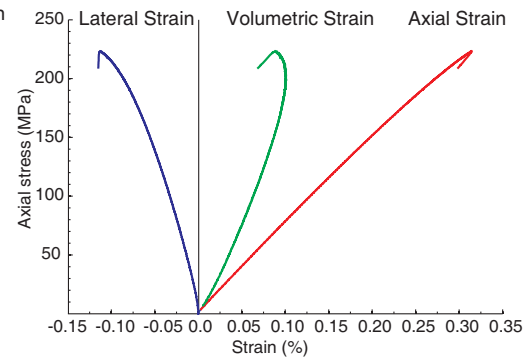
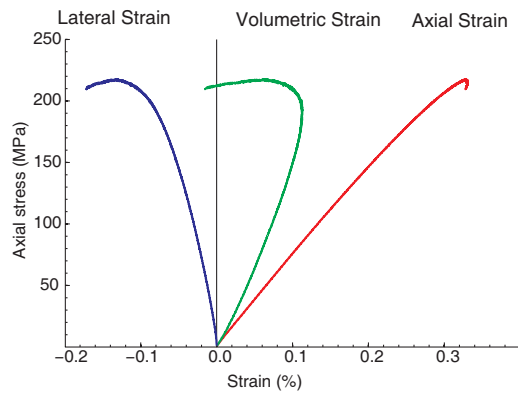
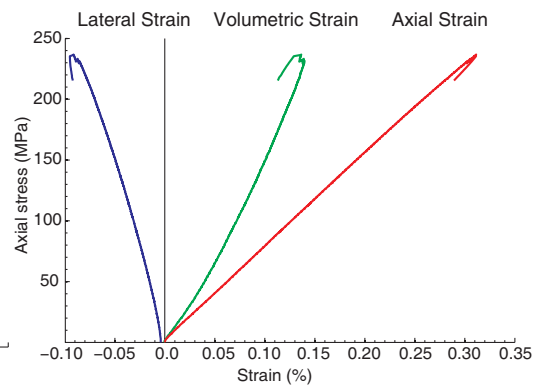


Figure A1.1: Äspö diorite stress-strain curves in unconfined compressive strength test

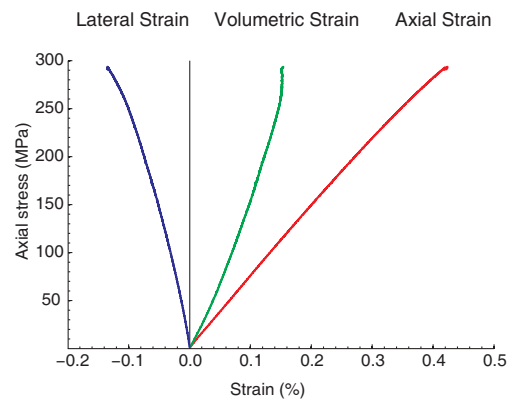
Specimen ID: 51G01-01



Specimen ID: 54G02-01



Specimen ID: 54G01-02



Specimen ID: 54G06-01

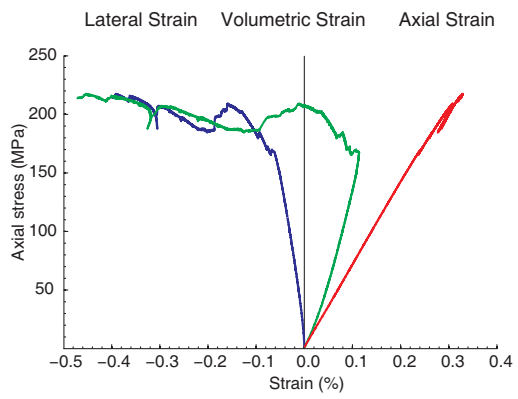
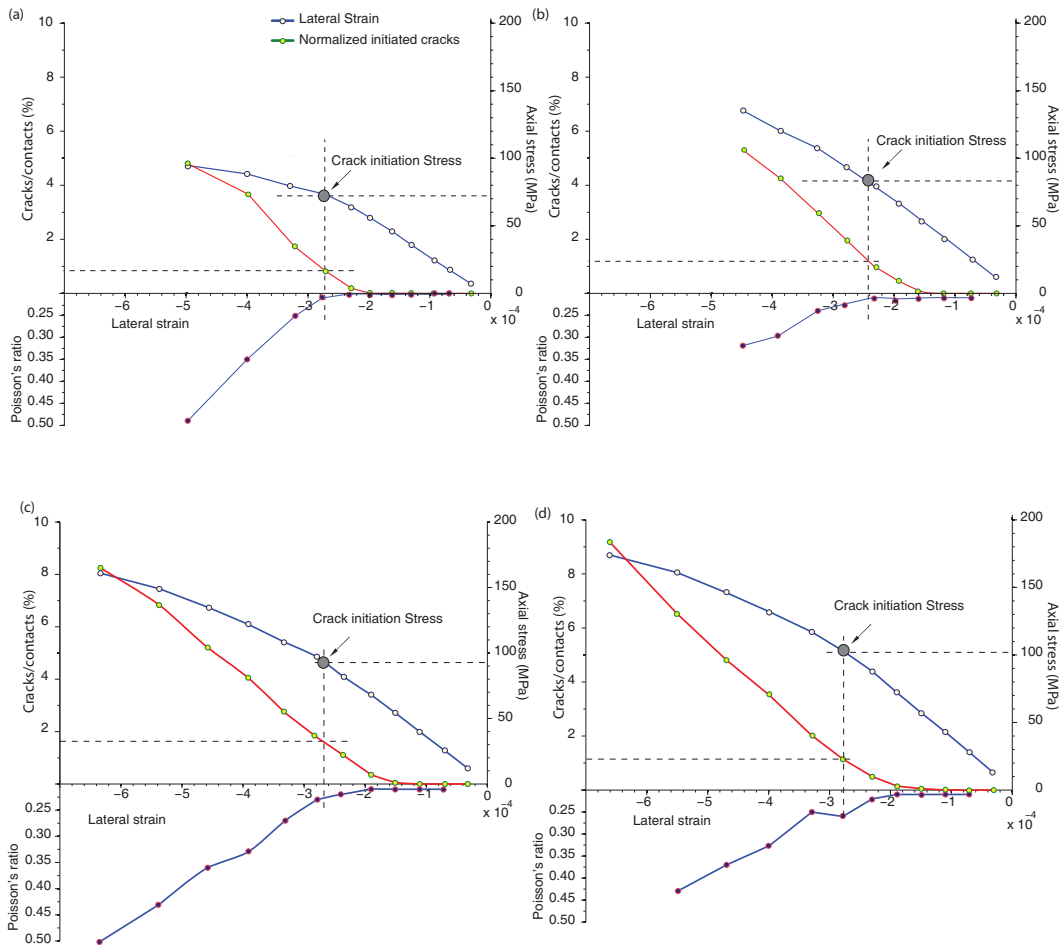
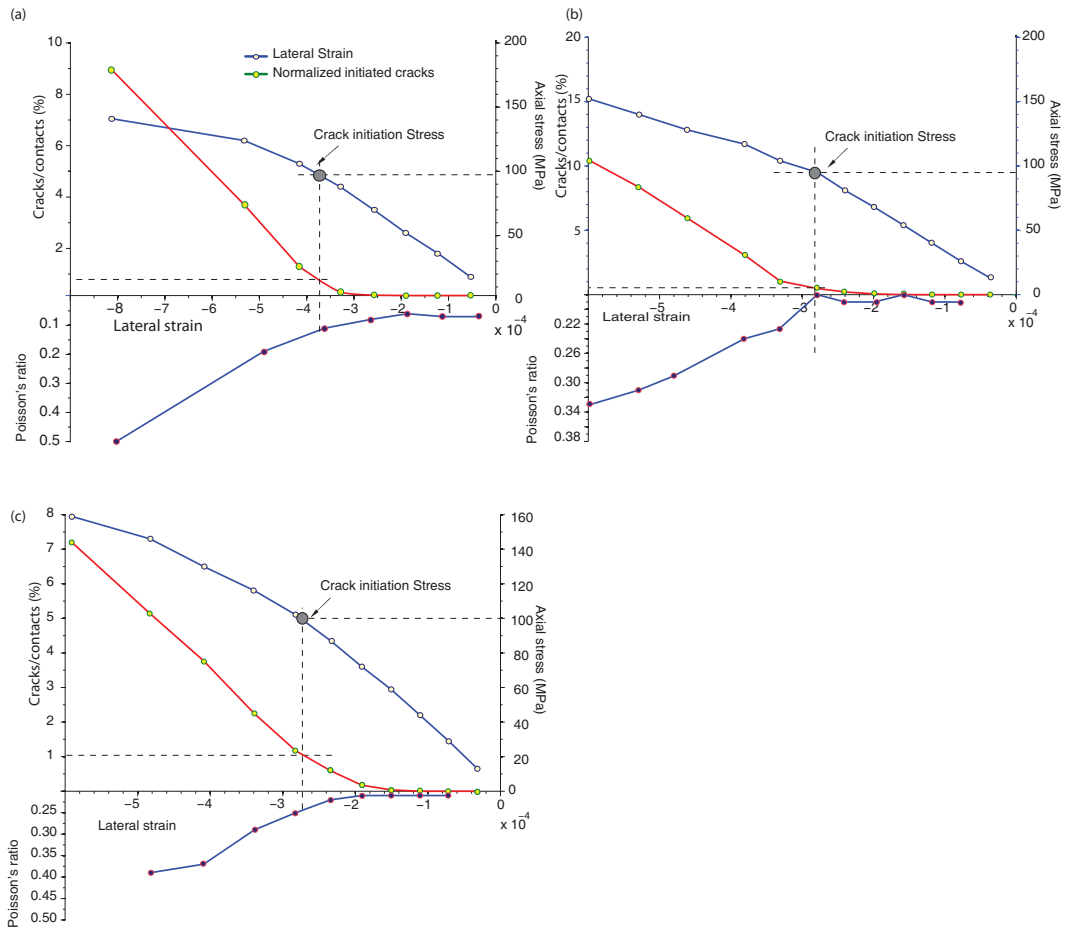


Figure A1.1: continued

# Appendix 2



**Figure A2.1: Lateral Strain, normalized tensile cracks and change in Poisson's ratio in models with different grain size distribution, (a)  $S_o= 1.50$ ; (b)  $S_o= 1.14$ ; (c)  $S_o= 1.05$  and (d)  $S_o=1.03$**



**Figure A2.2: Lateral Strain, normalized tensile cracks and change in Poisson's ratio in models with different average grain size, (a) fine; (b) fine to medium and (c) medium grain size**

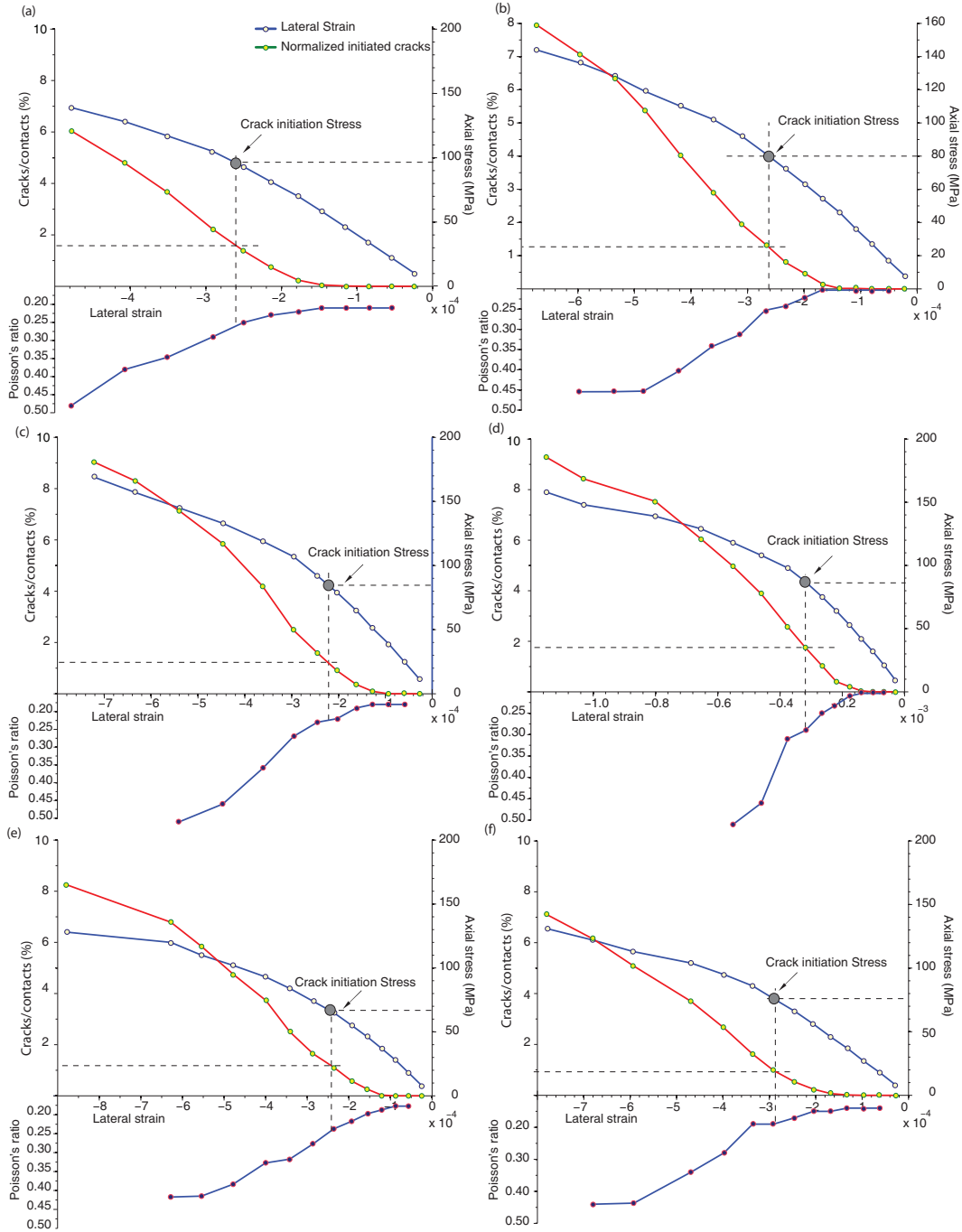


**Figure A2.3: Lateral strain, normalized tensile cracks and change in Poisson's ratio in models with various mineral contents. All models have uniform grain size distribution. Graphs a-f correspond to model 1-6, respectively.**

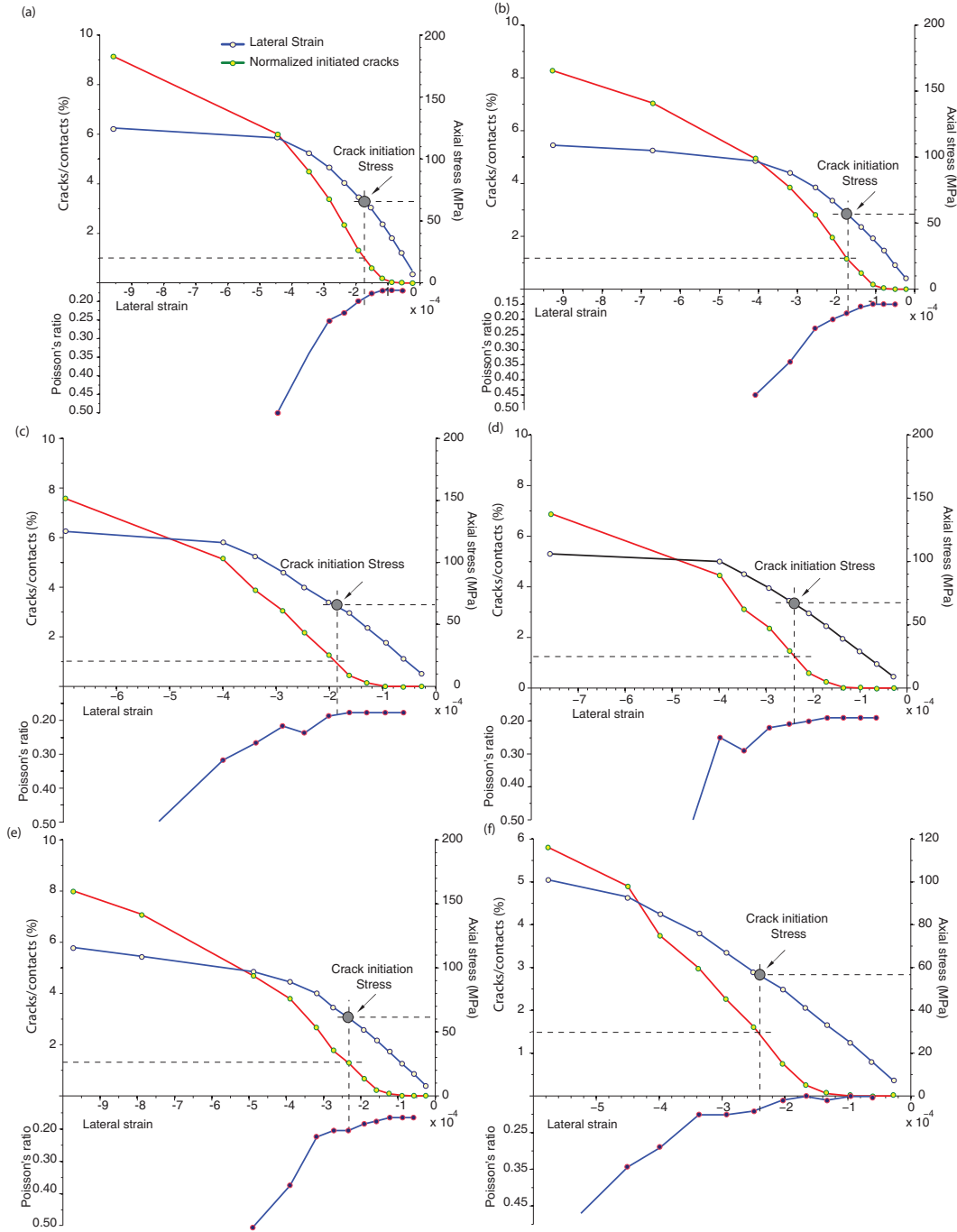


**Figure A2.4: Lateral Strain, normalized tensile cracks and change in Poisson's ratio in models with various mineral contents. All models have the same grain size distribution as Figure 5.7-a. Graphs a-f correspond to model 1-6 respectively.**

## Appendix 3

UDEC code model to create the base model:

---

```
new
round 0.00001
block -0.04 -0.02 -0.04 0.1487 0.0907 0.1487 0.0907 -0.02
crack -0.04 0.1287 0.0907 0.1287
crack -0.04 0 0.0907 0
crack 0 0 0 0.1287
crack 0.0507 0 0.0507 0.1287
prop jmat 3 jkn=4e14 jks=2e14 jcoh=0 jfri=30 jten=0
change jmat 3
del bl 782
del bl 562
voronoi edge 0.00225 iteration 300 seed 69069 &
range -0.002 0.051 -0.002 0.13
gen edge 0.0022 range -0.002 0.051 -0.002 0.13
gen quad 0.1014,0.02 range bl 342
gen quad 0.1014,0.02 range bl 202
save base.sav
```

---

## UDEC code to apply load

---

```
; 1- APPLY MATERIAL PROPERTIES

change cons 1

prop mat 1 d=2630 shear 30.204e9 bulk 44.85e9
prop mat 2 d=7750 shear 79.3e9 bulk 160e9

change mat 2 range bl 342
change mat 2 range bl 202

; -----
change jcons=5
set jcondf=5

; Continuously Yielding Parameters
prop jmat 1 jkn=43428.25e9 jks=26056e9 jfric=57.5 jcoh=42e6 &
jten=18e6 jdil=15 jrescoh=2e6 jrfric=15

; -----
set echo off

def temp
ntab=1
end
temp

; -----
; 2- DEFINE AUTO SAVE FUNCTION

def io4
name1='med_'+cyclD+'.sav'
end

; -----
; 3- DEFINE AXIAL-LATERAL STRAIN CURVE FUNCTION

def slip_load
ntab = ntab + 1
```

---

---

```

tot_str = 0.0
n_z = 0.0
x_z = 0.0
loop n (1,23)
x_z = float(n)
iz = z_near(x_z/454,0.1287)
tot_str = tot_str + z_syy(iz)
n_z = n_z + 1
endloop
; -----
; Axial Strain
p_ytp1L = gp_near(0,0.064)
p_ytp2L = gp_near(0.0127,0.064)
p_ytp3L = gp_near(0.0230,0.064)
p_ytp1R = gp_near(0.0507,0.064)
p_ytp2R = gp_near(0.0380,0.064)
p_ytp3R = gp_near(0.0240,0.064)
; Lateral Strain
p_xtp1L = gp_near(0,0.059)
p_xtp2L = gp_near(0,0.064)
p_xtp3L = gp_near(0,0.069)
; Lateral Strain
p_xtp4L = gp_near(0.0507,0.059)
p_xtp5L = gp_near(0.0507,0.064)
p_xtp6L = gp_near(0.0507,0.069)
y_disp1L = gp_ydis(p_ytp1L)
y_disp2L = gp_ydis(p_ytp2L)
y_disp3L = gp_ydis(p_ytp3L)
y_disp1R = gp_ydis(p_ytp1R)

```

---

---

```

y_disp2R = gp_ydis(p_ytp2R)
y_disp3R = gp_ydis(p_ytp3R)
x_disp1L = abs(gp_xdis(p_xtp1L))
x_disp2L = abs(gp_xdis(p_xtp2L))
x_disp3L = abs(gp_xdis(p_xtp3L))
x_disp4L = abs(gp_xdis(p_xtp4L))
x_disp5L = abs(gp_xdis(p_xtp5L))
x_disp6L = abs(gp_xdis(p_xtp6L))
; -----
y_dispL = (y_disp1L+y_disp2L+y_disp3L)/3
y_dispR=(y_disp1R+y_disp2R+y_disp3R)/3
y_disp=(y_dispR+y_dispL)/2
; -----
x_dispL1=(x_disp1L+x_disp2L+x_disp3L)
x_dispL2=(x_disp4L+x_disp5L+x_disp6L)
x_disp=(x_dispL1+x_dispL2)/6
; -----
ver_str = -tot_str / n_z
ax_stai=-y_disp/0.1287
lat_stai=-x_disp/0.0507
xtable(1,ntab) = ax_stai
ytable(1,ntab) = ver_str
xtable(2,ntab) = lat_stai
ytable(2,ntab) = ver_str
end
table 1 (0,0)
table 2 (0,0)
hist unbal
; -----

```

---

---

```
; 4- APPLY LOAD
def loop_load
loop h (1,200)
cyclD=string(h)
chk1=string(ver_str/10^6)
chk2=string(ax_stai)
chk3=string(lat_stai)
ID=out('This is load no.: '+cyclD)
prv1=out('Previous load was: '+chk1+'MPa')
prv2=out('Axial Strain was: '+chk2)
prv3=out('Lateral Strain was: '+chk3)
command
bound yvel=0 range bl 342
bound yvel=-0.02 range bl 342
cyc 5000
bound yvel=0.0 range bl 202
;-----
endcommand
loop sk1 (1,20)
if h=sk1*10
io4
command
save name1
endcommand
endif
endloop
slip_load
endloop
loop_load
```

---

UDEC FISH code to apply mineral heterogeneity

---

```
; GENERATE RANDOM NUMBER FOR MINERAL LOCATION
; THE GENERATED RANDOM NUMBER WILL BE USED TO
; ASSIGN MATERIAL TO THE RANDOM LOCATIONS
;=====
change cons 1
; QUART
prop mat 1 d 2650 shear 44e9 bulk 37e9
; PLAGIOCLASE
prop mat 2 d 2630 shear 29.3e9 bulk 50.8e9
; K-FELDSPAR
prop mat 3 d 2560 shear 27.2e9 bulk 53.7e9
; OTHER
prop mat 4 d 3050 shear 12.4e9 bulk 41.1e9
def proBL
; -----
; Mineral Fraction should be corrected
; -----
array qtzx(687) plgx(437) kfelx(112) othx(13)
array qtzy(687) plgy(437) kfely(112) othy(13)
min1=open('qtzx.dat',0,1)
min1=read(qtzx,687)
min1=close
min2=open('plgx.dat',0,1)
min2=read(plgx,437)
min2=close
min3=open('kfelx.dat',0,1)
min3=read(kfelx,112)
min3=close
```

---

```
min4=open('othx.dat',0,1)
```

```
min4=read(othx,13)
```

```
min4=close
```

```
min5=open('qtzy.dat',0,1)
```

```
min5=read/qtzy,687)
```

```
min5=close
```

```
min6=open('plgy.dat',0,1)
```

```
min6=read(plgy,437)
```

```
min6=close
```

```
min7=open('kfely.dat',0,1)
```

```
min7=read(kfely,112)
```

```
min7=close
```

```
min8=open('othy.dat',0,1)
```

```
min8=read(othy,13)
```

```
min8=close
```

```
; -----
```

```
loop i (1,687)
```

```
qtx=parse/qtzx(i),1)
```

```
qty=parse/qtzy(i),1)
```

```
bi1=b_near(qtx,qty)
```

```
b_mat(bi1)=1
```

```
endloop
```

```
loop i (1,437)
```

```
plx=parse/plgx(i),1)
```

```
ply=parse/plgy(i),1)
```

```
bi2=b_near(plx,ply)
```

```
b_mat(bi2)=2
```

```
endloop
```

```
loop i (1,112)
```

---

---

```
kfx=parse(kfelx(i),1)
kfy=parse(kfely(i),1)
bi3=b_near(kfx,kfy)
b_mat(bi3)=3
endloop
loop i (1,13)
otx=parse(othx(i),1)
oty=parse(othy(i),1)
bi4=b_near(otx,oty)
b_mat(bi4)=4
endloop
end
proBL
```

---

UDEC FISH code to define contact normal and shear stiffness based on mineralogy

---

```
; Contact Editor
; Quartz-Quartz
change jcons=5
set jcondf=5
prop jmat 1 jkn=43428e9 jks=26057e9 jfric=57.5 jcoh=42e6 &
jten=18e6 jdil=15 jrescoh=2e6 jrfric=15
; Plagioclase-Plagioclase
prop jmat 2 jkn=32450e9 jks=19548e9 jfric=57.5 jcoh=42e6 &
jten=18e6 jdil=15 jrescoh=2e6 jrfric=15
; K-Feldspar-K-Feldspar
prop jmat 3 jkn=8865e9 jks=5349e9 jfric=57.5 jcoh=42e6 &
jten=18e6 jdil=15 jrescoh=2e6 jrfric=15
; Quartz-Plagioclase
prop jmat 4 jkn=37939e9 jks=22763e9 jfric=57.5 jcoh=42e6 &
jten=18e6 jdil=15 jrescoh=2e6 jrfric=15
; Quartz-K-Feldspar
prop jmat 5 jkn=26146e9 jks=15687.9e9 jfric=57.5 jcoh=42e6 &
jten=18e6 jdil=15 jrescoh=2e6 jrfric=15
; Plagioclase-K-Feldspar
prop jmat 6 jkn=20657.5e9 jks=12444.28e9 jfric=57.5 jcoh=42e6 &
jten=18e6 jdil=15 jrescoh=2e6 jrfric=15
set jmatdf=1
def cmat
ci=contact_head
loop while ci # 0
bi=c_b1(ci)
```

---

---

```
bi2=c_b2(ci)
; Q
if b_mat(bi)=1
; Q-Q
if b_mat(bi2)=1
c_mat(ci)=1
endif
; Q-P
if b_mat(bi2)=2
c_mat(ci)=4
endif
; Q-K
if b_mat(bi2)=3
c_mat(ci)=5
endif
; Q-Bi
if b_mat(bi2)=4
c_mat(ci)=1
endif
endif
; P
if b_mat(bi)=2
; P-P
if b_mat(bi2)=2
c_mat(ci)=2
endif
; Q-P
if b_mat(bi2)=1
c_mat(ci)=4
```

---

---

```
endif
; P-K
if b_mat(bi2)=3
c_mat(ci)=6
endif
; P-Bi
if b_mat(bi2)=4
c_mat(ci)=4
endif
endif
; K
if b_mat(bi)=3
; K-K
if b_mat(bi2)=3
c_mat(ci)=3
endif
; K-P
if b_mat(bi2)=2
c_mat(ci)=6
endif
; Q-K
if b_mat(bi2)=1
c_mat(ci)=5
endif
; K-Bi
if b_mat(bi2)=4
c_mat(ci)=5
endif
endif
```

---

---

```
; Q
if b_mat(bi)=4
; Q-Q
if b_mat(bi2)=1
c_mat(ci)=1
endif
; Q-P
if b_mat(bi2)=2
c_mat(ci)=4
endif
; Q-K
if b_mat(bi2)=3
c_mat(ci)=5
endif
; Q-Bi
if b_mat(bi2)=4
c_mat(ci)=1
endif
endif
ci=c_next(ci)
endloop
end
cmat
```

---

## Appendix 4

Rock Type (Forsmark site area)	Grain Size classification	Crack initiation stress (MPa)	Crack Damage stress (MPa)	Unconfined Compressive Stress (MPa)	E (GPa)	$\nu$
Pegmatite	Medium grained	86	139	158	68	0.24
Pegmatite	Medium grained	71	125	187	69	0.23
Pegmatite	Medium grained	66	110	158	67	0.22
Pegmatite	Medium grained	131	212	285	77	0.27
Pegmatite	Medium grained	49	72	94	70	0.21
Pegmatite	Medium grained	79	132	153	70	0.16
Pegmatite	Medium grained	78	133	187	69	0.24
Pegmatite	Medium-grained	100	179	232	73	0.23
Pegmatite	Medium-grained	100	181	213	72	0.22
Pegmatite	Medium-grained	83	170	236	79	0.18
Pegmatite	Medium-grained	97	159	192	74	0.21
Pegmatite	Medium-grained	91	160	220	72	0.23
Granodiorite	fine granined	55	112	149	74	0.2
Granodiorite	fine granined	72	122	143	70	0.25
Granodiorite	fine granined	60	114	155	66	0.23
Granodiorite	fine granined	75	126	155	75	0.18
Granodiorite	Fine-grianed	136	240	295	67.8	0.20
Granodiorite	Fine-grianed	128	228	274	69.1	0.22
Granodiorite	Fine-grianed	105	198	249	66.8	0.22
Granodiorite	Fine-grianed	95	195	287	63.9	0.23
Granodiorite	Fine-grianed	88	183	233	63.4	0.22
Granodiorite	Fine-grianed	98	189	264	64.0	0.25
Granodiorite	Fine-grianed	107	185	234	65.6	0.25
Granodiorite	Fine-grianed	153	265	323	74.2	0.22
Granodiorite	Fine-grianed	143	228	298	72.6	0.26
Granodiorite	Fine-grianed	133	217	277	62.5	0.23
Tonalite	fine granined	83	148	170	80	0.23
Tonalite	fine granined	80	139	169	74	0.21
Tonalite	fine granined	82	139	162	74	0.2
Tonalite	fine granined	86	144	176	75	0.21
Tonalite	fine granined	70	120	140	67	0.17
Tonalite	fine granined	106	172	214	72	0.27
Tonalite	fine granined	97	184	228	76	0.23
Tonalite	fine granined	94	187	228	74	0.24
Tonalite	fine granined	109	189	227	76	0.25
Granite	Medium grained	108	202	246	76	0.23
Granite	Medium grained	127.34	231	270.125	82	0.18

Rock Type (Forsmark site area)	Grain Size classification	Crack initiation stress (MPa)	Crack Damage stress (MPa)	Unconfined Compressive Stress (MPa)	E (GPa)	$\nu$
Granite	Medium grained	96	166.2	187.4	72	0.19
Granite	Medium grained	104	200	236	76	0.19
Granite	Medium grained	128	211	253	77	0.17
Granite	Medium grained	98	173	218	70	0.18
Granite	Medium grained	98	180	239	72	0.2
Granite	Medium grained	104	198	245	77	0.21
Granite	Medium grained	99	175	221	75	0.21
Granite	Medium grained	98	167	221	73	0.19
Granite	Medium grained	89	159	208	70	0.2
Granite	Medium grained	90	165	199	73	0.19
Granite	Medium grained	97	175	205	71	0.19
Granite	Medium grained	98	164	192	67	0.18
Granite	Medium-grained	130	220	269	80	0.21
Granite	Medium-grained	118	210	265	78	0.22
Granite	Medium-grained	105	203	248	76	0.22
Granite	Medium-grained	111	209	255	80	0.19
Granite	Medium-grained	116	214	261	78	0.2
Granite	Medium-grained	90	176	233	77	0.22
Granite	Medium-grained	111	202	244	80	0.16
Granite	Medium-grained	114	201	243	78	0.18
Granite	Medium-grained	104	192	228	77	0.18
Granite	Medium-grained	117	207	246	78	0.19
Granite	Medium-grained	102	181	214	75	0.2
Granite	Medium-grained	60	112	126	76	0.14
Granite	Medium-grained	88	162	181	74	0.22
Granite	Medium-grained	83	151	171	71	0.23
Granite	Medium-grained	75	143	180	71	0.21
Graanodiorite	Medium grained	103	182	227	75	0.21
Graanodiorite	Medium grained	99	166	203	74	0.17
Graanodiorite	Medium grained	111	177	217	74	0.21
Graanodiorite	Medium grained	108	176	203	71	0.21
Graanodiorite	Medium grained	119	198	233	76	0.17
Graanodiorite	Medium grained	114	183	226	77	0.17
Granodiorite	Medium grained	98	135	193	88	0.36
Granodiorite	Medium grained	116	186	188	72	0.25
Granodiorite	Medium grained	92	186	192	71	0.22
Graanodiorite	Medium grained	108	185	227	81	0.21
Granite	Fine-grained	145	276	336	68.4	0.23
Granite	Fine-grained	109	219	284	71.2	0.21
Granite	Fine-grained	116	230	271	62.6	0.23

Rock Type (Forsmark site area)	Grain Size classification	Crack initiation stress (MPa)	Crack Damage stress (MPa)	Unconfined Compressive Stress (MPa)	E (GPa)	$\nu$
Granite	Fine-grained	102	195	279	67.5	0.22
Granite	Fine-grained	121	221	266	63.2	0.26
Granite	Fine-grained	146	227	292	70.3	0.25
granite	Fine-grained	137	225	249	75	0.21
granite	Fine-grained	125	198	241	79	0.24
granite	Fine-grained	121	197	222	80	0.16
granite	Fine-grained	119	191	230	77	0.19
Granite	fine grained	156	300	371	82	0.22
Granite	fine grained	126	233	309	85	0.2
Granite	fine grained	191	312	358	83	0.21
Granite	Medium grained	76	168	218	71.50	0.22
Granite	Medium grained	114	193	218	72.80	0.27
Granite	Medium grained	110	199	224	75.20	0.29
Granite	Medium grained	126	218	242	75.92	0.26
Granodiorite	Medium grained	123	187	214	73	0.25
Granite	fine grained	110	179	189	83	0.17

Rock Type (Laxemar site area)	Grain Size classification	Crack initiation stress (MPa)	Crack Damage stress (MPa)	Unconfined Compressive Stress (MPa)	E (GPa)	$\nu$
Quartz monzodiorite	Fine-grained	86	146	182	85	0.2
Quartz monzodiorite	Fine-grained	84	152	188	85	0.2
Quartz monzodiorite	Fine-grained	103	183	215	89	0.22
Quartz monzodiorite	Fine-grained	98	166	194	87	0.25
Quartz monzodiorite	Fine-grained	83	142	182	83	0.19
Quartz monzodiorite	Medium grained	77	146	187	70	0.26
Quartz monzodiorite	Medium grained	85	147	186	71	0.23
Quartz monzodiorite	Medium grained	101	176	214	79	0.2
Quartz monzodiorite	Medium grained	120	179	209	76	0.23
Quartz monzodiorite	Medium grained	94	144	161	75	0.25
Quartz monzodiorite	Medium grained	97	165	201	77	0.26
Quartz monzodiorite	Medium grained	104	171	209	77	0.23
Quartz monzodiorite	Medium grained	90	150	183	70	0.25
Quartz monzodiorite	Medium grained	68	121	155	67	0.22
Quartz monzodiorite	Medium grained	103	154	182	77	0.25
Quartz monzodiorite	Medium grained	105	167	193	78	0.24
Quartz monzodiorite	Medium grained	70	123	167	76	0.25
Quartz monzodiorite	Medium grained	131	190	240	76	0.29
Quartz monzodiorite	Medium grained	103	179	218	70	0.24
Quartz monzodiorite	Medium grained	96	169	212	69	0.28
Quartz monzodiorite	Medium grained	115	194	241	75	0.25
Quartz monzodiorite	Medium grained	137	245	320	73	0.24
Quartz monzodiorite	Medium grained	61	141	170	76	0.27
Quartz monzodiorite	Medium grained	102	174	212	83	0.26
Quartz monzodiorite	Medium grained	107	174	207	82	0.24

Rock Type (Laxemar site area)	Grain Size classification	Crack initiation stress (MPa)	Crack Damage stress (MPa)	Unconfined Compressive Stress (MPa)	E (GPa)	$\nu$
Quartz monzodiorite	Medium grained	77	159	192	83	0.17
Quartz monzodiorite	Medium grained	84	150	191	83	0.27
Quartz monzodiorite	Medium grained	106	168	205	84	0.28
Quartz monzodiorite	Medium grained	87	145	163	65	0.26
Quartz monzodiorite	Medium grained	95	148	169	66	0.29
Quartz monzodiorite	Medium grained	48	94	110	51	0.23
Quartz monzodiorite	Medium grained	78	155	192	75	0.27
Granite (Ävrö)- Granite	Medium grained	87	158	175	75	0.17
(Ävrö)- Granite	Medium grained	90	162	188	73	0.15
(Ävrö)- Granite	Medium grained	86	151	179	69	0.18
(Ävrö)- Granite	Medium grained	102	180	208	76	0.12
(Ävrö)- Granite	Medium grained	113	188	216	74	0.15
(Ävrö)- Granite	Medium grained	104	182	216	73	0.15
(Ävrö)- Granite	Medium grained	107	188	228	86	0.21
(Ävrö)- Granite	Medium grained	91	166	214	76	0.17
(Ävrö)- Granite	Medium grained	97	154	194	74	0.21
(Ävrö)- Granite	Medium grained	99	159	181	74	0.17
Granite (Ävrö)- Granite	Medium grained	109	180	212	73	0.17
(Ävrö)- Granite	Medium grained	114	180	207	76	0.18
(Ävrö)- Granite	Medium grained	93	167	203	73	0.22
(Ävrö)- Granite	Medium grained	95	171	206	75	0.15
(Ävrö)- Granite	Medium grained	84	154	196	71	0.15
(Ävrö) Granite	Medium grained	62	138	173	77	0.17
(Ävrö) Granite	Medium grained	63	147	179	37	0.19
(Ävrö) Granite	Medium grained	87	150	179	84	0.26

Rock Type (Laxemar site area)	Grain Size classification	Crack initiation stress (MPa)	Crack Damage stress (MPa)	Unconfined Compressive Stress (MPa)	E (GPa)	$\nu$
Granite (Ävrö)	Medium grained	64	141	175	74	0.15
Granite (Ävrö)	Medium grained	84	145	180	80	0.27
Granite (Ävrö)	Medium grained	67	124	164	67	0.2
Granite (Ävrö)	Medium grained	72	132	171	74	0.19
Granite (Ävrö)	Medium grained	65	127	167	73	0.22
Granite (Ävrö)	Medium grained	72	134	166	70	0.2
Granite (Ävrö)	Medium grained	75	153	197	76	0.2
Granite (Ävrö)	Medium grained	78	148	210	83	0.19
Granite (Ävrö)	Medium grained	81	153	205	71	0.18
Granite (Ävrö)	Medium grained	81	147	196	68	0.18
Granite (Ävrö)	Medium grained	86	157	202	74	0.22
Granite (Ävrö)	Medium grained	76	128	155	70	0.2
Granite (Ävrö)	Medium grained	79	140	159	65	0.19
Granite (Ävrö)	Medium grained	81	133	157	71	0.2
Granite (Ävrö)	Medium grained	79	128	150	69	0.15
Granite (Ävrö)	Medium grained	63	133	167	74	0.18
Granite (Ävrö)	Medium grained	93	149	188	73	0.18
Granite (Ävrö)	Medium grained	75	136	181	72	0.18
Granite (Ävrö)	Medium grained	85	156	188	69	0.12
Granite (Ävrö)	Medium grained	86	151	181	73	0.12
Granite (Ävrö)	Medium grained	79	149	186	70	0.15
Granite (Ävrö)	Medium grained	79	144	184	70	0.22
Granite (Ävrö)	Medium grained	70	142	182	61	0.21
Granite (Ävrö)	Medium grained	88	153	201	71	0.26
Granite (Ävrö)	Medium grained	68	133	166	74	0.26
Granite (Ävrö)	Medium grained	70	131	168	72	0.25

Rock Type (Laxemar site area)	Grain Size classification	Crack initiation stress (MPa)	Crack Damage stress (MPa)	Unconfined Compressive Stress (MPa)	E (GPa)	$\nu$
Granite (Ävrö)	Medium grained	96	144	187	70	0.28
Granite (Ävrö)	Medium grained	78	135	165	71	0.23
Granite (Ävrö)	Medium grained	64	127	173	68	0.19
Granite (Ävrö)	Medium grained	57	112	162	46	0.14
Granite (Ävrö)	Medium grained	79	165	201	70	0.22
Granite (Ävrö)	Medium grained	60	117	140	62	0.18
Granite (Ävrö)	Medium grained	93	160	188	67	0.22
Granite (Ävrö)	Medium grained	69	150	199	68	0.22
Granite (Ävrö)	Medium grained	104	182	218	72	0.23
Granite (Ävrö)	Medium grained	97	178	224	71	0.24
Granite (Ävrö)	Medium grained	111	195	239	72	0.24
Granite (Ävrö)	Medium grained	60	119	145	57	0.21
Granite (Ävrö)	Medium grained	88	157	170	74	0.25
Granite (Ävrö)	Medium grained	70	139	150	61	0.21
Granite (Ävrö)	Medium grained	67	119	125	56	0.2
Diorite	Medium grained	72	146	215	90	0.3
Diorite	Medium grained	86	159	216	88	0.27
Diorite	Medium grained	132	209	268	91	0.3
Diorite	Medium grained	84	162	219	79	0.25
Diorite	Medium grained	106	181	225	81	0.27
Diorite	Medium grained	78	139	199	73	0.29
Diorite	Medium grained	76	156	201	73	0.26
Diorite	Medium grained	111	177	231	76	0.27
Diorite	Medium grained	119	182	229	77	0.27
Diorite	Medium grained	112	179	224	81	0.25
Diorite	Fine-grained	112	192	233	75	0.19
Diorite	Fine-grained	125	218	254	86	0.26
Diorite	Fine-grained	112	179	224	81	0.25
Diorite	Fine-grained	132	235	269	76	0.31
Diorite	Fine-grained	130	247	314	73	0.24
Diorite	Fine-grained	171	272	342	76	0.29
Diorite	Fine-grained	154	266	349	76	0.25

Rock Type (Hometake site area)	Grain Size classification	Crack initiation stress (MPa)	Crack Damage stress (MPa)	Unconfined Compressive Stress (MPa)	E (GPa)	$\nu$
Rhyolite	Very fine	73	139	161	57	0.2
Rhyolite	Very fine	33	47	59	40	0.21
Rhyolite	Very fine	106	185	222	57	0.23
Rhyolite	Very fine	56	125	144	53	0.2
Rhyolite	Very fine	32	53	68	40	0.21

Rock Type (Bruce site area)	Grain Size classification	Crack initiation stress (MPa)	Crack Damage stress (MPa)	Unconfined Compressive Stress (MPa)	E (GPa)	$\nu$
Anhydrite / gypsum	fine to medium grained	19	25	35	13	0.11
Anhydrite / gypsum	fine to medium grained	35	53	60	3	0.19
Argillaceous limestone	fine to medium grained	44	85	95	6	0.08
Argillaceous limestone	fine to medium grained	19	34	50	39	0.15
Argillaceous limestone	fine to medium grained	59	110	145	22	0.05
Argillaceous limestone	fine to medium grained	32	56	78	26	0.1
Argillaceous limestone	fine to medium grained	26	49	58	29	0.18
Argillaceous limestone	fine to medium grained	60	94	114	18	0.37
Argillaceous limestone	fine to medium grained	37	57	81	26	0.37
Argillaceous limestone	fine to medium grained	48	68	85	50	0.3
Argillaceous limestone	fine to medium grained	54	99	114	28	0.13
Argillaceous limestone	fine to medium grained	71	119	140	22	0.11
Argillaceous limestone	fine to medium grained	57	97	141	8	0.37
Argillaceous limestone	fine to medium grained	77	113	141	3	0.26
Argillaceous limestone	fine to medium grained	49	73	91	15	0.14
Argillaceous limestone	fine to medium grained	41	77	93	3	0.09
Argillaceous limestone	fine to medium grained	64	102	132	22	0.28
Argillaceous limestone	fine to medium grained	51	79	124	42	0.36
Argillaceous limestone	fine to medium grained	28	61	100	41	0.34
Argillaceous limestone	fine to medium grained	47	76	96	43	0.35
Argillaceous limestone	fine to medium grained	41	77	118	36	0
Argillaceous limestone	fine to medium grained	45	72	75	40	0.33
Argillaceous limestone	fine to medium grained	48	85	116	33	0.41
Calcareous shale	very fine grained	27	49	61	12	0.32
Calcareous Shale	very fine grained	22	56	56	32	0.13

Rock Type (Bruce site area)	Grain Size classification	Crack initiation stress (MPa)	Crack Damage stress (MPa)	Unconfined Compressive Stress (MPa)	E (GPa)	$\nu$
Calcareous Shale	very fine grained	60	102	115	22	0.3
Calcareous Shale	very fine grained	57	105	119	25	0.33
Shale	very fine grained	13	16	21	43	0.15
Shale	very fine grained	12	17	22	28	0.22
Shale	very fine grained	27	46	53	37	0.36
Shale	very fine grained	8	12	15	31	0.36
Shale	very fine grained	24	30	42	34	0.18
Shale	very fine grained	11	14	16	22	0.2

Rock Type (Homestaksite area)	Grain Size classification	Crack initiation stress (MPa)	Crack Damage stress (MPa)	Unconfined Compressive Stress (MPa)	E (GPa)	$\nu$
Amphibolite		55	104	115	62	0.26
Amphibolite		36	67	107	52.1	0.25
Amphibolite		84	149	216	85	0.32
Amphibolite		78	127	150	87	0.27
Amphibolite		71	121	140	71	0.34
Amphibolite		45	73	84	81	0.29

Rock Type (Forsmark site area)	Grain Size classification	Crack initiation stress (MPa)	Crack Damage stress (MPa)	Unconfined Compressive Stress (MPa)	E (GPa)	$\nu$
Metagranite	Medium grained	97	178	221	81	0.19
Metagranite	Medium grained	112	193	221	76	0.17
Metagranite	Medium grained	121	191	227	76	0.19
Metagranite	Medium grained	99	174	216	78	0.21
Metagranite	Medium grained	109	181	209	75	0.17
Metagranite	Medium grained	77	132	166	78	0.19
Metagranite	Medium grained	102	213	242	78	0.16
Metagranite	Medium grained	58	104	119	76	0.2
Metagranite	Medium grained	109	185	222	77	0.19
Metagranite	Medium grained	87	182	202	73	0.15
Metagranite	Medium grained	124	199	220	72	0.15
Metagranite	Medium grained	106	189	209	77	0.2
Metagranite	Medium grained	109	188	214	75	0.18
Metagranite	Medium grained	127	231	270	82	0.18
Metagranite	Medium grained	112	205	227	82	0.22
Metagranite	Medium grained	96	166	187	72	0.19
Metagranite	Medium grained	123	200	223	76	0.18
Metagranite	Medium grained	140	229	262	76	0.2
Metagranite	Medium grained	122	199	239	73	0.17
Metagranite	Medium grained	107	199	225	78	0.22
Metagranite	Medium grained	118	208	248	77	0.18
Metagranite	Medium grained	106	175	248	73	0.12
Metagranite	Medium grained	121	214	249	79	0.19
Metagranite	Medium grained	117	224	277	68.8	0.2
Metagranite	Medium grained	115	196	247	67.6	0.2
Metagranite	Medium grained	110	209	263	64.1	0.21
Metagranite	Medium grained	106	210	256	65.1	0.18
Metagranite	Medium grained	114	217	268	66.8	0.18
Metagranite	Medium grained	118	211	256	66.7	0.18
Metagranite	Medium grained	129	214	267	69.4	0.22
Metagranite	Medium grained	111	205	274	68.70	0.23
Metagranite	Medium grained	118	219	282	67.10	0.19

Rock Type (Olkilouto site area)	Grain Size classification	Crack initiation stress (MPa)	Crack Damage stress (MPa)	Unconfined Compressive Stress (MPa)	E (GPa)	$\nu$
Mica gneiss	Medium grained	35	106	127	66.80	0.26
Mica gneiss	Medium grained	65	98	120	58.10	0.23
Mica gneiss	Medium grained	43	121	139	59.90	0.19
Mica gneiss	Medium grained	44	94	116	58.50	0.19
Mica gneiss	Medium grained	55	94	113	59.90	0.25
Mica gneiss	Medium grained	47	102	119	57.01	0.28
Mica gneiss	Medium grained	66	106	119	75.16	0.33
Mica gneiss	Medium grained	51	85	123	68.07	0.23
Mica gneiss	Medium grained	50	85	105	63.77	0.30
Mica gneiss	Medium grained	59	113	144	67.97	0.26
Mica gneiss	Medium grained	64	112	137	66.35	0.27
Mica gneiss	Medium grained	50	97	116	62.23	0.27
Mica gneiss	Medium grained	40	77	97	58.86	0.27
Mica gneiss	Medium grained	61	134	162	68.84	0.25
Mica gneiss	Medium grained	49	93	122	64.91	0.26
Mica gneiss	Medium grained	59	90	114	64.60	0.37
Mica gneiss	Medium grained	86	156	184	71.85	0.26
Mica gneiss	Medium grained	34	40	45	38.72	0.34
Mica gneiss	Medium grained	51	94	116	57.10	0.28
Mica gneiss	Medium grained	35	69	88	45.29	0.32
Mica gneiss	Medium grained	36	64	78	44.68	0.29
Mica gneiss	Medium grained	40	63	76	50.44	0.33
Mica gneiss	Medium grained	33	43	48	48.14	0.30
Mica gneiss	Medium grained	38	65	78	55.64	0.28
Mica gneiss	Medium grained	40	75	89	52.22	0.30
Mica gneiss	Medium grained	44	69	91	57.10	0.27
Mica gneiss	Medium grained	40	66	82	58.15	0.29
Mica gneiss	Medium grained	54	105	129	60.92	0.29
Mica gneiss	Medium grained	62	98	111	72.44	0.28
Mica gneiss	Medium grained	42	72	90	60.67	0.28
Mica gneiss	Medium grained	44	98	116	61.77	0.29
Mica gneiss	Medium grained	41	83	105	55.52	0.32
Mica gneiss	Medium grained	42	63	71	52.56	0.28
Mica gneiss	Medium grained	42	65	88	58.67	0.27
Mica gneiss	Medium grained	49	60	71	55.89	0.26
Mica gneiss	Medium grained	52	86	107	62.93	0.22
Mica gneiss	Medium grained	44	75	99	54.65	0.29
Mica gneiss	Medium grained	51	98	123	59.50	0.28

Rock Type (Olkilouto site area)	Grain Size classification	Crack initiation stress (MPa)	Crack Damage stress (MPa)	Unconfined Compressive Stress (MPa)	E (GPa)	$\nu$
Mica gneiss	Medium grained	40	87	102	41.10	0.22
Mica gneiss	Medium grained	58	104	126	64.20	0.26
Mica gneiss	Medium grained	70	120	166	65.40	0.26
Mica gneiss	Medium grained	69	128	142	59.50	0.23
Mica gneiss	Medium grained	57	94	112	60.60	0.26
Mica gneiss	Medium grained	31	48	57	37.80	0.28
Mica gneiss	Medium grained	53	85	102	61.60	0.25
Mica gneiss	Medium grained	58	96	119	63.30	0.27
Mica gneiss	Medium grained	42	66	83	47.10	0.28
Mica gneiss	Medium grained	50	85	103	61.20	0.28
Mica gneiss	Medium grained	61	104	123	65.20	0.25
Mica gneiss	Medium grained	49	74	97	56.60	0.28
Mica gneiss	Medium grained	50	92	113	65.00	0.27
Mica gneiss	Medium grained	48	87	99	56.90	0.27
Mica gneiss	Medium grained	56	98	116	72.20	0.25

	Rock Type (Grain size)	Confining Stress (MPa)	Crack initiation stress (MPa)	Peak Stress (MPa)	
Forsmark site area	Granite (medium grain)	5	200	360.5	
		10	220	410.2	
		10	200	345.6	
		20	265	462.8	
	Pegmatite (medium grain)	5	145	284.3	
		10	125	244.9	
		10	160	321.1	
		20	230	448	
		20	190	348	
		20	205	358.9	
		Qtz monzodiorite (medium grain)	5	115	207.3
	10		135	267.5	
	10		150	271.8	
	20		190	361.2	
5	185		277.4		
10	165		313.9		
10	160		308.3		
20	170		332.3		
Laxemar site area	Granite (Avro: medium grain)		2	130	223.9
			2	120	187.5
		2	120	207.6	
		7	150	271	
		7	150	294.7	
		7	110	231.7	
		7	130	243	
		7	100	247.4	
		7	130	233	
		10	180	332.9	
		10	210	346.8	
		15	165	303.3	
		20	180	329.7	
		20	175	324.7	
		5	135	250.4	
		5	160	285.3	
10	135	281.3			
10	170	326.5			
20	220	405.8			
20	220	437.7			

	Rock Type (Grain size)	Crack initiation stress (MPa)	Peak Stress (MPa)	Rock Type (Grain size)
Lac du Bonnet	Granite (Medium grain)	2	125	234
		4	148	277
		6	145	280
		8	154	287
		10	188	323
		15	192	373
		20	213	421
		40	284	563
		50	380	600
		60	336	602
		2	121	255
		4	136	298
	6	168	344	
	8	165	368	
	10	197	391	
	15	205	432	
	20	220	471	
	30	269	591	
	40	284	593	
	60	394	712	

	Rock Type (Grain size)	Crack initiation stress (MPa)	Peak Stress (MPa)	Rock Type (Grain size)
Forsmark site area	Metagranite (fine grain)	5	200	360.5
		10	220	410.2
		10	200	345.6
		20	265	462.8
Olikilouto site	Mica gneiss (Medium grain)	0.5	48.7	94.9
		0.5	54.1	111.9
		0.5	68.5	168.2
		0.5	61.3	88.5
		0.5	46.0	79.1
		0.5	43.6	96.6
		0.5	42.4	83.8
		0.5	44.1	86.1
		1.0	41.6	77.4
		1.0	30.7	39.4
		1.0	36.3	64.9
		1.0	62.5	83.3
		1.0	48.1	104.9
		1.0	55.1	90.8
		1.0	50.7	105.4
		1.0	58.0	102.2
		3.0	45.9	94.4
		3.0	48.8	126.2
		3.0	75.0	168.6
		3.0	38.4	71.3
		3.0	42.3	93.2
		3.0	61.6	104.5
		3.0	58.2	121.2
		3.0	47.1	63.3
		5.0	44.4	95.5
		5.0	41.7	72.2
		5.0	48.3	70.0
		5.0	64.0	96.0
		5.0	48.4	137.1
		5.0	38.4	95.0
		5.0	58.9	105.6
		5.0	49.8	99.5
15.0	84.1	160.5		
15.0	102.5	166.1		
15.0	98.3	238.2		

	Rock Type (Grain size)	Crack initiation stress (MPa)	Peak Stress (MPa)	Rock Type (Grain size)
Olikilouto site	Mica gneiss (Medium grain)	15.0	58.2	112.3
		15.0	57.3	127.3
		15.0	88.2	156.2
		15.0	58.4	118.2
		15.0	75.4	145.1